2015-02-25

The Role of Sodium-Calcium Exchanger in the Regulation of Endothelial Function

Liao, Chiu-Hsiang

UNIVERSITY OF CALGARY

The Role of Sodium-Calcium Exchanger in the Regulation of Endothelial Function

by

Chiu-Hsiang Liao

A THESIS

SUBMITTED TO THE FACULTY OF GRADUATE STUDIES

IN PARTIAL FULFILMENT OF THE REQUIREMENTS FOR THE

DEGREE OF DOCTOR OF PHILOSOPHY

DEPARTMENT OF CARDIOVASCULAR & RESPIRATORY SCIENCES

CALGARY, ALBERTA

FEBRUARY, 2015

Abstract

Appropriate release of nitric oxide (NO) is critical for normal physiological functioning of the cardiovascular system. Although a rise in intracellular Ca^{2+} concentration ($[Ca^{2+}]_i$) in endothelial cells (ECs) is thought to play an important role in the coordination of NO release, the molecular mechanism underlying this influx is poorly understood. The work presented here outlines the molecular mechanisms responsible for regulating endothelial $[Ca^{2+}]_i$ and its implication to NO production and release, and involved two major areas of study. Firstly, we identified the presence of a signaling complex comprised of stromal interaction molecule 1 (STIM1), transient receptor potential protein (canonical subtype) 1 (TRPC1), and the Na^+/Ca^{2+} exchanger 1 (NCX1) in cultured ECs, which may be an important component of the Ca^{2+} influx pathway necessary for the activation of endothelial NO synthase (eNOS) during agonist stimulation. Secondly, recruitment of the NCX in reverse mode was shown to play an important role in flow-mediated dilation and the corresponding phosphorylation of serine-1177 of eNOS (S1177-eNOS). This is the first study to identify S1177-eNOS phosphorylation in response to flow in small (< 300 μm), pressurized, myogenic rat cerebral arteries. These findings are significant because the potential involvement of a TRP-NCX signaling complex in ECs has been an unresolved issue for some time. Therefore the work of this thesis provides unique insight into the molecular mechanisms that contribute to the regulation of endothelial $[Ca^{2+}]_i$.

Acknowledgements

I would like to thank my supervisor, Dr. William Cole, for his support and guidance and also my supervisory committee, Dr. Andrew Braun and Dr. Michael Walsh. I would also like to acknowledge the contribution of Emma Walsh who helped with the set-up of the open-system myograph in Chapter 4. I would also like to thank Dr. Wayne Chen who provided the equipment for the Ca^{2+} imaging experiments carried out in Chapter 3, Dr. Jonathan Lytton for providing us with R3F1 antibody used in Chapter 3, Dr. Ray Turner who has provided us with the opportunity to generate fluorescent micrographs in Chapters 3 and 5 on the Zeiss axioimager in his laboratory, and Ms. Mirna Kruskic for her excellent technical assistance in operating the axioimager. Also, I would like to thank the members of the Cole lab for their valuable input.

For my family

Table of Contents

List of Figures

List of Symbols, Abbreviations and Nomenclature

Abbreviation	***Full Name***
Akt	Protein kinase B
ATP	Adenosine 5'-trisphosphate
$[Ca^{2+}]_i$	Cytosolic calcium concentration
CaM	Calmodulin
CaMKII	Calmodulin-dependent protein kinase II
COX	Cyclooxygenase
DAG	Diacylglycerol
EC	Endothelial cell
EDHF	Endothelium-dependent hyperpolarizing factor
E_m	Membrane potential
eNOS	Endothelial nitric oxide synthase
ER	Endoplasmic reticulum
FMD	Flow-mediated dilation
GSK	GSK1016790A
IEL	Internal elastic lamina
I_{NSCC}	Non-selective cation current
IP_3	Inositol 1,4,5-trisphosphate
I_{SOC}	Currents mediated by SOC
KBR	KB-R7943
LC_{20}	20 kDa myosin light chain
MLCK	Myosin light chain kinase
MLCP	Myosin light chain phosphatase
MYPT1	Myosin phosphatase targeting subunit 1
NCX	Sodium calcium exchanger
NO	Nitric oxide
NSCC	Non-selective cation current
PKG	Protein kinase G
PLA	Proximity ligation assay
RCA	Rat cerebral arteries
ROC	Receptor operated channel
ROK	Rho-associated kinase
SERCA	(Sarco)endoplasmic reticulum calcium ATPase
SK_{Ca}/IK_{Ca}	Small and intermediate conductance Ca^{2+}-activated potassium channels
SKF	SKF96365

SMC	Smooth muscle cell
SOC	Store operated channel
SR	Sarcoplasmic reticulum
STIM1	Stromal interaction molecule 1
TRP	Transient receptor potential protein
TRPC	Transient receptor potential protein, canonical family
TRPV	Transient receptor potential protein, vanilloid family
VASP	Vasodilator stimulated phosphoprotein
VGCC	Voltage gated calcium channel
VSMC	Vascular smooth muscle cell
XIP	Exchanger inhibitory peptide

Chapter 1: General Introduction

1.1 Structure of blood vessel

Arteries transport blood from the heart to all other organs and consist of three layers: the *tunica intima*, *tunica media*, and *tunica adventitia*. Depending on the vascular bed and the size of the artery, the relative size of each layer can be variable.

The *tunica adventitia* consists of connective tissues, such as elastin, collagen, fibroblasts, mast cells and macrophages (Martinez-Lemus, 2012). The adventitia confers structural support to the artery by anchoring it to surrounding tissue. Perivascular nerves also make contact with arteries at the adventitia layer, conferring innervation to the artery.

The *tunica media* is generally the thickest layer in arteries and consists of layers of long spindle-shaped smooth muscle cells (SMC) and elastic tissue. SMCs are arranged circumferentially around the lumen. The thickness of the SMC layer is variable. For example, in small arteries, the *tunica media* can be composed of anywhere from a single layer of SMC in the smallest arterioles to slightly larger arteries having 3-4 layers of SMC (Perrotta, 2013). In larger arteries, the *tunica media* also contains elastic fibers interspersed between muscle bundles. With increasing size of arteries, there is a gradual increase in the amount of elastic tissue relative to that of the smaller arteries. The elastic tissue in these larger arteries provides them with the ability to stretch and distend

in response to each heartbeat and prevents overextension in response to systolic pressure.

The *tunica intima* consists of a single layer of endothelial cells (ECs) and is supported by the internal elastic lamina (IEL), which separates the *tunica intima* from the *tunica media*. ECs also send finger-like processes through the IEL to make contact with the SMC layer. The endothelium lines the entire circulatory system and plays an important role in the regulation of vascular tone. The structural specialization of the endothelium can also vary in a vascular bed-specific and function-dependent manner. For example, in the cerebral and pulmonary circulations, the controlled passage of molecules across the endothelium dictates that ECs form specialized cell-to-cell tight junctions with each other (Dyer & Patterson, 2010). Conversely, in regions where a high rate of solute and solvent exchange are known to occur, such as in the glomerulus of the renal circulation, ECs form fenestrations, or transcellular holes, to facilitate fluid movement (Satchell & Braet, 2009).

1.2 Regulation of blood flow

Proper circulation of blood is necessary for delivery and removal of substances required for, and by-products of, cellular metabolism. The cardiovascular system, comprised of systemic and pulmonary circulations, facilitates the transport of blood throughout the body. This system works synergistically to oxygenate and propagate the blood to respective tissues and cells. Although the heart is important in providing the initial propagating force of

propulsion, regulation of vascular tone plays a key role in the overall control of blood flow and pressure.

The maintenance of appropriate blood flow to the various organs of the body is critical to normal physiological functions. Regulation of blood flow is determined by arterial diameter and vascular resistance, both of which are dependent on the contractile state of vascular SMCs. For example, stimuli that cause vasoconstriction result in decreased blood flow, increased vascular resistance and increased systemic pressure. Conversely, vasodilation results in increased blood flow, decreased vascular resistance and decreased pressure.

The relationship between arterial diameter and blood flow regulation can be approximated by Poiseuielle's law, which states that flow is related to pressure difference (ΔP), blood viscosity (η), the length of the vessel (L), and the fourth power of vessel radius:

$$F = \frac{\pi \times \Delta P \times r^4}{8\eta L}$$

This approximation assumes that blood flow is steady and uniform through a non-distensible, long and straight tube (Cipolla, 2009). The relationship between the radius to the fourth power and flow indicates that a small change in arterial diameter exerts a significant influence over blood flow and control of blood supply to vital organs.

1.3 Role of vascular SMC (VSMC) in the regulation of peripheral resistance

1.3.1 Overview

Arterial diameter is a critical determinant of peripheral vascular resistance and is dependent on the level of activation of VSMCs, given these cells are

responsible for force generation. The contractile state of VSMCs is determined by both intrinsic and extrinsic factors affecting cross-bridge cycling and force transmission to the extracellular matrix. The contributions of these intrinsic and extrinsic factors are important in establishing resting vascular tone, which enables arteries at rest to exist in a partially constricted state and is physiologically important because it allows arteries to either dilate or constrict in response to vasomotor stimuli to increase or decrease blood flow.

1.3.2 Myogenic response

1.3.2.1 Myogenic response defined

The myogenic response refers to the inherent ability of VSMCs in an artery/arteriole to contract in response to an increase in intraluminal pressure, and to relax in response to decrease in pressure thus maintaining appropriate flow and perfusion. The myogenic response is not present in large conduit vessels, but is prevalent in resistance arteries and arterioles (Davis & Hill, 1999; Hill *et al.*, 2001). The pressure-diameter relationship of a myogenic artery is illustrated in Figure 1.1A. This demonstrates that when intraluminal pressure increases, the artery initially passively dilates (i.e. diameter expands), followed by an immediate transient and a subsequent sustained component of constriction, reducing arterial diameter. Conversely, when there is a sudden drop in vascular pressure, the blood vessel first transiently collapses, and then dilates.

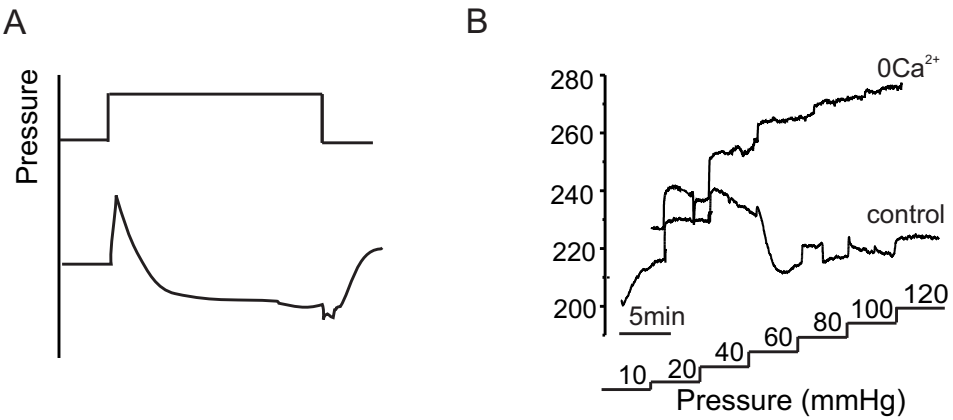

Figure 1.1: Pressure-diameter relationship of an artery displaying a myogenic response.

A, Representative recording of the pressure-diameter relationship of an artery displaying the myogenic response. B, Typical pressure myograph recording of the change in rat cerebral arterial diameter in response to a series of increasing luminal pressure steps from 10 mmHg to 120 mmHg in the presence and absence of extracellular Ca^{2+}.

The use of pressure myography permits the study of blood vessel functions *in vitro* at known levels of intraluminal pressure (Davis & Hill, 1999). Figure 1.1B displays a typical pressure myograph recording of the response of rat cerebral arterial diameter to a series of increasing intraluminal pressure steps from 20 mmHg to 120 mmHg in increments of 20 mmHg. Pressure-induced vessel constriction and arterial diameter reduction occurred at pressures greater than 40-60 mmHg. Passive dilation is observed in the absence of extracellular Ca^{2+} in response to an increase in pressure. The difference in diameter in the presence and absence of extracellular Ca^{2+} represents the extent of active myogenic constriction as a result of pressure-dependent activation of myogenic mechanisms inherent to VSMCs. The physiological pressure range for myogenic constriction varies between different species and vascular beds. For example, myogenic constriction occurs between 60 and 140 mmHg in cerebral arteries (Knot & Nelson, 1998), whereas renal afferent arterioles exhibit myogenic reactivity at pressures as high as 200 mmHg (Loutzenhiser *et al.*, 2004).

1.3.2.2 Physiological significance of the myogenic response

The myogenic response serves two important physiological functions: (1) determination of the basal vascular tone and (2) autoregulation of blood flow.

The presence of a basal vascular tone is important, as it allows arterial diameter to be increased or decreased, depending on a given stimulus in order to match blood flow to physiological demands. The blood pressure and vascular tone *in vivo* consists of the combined effect of maintained and spontaneously-generated myogenic tone (Davis & Hill, 1999).

The myogenic response has also been suggested to play a central role in blood flow autoregulation, which is the maintenance of near-constant blood flow during changes in arterial pressure. The ability of arteries to constrict/dilate in response to increasing/decreasing intraluminal pressure allows for maintenance of constant blood flow despite variations in intraluminal pressure (Koller & Toth, 2012). This mechanism is especially critical in certain vascular beds, such as the cerebral and renal circulations, where constant blood flow is critical for organ function. For example, in the cerebral circulation, constant blood flow needs to be maintained since insufficient blood flow would result in ischemia and excessive perfusion would result in an increase in intracranial pressure, and, possibly, cerebral edema (Koller & Toth, 2012).

1.3.2.3 E_m and $[Ca^{2+}]_i$ in the myogenic response

SMC contraction is determined by forces generated in response to cross-bridge cycling between myosin heads and actin. Myosin is composed of two heavy chains with actin-binding domains and ATP pockets, two essential light chains and two 20 kDa regulatory light chains (LC_{20}). Monophosphorylation of LC_{20} at serine-19 (S19) or diphosphorylation at S19 and threonine-18 is critical for activation of the actomyosin ATP-ase and initiation of cross-bridge cycling in SMCs. Phosphorylation of LC_{20} is mediated by myosin light chain kinase (MLCK) in a Ca^{2+}-dependent manner. An increase in intracellular Ca^{2+} concentration ($[Ca^{2+}]_i$) leads to binding of Ca^{2+} to calmodulin (CaM) forming a Ca^{2+}/CaM complex that activates MLCK (Davis & Hill, 1999; Cole & Welsh, 2011).

The classical view of the myogenic response suggests the occurrence of the following cellular events: (1) E_m depolarization due to the activation of non-selective cation channels (NSCCs) and stretch-activated chloride or Ca^{2+} channels in response to an increase in pressure (Doughty & Langton, 2001; Welsh *et al.*, 2002; Bulley *et al.*, 2012), (2) depolarization induces the activation of voltage-gated Ca^{2+} channels (VGCCs) and other Ca^{2+} influx pathways, resulting in an increase in $[Ca^{2+}]_i$ that leads to Ca^{2+}-CaM-MLCK-dependent phosphorylation of LC_{20} and, ultimately, contraction (Davis & Hill, 1999).

E_m and $[Ca^{2+}]_i$ elevation are important in regulating myogenic constriction. An increase in intraluminal pressure from 10 to 60 mmHg is associated with E_m depolarization from -65 to -40 mV and a corresponding increase in $[Ca^{2+}]_i$ from ~100 to 200 nM (Osol *et al.*, 2002). Although VGCCs are believed to be the primary Ca^{2+} influx pathway, other Ca^{2+} entry pathways, such as NSCC and sodium-calcium exchangers (NCX), and Ca^{2+} release from the ER store have also been suggested to contribute to the $[Ca^{2+}]_i$ increase during myogenic constriction (McCarron *et al.*, 1997; Hill *et al.*, 2001; Potocnik & Hill, 2001; Earley *et al.*, 2005; Morita *et al.*, 2007; Raina *et al.*, 2008; Mufti *et al.*, 2010).

However, changes in $[Ca^{2+}]_i$ alone do not account for myogenic constriction. For example, over the pressure range of 60 mmHg to 120 mmHg, an increase in myogenic tone was observed despite minimal change in $[Ca^{2+}]_I$ (Knot & Nelson, 1998; Davis & Hill, 1999). Thus, other mechanisms are likely involved in pressure-induced contraction.

1.3.2.4 Ca^{2+} sensitization in the myogenic response

LC_{20} phosphorylation is a major determinant in the regulation of SMC contraction and the level of its phosphorylation is the net contribution of MLCK and myosin light chain phosphatase (MLCP) activities. MLCP is a protein serine and threonine phosphatase that is composed of a ~38 kDa catalytic subunit (PP1cδ), a 110~130 kDa myosin phosphatase targeting subunit 1 (MYPT1) and a ~20 kDa subunit of unknown function (Grassie *et al.*, 2011). MYPT1 is important in the regulation of MLCP activity: phosphorylation of MYPT1 at T853 and T696 (human sequence) is known to inhibit MLCP activity (Somlyo & Somlyo, 2003; Grassie *et al.*, 2011).

The classical view of myogenic constriction maintains that MLCK-mediated LC_{20} phosphorylation is the primary mechanism underlying pressure-induced contraction. However, in addition to MLCK-dependent phosphorylation of LC_{20}, Ca^{2+} sensitization has also been shown to occur as the result of increased phosphorylation of LC_{20} following inhibition of MLCP activity. Ca^{2+} sensitization was initially characterized in agonist-induced contraction: stimulation of $G_{12/13}$ and the small GTPase, RhoA, activates Rho-associated kinase (ROK), which phosphorylates MYPT1 to inhibit MLCP activity (Somlyo & Somlyo, 2003). This process has been shown to increase LC_{20} phosphorylation and force generation independent of changes in $[Ca^{2+}]_i$ (Somlyo & Somlyo, 2003).

ROK-mediated Ca^{2+}-sensitization has been shown to contribute to the myogenic response. For example, in conditions where E_m was clamped or $[Ca^{2+}]_i$ was held constant by α-toxin-permeabilization, inhibition of ROK suppressed the

myogenic response without significant change in $[Ca^{2+}]_i$ (Lagaud *et al.*, 2002; Gokina *et al.*, 2005). Recent findings show that pressure-induced constriction of rat cerebral and gracilis arteries coincides with an increase in LC_{20} phosphorylation at S19 and MYPT1 phosphorylation at T855 (rat equivalent of T853). Myogenic constriction and associated phosphorylation of MYPT1 and LC_{20} were suppressed in the presence of the ROK inhibitor, H1152 (Johnson *et al.*, 2009; Moreno-Dominguez *et al.*, 2013). Combined, these data indicate that Ca^{2+} sensitization contributes to myogenic constriction.

1.3.2.5 Cytoskeletal re-arrangement in the myogenic response

The actin cytoskeleton consists of actin and actin-associated proteins. Actin is interconnected at cytosolic dense bodies and anchored to the PM at focal adhesions, which are large protein complexes that include, for example, actin, integrins and other actin-binding and focal adhesion proteins. The interconnection of actin and actin-associated proteins provides a structural framework that permits force transmission from the contractile filaments to the PM and extracellular matrix. Contractile SMCs have been assumed to possess a largely static actin cytoskeleton; however, emerging evidence suggests that the actin cytoskeleton undergoes dynamic remodeling during smooth muscle contraction/relaxation, and may contribute to force generation (Gunst & Tang, 2000; Gunst & Zhang, 2008).

Actin exists in a dynamic equilibrium between two forms of actin: filamentous actin (F-actin) and globular actin (G-actin) and can depolymerize (conversion of F-actin to G-actin) or polymerize (conversion of G-actin to F-actin).

It is proposed that there are two pools of SMC actin: contractile and cytoskeletal actin. Contractile actin interacts with myosin during cross-bridge cycling and exists in the F-actin form. Cytoskeletal actin, on the other hand, exists as either F-actin or G-actin; the dynamic polymerization and depolymerization of cytoskeletal actin are thought to be involved during SMC contraction and relaxation, respectively. An increase in F-actin (and a decrease in G-actin) in response to contractile stimuli is thought to strengthen the actin skeleton and enhance force transmission (Gunst & Tang, 2000; Gunst & Zhang, 2008). A role for cytoskeleton rearrangement has been implicated in the myogenic response; specifically, pressure-induced contraction was associated with a decrease in G-actin content in rat cerebral and gracilis arteries (Cipolla & Osol, 1998; Cipolla *et al.*, 2002; Flavahan *et al.*, 2005; Moreno-Dominguez *et al.*, 2013). Moreover, sequestration of G-actin by latrunculin B significantly reduced myogenic constriction.

In addition to re-organization of cytoskeletal actin, recruitment of several cytoskeletal-associated proteins to the focal adhesion sites has been reported. These proteins include β-integrin, focal adhesion kinase (FAK), paxillin (PAX), vinculin, α-actinin, vasodilator-stimulated phosphoprotein (VASP) (Walsh & Cole, 2013). The recruitment of these proteins is thought to be important in actin (de)polymerization and/or provides an anchor for transmission of force (Gunst & Zhang, 2008).

1.4 Extrinsic control of vascular tone

In addition to the intrinsic ability of SMCs to contract/relax in response to

a(n) increase/decrease in intraluminal pressure, blood vessels are modulated by various extrinsic factors that regulate vascular tone and blood flow to meet physiological demand. Numerous metabolic, neural, and/or endothelial factors can superimpose vasoconstriction or vasodilation on the basal level of myogenic tone. Thus extrinsic factors, together with the intrinsic myogenic response, modulate arterial diameter to optimize blood delivery in dynamic physiological conditions.

Several major extrinsic factors contribute to the regulation of arterial diameter. These include: (1) neurotransmitters released by nerve fibers, (2) circulating factors, (3) metabolic products and (4) endothelium-derived vasoactive factors (Davis & Hill, 1999). Among the extrinsic factors, endothelium-derived vasoactive factors are the most abundant and chemically diverse.

As the innermost lining of arteries, the endothelium is exposed to a variety of stimuli in the form of circulating agonists, neurotransmitters, inflammatory mediators, as well as shear stress that is generated as a result of constant blood flow across the luminal surface of the endothelium. In response to these stimuli, the endothelium releases vasoactive substances that can influence SMCs and impose additional control of arterial diameter and consequently blood pressure and flow. The factors released by the endothelium include constrictors (e.g. prostaglandin E_2, thromboxane A_2 (Wong & Vanhoutte, 2010) and reactive oxygen species (Tang & Vanhoutte, 2009)) and dilators (e.g. nitric oxide (NO), prostacyclin (PGI_2) (Fleming & Busse, 1999) and endothelium-derived hyperpolarizing factors (EDHF) (Edwards *et al.*, 2010)).

1.5 Endothelium-dependent regulation of vascular tone

1.5.1 Endothelium-dependent relaxing factors (EDRFs)

The presence of an EDRF within the vasculature was first elucidated by Furchgott and Zawadski (Furchgott & Zawadzki, 1980). They found acetylcholine-mediated dilation of rabbit aorta depended on the presence of the endothelium. This prompted a search for the chemical mediator(s) underlying this endothelium-dependent relaxation. An EDRF must satisfy at least three criteria in order for it to be physiologically relevant: (1) it should be secreted/released by the endothelium, (2) it should relax VSMCs, and (3) the concentration at which it exerts its effect should be within the physiological range.

Nitric oxide (NO) was later identified as the "factor" underlying endothelium-dependent relaxation (Palmer *et al.*, 1987) (see Chapter 1.6). Other factors have also been reported to have vasodilatory effects in a species- and vascular bed-dependent manner. Next to NO, PGI_2, the principal metabolite of cyclooxygenase (COX), has also been shown to elicit vasodilation (Gryglewski *et al.*, 1986). Vasodilatory peptides, such as C-Type natriuretic peptide (Wright *et al.*, 1996), have also been suggested as putative EDRFs.

1.5.2 Endothelium-dependent hyperpolarization factors (EDHFs)

EDHF manifests as the residual component of endothelium-dependent vasodilation in the presence of L-NAME and indomethacin, inhibitors of endothelial nitric oxide synthase (eNOS) and COX, respectively, in an experimental setting. By definition, EDHF is a factor and/or electrical signal that is released by and/or initiated in the endothelium and induces E_m

hyperpolarization in VSMC (Feletou & Vanhoutte, 1999).

The concept of EDHF comes from experiments showing that some vasodilators can cause endothelial membrane potential (E_m) hyperpolarization, followed by subsequent membrane hyperpolarization in VSMCs (Chen *et al.*, 1988). Later studies indicated that EC hyperpolarization is the result of intermediate and small conductance Ca^{2+}-activated K^+ channel (IK_{Ca} and SK_{Ca}) activation, and the electrical coupling between ECs and SMCs via myoendothelial gap junctions enables this transfer of hyperpolarization from cell-to-cell from the endothelium to underlying SMCs (Harris *et al.*, 2000; Sandow & Hill, 2000; McSherry *et al.*, 2005; McNeish *et al.*, 2006). In addition to gap junctions, the ultrastructural composition of vascular endothelium and SMCs within the IEL regions, where finger-like projections extend from ECs through the IEL to make contact with SMCs, has also been suggested to facilitate this electrical communication (Sandow *et al.*, 2006; Sandow *et al.*, 2009). Hydrogen peroxide (H_2O_2) (Zembowicz *et al.*, 1993), carbon monoxide (Wang *et al.*, 1997), hydrogen sulfide (H_2S) (Mustafa *et al.*, 2011), metabolites of cytochrome P450, such as epoxyeicosatrienoic acids (EETs) (Carroll *et al.*, 1990) have also been suggested as putative EDHFs (summarized in Figure 1.2).

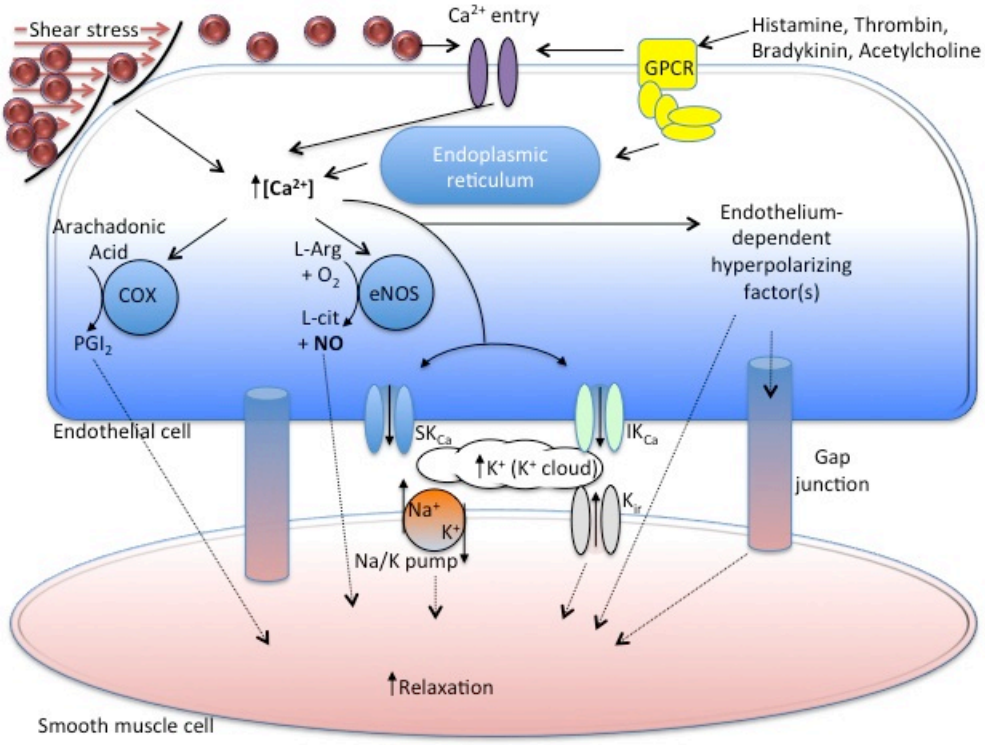

Figure 1.2: Overview of endothelium-dependent release of vasoactive factors.

In response to agonist and shear stress, a combination of ER Ca^{2+} release and Ca^{2+} influx increases $[Ca^{2+}]_i$ and is associated with the release of vasodilators (e.g. nitric oxide (NO), prostacyclin (PGI_2), endothelium-derived hyperpolarizing factor (EDHF)). (Abbreviations: L-arg – L-arginine, L-cit – L-citrulline, IK_{Ca}/SK_{Ca} – intermediate and small conductance Ca^{2+}-activated K^+ channels, K_{ir} – inward rectifying K^+ channels). Modified by Dr. Barry Kyle from Luksha *et al.* (2009).

In addition to a direct spread of E_m hyperpolarization, K^+ released from endothelial IK_{Ca} and SK_{Ca} channels has been suggested to cause a sufficient localized increase in $[K^+]$ in the extracellular space to hyperpolarize SMC by activating inwardly rectifying K^+ (K_{ir}) channels and/or Na^+/K^+ ATPase (NKA) activity on the SMC (Edwards *et al.*, 1998). Small diffusible molecules, such as H_2O_2 and H_2S, have also been proposed to be putative EDHFs (Mustafa *et al.*, 2011), but this remains controversial.

1.6 NO-mediated vasodilation

1.6.1 Overview

The endothelium is considered to be a key determinant of vascular health, with the appropriate release of NO from ECs apparently critical for normal physiological function of the cardiovascular system. NO is a principal mediator of all endothelial protective effects, contributing to blood pressure regulation through its ability to induce smooth muscle relaxation and arterial dilation, but also by its anti-inflammatory, anti-proliferative, and immunomodulatory properties (Hooper *et al.*, 2007). Endothelial dysfunction, which manifests as an inability of blood vessels to dilate appropriately, plays a crucial role in several diseases, such as type 2 diabetes, hypertension, and atherosclerosis (Rudic & Sessa, 1999). The loss of NO bioavailability in the endothelium is an early biochemical marker of endothelial dysfunction and is apparent in several cardiovascular diseases.

1.6.2 NO-mediated SMC relaxation

NO produced by the endothelium diffuses to the smooth muscle cells, where it exerts its vasodilatory effects. NO interacts with the enzyme soluble guanylyl cyclase (sGC), which in turn converts guanosine 5'-triphosphate (GTP) to cyclic guanosine 3'-,5'-monophosphate (cGMP). Activation of protein kinase G (PKG) downstream of an increase in intracellular [cGMP] is a common feature underlying many of NO's biological functions. PKG has several potential targets in SMC that can be phosphorylated to alter SMC contractility by either: (1) reducing $[Ca^{2+}]_i$, (2) altering Ca^{2+} sensitization, or (3) affecting cytoskeletal reorganization.

Several proteins that either directly or indirectly modulate $[Ca^{2+}]_i$ have been reported to be targets of PKG. Phosphorylation of VGCC and sarcoplasmic reticulum Ca^{2+} ATPase (SERCA) by PKG has been reported to inhibit Ca^{2+} entry and enhance sequestration of Ca^{2+}, leading to an overall reduction in $[Ca^{2+}]_i$ (Cornwell *et al.*, 1991; Liu *et al.*, 1997). Moreover, PKG-mediated phosphorylation of IP_3 receptor-associated PKG substrate (IRAG) has been shown to reduce IP_3R-mediated Ca^{2+} release from the store, thereby reducing $[Ca^{2+}]_i$ (Casteel *et al.*, 2005). NO-dependent phosphorylation of large conductance Ca^{2+}-sensitive K^+ channels (BK_{Ca}) is associated with an enhancement of BK_{Ca}-mediated outward current, leading to membrane hyperpolarization and reduced $[Ca^{2+}]_i$ (Kyle *et al.*, 2013).

PKG can also influence Ca^{2+} sensitization. Specifically, phosphorylation by PKG has been reported to increase MLCP activity in VSMCs (Pfitzer, 2001).

As mentioned previously, phosphorylation of MYPT1 at S855 and T696 (human sequence) is associated with an inhibition of MLCP activity (Somlyo & Somlyo, 2003; Grassie *et al.*, 2011). However, PKG has been reported to phosphorylate MYPT1 at other residues. Specifically, PKG was shown to phosphorylate S692, S695, and S852 residues of MYPT1 *in vitro* (human sequence) by the Somlyo group (Wooldridge *et al.*, 2004). Further characterization of PKG-mediated effects in ileum smooth muscle revealed S695 phosphorylation prevented T696 phosphorylation and inhibited Ca^{2+} sensitization (Ca^{2+} desensitization) (Wooldridge *et al.*, 2004). Interestingly, crosstalk between ROK and cyclic nucleotide-dependent protein kinases appears to exist in the regulation of myosin phosphatase activity. Specifically, dual phosphorylation at S696/T697 and S854/T855 by cyclic nucleotide-dependent protein kinases had no effect on myosin phosphatase activity, whereas phosphorylation at T697 and T855 by ROK inhibited phosphatase activity and prevented phosphorylation by cAMP-dependent protein kinase at the neighboring serine residues (Grassie *et al.*, 2012)

NO-mediated SMC relaxation is also thought to involve actin cytoskeletal reorganization. The complex regulation of actin cytoskeletal structure requires coordinated action of several actin-associated proteins (Chapter 1.3.2.5), one of which is VASP, a PKG target that has been extensively studied. An increase in phosphorylation of VASP at S157 and/or S239 coincides with NO-mediated relaxation in rat/rabbit aortae (Oelze *et al.*, 2000; Schafer *et al.*, 2003). Our lab has also recently shown that NO-evoked vasodilation of cerebral arteries is

associated with an increase in VASP S157 phosphorylation (Zoe Zhong, unpublished observation).

1.6.3 Mechanism of NO production

NO is produced from conversion of L-arginine to L-citrulline, in a reaction that is catalyzed by three different forms of nitric oxide synthase (NOS). The isoenzymes are referred to as neuronal 'n'NOS (or NOS I), inducible 'i'NOS (or NOS II), and endothelial 'e'NOS (or NOS III). All three isoenzymes play a role in the cardiovascular system: nNOS releases NO via nitridergic synapses and contributes to control of perfusion of some vascular beds (Lee *et al.*, 2012), constitutively active iNOS plays a role in inflammation and in conditions such as septic shock (Forstermann & Sessa, 2012), and eNOS is expressed in the endothelium and releases NO in response to various stimuli. Although NO derived from all three isozymes of NOS can affect smooth muscle contractility, the involvement of eNOS in the regulation of vascular tone has been the most extensively characterized.

NO is generated via a series of oxidation-reduction reactions, with L-arginine as the primary substrate and molecular oxygen and reduced nicotinamide adenine dinucleotide phosphate (NADPH) as co-substrates. Ca^{2+} is thought to be important in the formation of NO in response to agonist- or shear-stimulation. An increase in $[Ca^{2+}]_i$ coincides with release of NO. However, increasing evidence suggests that in addition to an increase in $[Ca^{2+}]_i$, eNOS activation is under the control of multiple regulatory mechanisms (Papapetropoulos *et al.*, 1999; Fulton *et al.*, 2001). For example, estrogen and

insulin have been reported to increase NO production in the absence of bulk $[Ca^{2+}]_i$ elevation (Kuchan & Frangos, 1994; Caulin-Glaser *et al.*, 1997). This suggests other mechanisms, in addition to changes in $[Ca^{2+}]_i$, may be involved in eNOS activation.

1.7 Regulation of eNOS

1.7.1 Overview

Multiple mechanisms are involved in the regulation of eNOS. As alluded to in the previous section, eNOS activation is sensitive to changes in $[Ca^{2+}]_i$. However, eNOS is also heavily regulated by other mechanisms, such as stabilization of mRNA, post-translational modification, and specific targeting to the plasma membrane (PM). For example, chronic exposure to shear stress can trigger adaptive mechanisms, such as induction of eNOS mRNA expression and/or stabilization of mRNA, contributing to overall eNOS expression (Moore *et al.*, 2010; Ishibazawa *et al.*, 2011). Specific targeting of eNOS to PM by post-translational modifications, such acylation and palmitoylation, is thought to be important in the functional regulation of eNOS (Liu *et al.*, 1996; Shaul *et al.*, 1996). Phosphorylation at serine, threonine, and tyrosine residues on eNOS has also been suggested to be a key post-translational modification that influences its activity. Several known protein-binding partners of eNOS also confer regulatory control of eNOS activity (Fulton *et al.*, 2001). Depending on the type and duration of stimulation, a combination of regulatory mechanisms could be involved in the activation of eNOS.

1.7.2 Role of $[Ca^{2+}]_i$ in the regulation of eNOS

1.7.2.1 Overview of Ca^{2+} dynamics

Ca^{2+} is an ubiquitous signaling molecule in cells. Changes in $[Ca^{2+}]_i$ are tightly regulated as a sustained, elevated $[Ca^{2+}]_i$ is cytotoxic and needs to be avoided to prevent detrimental effects. Precise spatio-temporal regulation of $[Ca^{2+}]_i$ is facilitated by strategic spatial organization of Ca^{2+} handling proteins, which is important for regulation of physiological functions that occur in restricted cellular environments.

Ca^{2+} concentration is maintained at relatively low levels in the cytosol and high in the endoplasmic reticulum (ER). The ER compartment is a storage site for Ca^{2+} at rest. When ECs are stimulated with an agonist, the activation of phospholipase C (PLC) leads to the generation of inositol 1,4,5-trisphosphate (IP_3) and diacylglycerol (DAG). IP_3-dependent activation of IP_3 receptors (IP_3R) on the ER releases Ca^{2+} from the ER and DAG activates non-selective cation channels (NSCC) on the plasma membrane, allowing for Ca^{2+} entry. The combination of ER Ca^{2+} release and Ca^{2+} entry contributes to the overall observed increase in $[Ca^{2+}]_i$. As the ER $[Ca^{2+}]$ ($[Ca^{2+}]_{ER}$) decreases, the fall in $[Ca^{2+}]_{ER}$ also activates Ca^{2+} entry pathways, such as NSCC. The molecular identity underlying this Ca^{2+} entry pathway is still controversial, although there are several potential candidates (see Chapter 1.8).

Effective removal of Ca^{2+} from the cytosol is crucial upon cessation of stimulation. Reuptake of Ca^{2+} back to the ER is mediated by SERCA. On the PM, the sodium-calcium exchanger (NCX), which extrudes 1 Ca^{2+} for intake of 3 Na^+,

and the PM Ca^{2+}-ATP-ase (PMCA) are two primary mechanisms for extruding Ca^{2+} from the cell.

1.7.2.2 Ca^{2+}-dependent activation of eNOS

While the mechanisms that regulate NO production and release are not clearly understood, some aspects of the mechanism are clearly established, such as the role played by increased $[Ca^{2+}]_i$ in the activation of eNOS and subsequent NO production (see Chapter 1.7.3.3). Although an increased $[Ca^{2+}]_i$ is necessary for activation of eNOS, several studies have indicated that Ca^{2+} entry, specifically, is necessary for the activation of eNOS (Singer & Peach, 1982; Luckhoff *et al.*, 1988; Forstermann *et al.*, 1991; Kruse *et al.*, 1994). For example, Isshiki *et al*. (2002), by simultaneously measuring $[Ca^{2+}]_i$ and NO production in bovine aortic endothelial cells, showed that Ca^{2+} influx preceded NO production (Isshiki *et al.*, 2002b). A similar observation was made using intact rat superior mesenteric arteries, where removal of extracellular Ca^{2+} inhibited acetylcholine-mediated NO production (Stankevicius *et al.*, 2006). These data suggest Ca^{2+} influx from the extracellular space is important for the production of NO.

1.7.3 Interacting partners of eNOS

1.7.3.1 Overview

There are several known protein regulators of eNOS. Caveolin-1 and calmodulin (CaM) are two of the most well-characterized binding partners of eNOS and are known to negatively and positively regulate the activity of eNOS, respectively (Chapter 1.7.3.2 and 1.7.3.3). Although other protein binding partners of eNOS, such as heat shock protein 90 (HSP90) and NOS-interacting

protein (NOSIP), have been identified, the mechanism of action of these proteins and their roles in the regulation of eNOS activity are poorly understood. For example, HSP90 has been shown to act as an activator of eNOS (Garcia-Cardena *et al.*, 1998; Presley *et al.*, 2008). However, it is unclear whether HSP90 is a direct activator of eNOS since it has been reported to enhance protein kinase B (Akt)-mediated phosphorylation of eNOS at S1177, suggesting HSP90 may be involved in post-translational modification of eNOS (Takahashi & Mendelsohn, 2003). Another protein, NOSIP, has been shown to bind to eNOS *in vivo* and *in vitro* (Dedio *et al.*, 2001). However, the functional relevance of this protein binding is still under investigation as indicated by findings of Dedio *et al* (2001). In their study, while the activity of eNOS was unaffected by NOSIP *in vitro*, co-expression of NOSIP with eNOS in cultured cells reduced ionomycin-induced production of NO (Dedio *et al.*, 2001), suggesting NOSIP-dependent regulation of eNOS is more complex than direct binding. Despite these observations, the mechanism by which NOSIP regulates eNOS activity is still unidentified.

1.7.3.2 CaM

CaM has been proposed to be involved in the Ca^{2+}-dependent activation of eNOS (Busse & Mulsch, 1990; Forstermann *et al.*, 1991). As $[Ca^{2+}]_i$ increases, a complex forms comprised of Ca^{2+}/CaM, leading to an enhancement of CaM binding to eNOS, which subsequently removes the inhibitory effect of caveolin-1. The idea that the Ca^{2+}/CaM complex formation precedes binding of CaM to eNOS was supported by findings of the Michel group, whereby co-immunoprecipitation of CaM and eNOS required the presence of Ca^{2+} (Michel *et*

al., 1997a). On the other hand, Cho *et al.* (1992) reported that the amount of CaM immunoprecipitated with eNOS remained unchanged in response to estrogen stimulation in ECs, which suggests that CaM tightly binds to eNOS regardless of whether an external stimulus is present, and responds to subtle changes in $[Ca^{2+}]_i$ to regulate eNOS function (Cho *et al.*, 1992).

Interaction between CaM and eNOS has been proposed to facilitate NO production by bringing together the oxygenase and reductase domains of eNOS (Abu-Soud & Stuehr, 1993). NO production requires a controlled sequence of oxidation-reduction reactions and the proper alignment of oxygenase and reductase domains within eNOS is thought to be necessary for its function. Although the mechanism underlying the CaM-dependent regulation of eNOS is still poorly understood, certain aspects, such as binding of CaM to eNOS, are thought be necessary for the dynamic regulation of eNOS.

1.7.3.3 Caveolin-1

Caveolin-1 is one of the most well-characterized, negative regulators of eNOS. Caveolin-1 is a 21 kDa scaffolding protein that forms the main structural component of caveolae, which are PM regions that are enriched in cholesterol and sphingolipid where diverse membrane signaling proteins are targeted. Caveolin-1 is thought to be tightly bound to eNOS at rest, rendering eNOS inactive. Agonist stimulation of EC results in formation of the Ca^{2+}/CaM complex, which displaces caveolin-1 from eNOS and facilitates the activation of eNOS.

The direct interaction between eNOS and caveolin-1 has been analyzed employing recombinant proteins, yeast 2-hybrid and co-immunoprecipitation

experiments (Garcia-Cardena *et al.*, 1997; Ju *et al.*, 1997). These studies determined eNOS/caveolin-1 interaction was mediated by a 20-amino acid sequence in caveolin-1 (amino acids 82-101), known as the caveolin-1 scaffolding domain (CSD) (Garcia-Cardena *et al.*, 1997; Ju *et al.*, 1997). Interestingly, consistent with the view that caveolin-1 is bound to eNOS at rest and displaced by Ca^{2+}/CaM during stimulation, Michel *et al.* (1997b) reported that co-immunoprecipitation of eNOS with caveolin-1 was inhibited by the presence of added Ca^{2+} (Michel *et al.*, 1997b).

The current literature supports the notion that binding of caveolin-1 to eNOS inhibits eNOS activity. For example, it was shown by the Michel lab that enzymatic activity of eNOS was reduced in COS-7 cells overexpressing eNOS and caveolin-1, while over-expression of caveolin-1 did not affect nNOS or iNOS activity (Michel *et al.*, 1997a; Michel *et al.*, 1997b). The inhibitory effect of caveolin-1 on eNOS activity has been attributed to direct binding of CSD to eNOS. Specifically, it was shown *in vitro* that CSD-peptide inhibited eNOS activity in a concentration-dependent manner (Garcia-Cardena *et al.*, 1997; Ju *et al.*, 1997). Moreover, delivery of cell-permeable CSD peptide, made from fusing an internalization sequence from antennapedia (AP) with the peptide, blocked VEGF-induced NO release from bovine aortic endothelial cells (Bernatchez *et al.*, 2005). These data indicate that caveolin-1 serves as an important negative regulator of eNOS activity through dynamic protein interactions.

1.7.4 Regulation of eNOS by phosphorylation

In addition to sensitivity to Ca^{2+} and protein-protein interactions, eNOS is also regulated by phosphorylation. Phosphorylation at various sites on eNOS has been suggested to facilitate sustained activation of eNOS. Specifically, S617, S635, S1177, T495, Y81, and Y567 residues on eNOS (human sequence) have been identified as phosphorylation sites, the phosphorylation of which is thought to influence the catalytic activity of eNOS (Fulton *et al.*, 2001).

The most extensively studied phosphorylation site on eNOS is S1177. S1177 phosphorylation is associated with increased eNOS activity and NO production; specifically, S1177 phosphorylation is thought to enhance eNOS activity by strengthening the interaction between CaM/eNOS (McCabe *et al.*, 2000; Tran *et al.*, 2008). Phosphorylation of S1177 is thought to be Ca^{2+}-dependent, with an increase in $[Ca^{2+}]_i$ promoting formation of Ca^{2+}/CaM, followed by activation of CaM-dependent kinase II (CaMKII)-mediated phosphorylation of S1177 (Fleming *et al.*, 2001). S1177 has also been reported to be phosphorylated independent of changes in $[Ca^{2+}]_i$ through shear stress-mediated activation of Akt (Dimmeler *et al.*, 1999). Protein kinase A (PKA) and adenosine 5'-monophosphate-activated protein kinase (AMPK) have also been implicated as kinases that mediate S1177 phosphorylation (Thors *et al.*, 2004).

Interestingly, dephosphorylation of T495 during agonist stimulation usually accompanies S1177 phosphorylation (Fleming *et al.*, 2001). T495 is thought to be basally phosphorylated by PKC and AMPK and becomes transiently dephosphorylated upon stimulation by agonists, such as bradykinin (Chen *et al.*,

1999; Michell *et al.*, 2001). Basal phosphorylation of T495 is thought to inhibit eNOS activity by preventing binding of CaM to eNOS. It was observed by the Busse group that agonist-induced dephosphorylation of T495 enhanced CaM-eNOS interaction in cell lysates collected from human umbilical vein endothelial cells (Fleming *et al.*, 2001). Moreover, they showed that phosphomimetic T495-eNOS mutant, in which T495 was replaced by an aspartate, was unable to bind to CaM when overexpressed in COS-7 cells (Fleming *et al.*, 2001). These data suggest that basal phosphorylation of T495 prevents binding of CaM to eNOS and is associated with an inhibition of eNOS activity.

Phosphorylation of Y81 and Y567 has been reported in response to agonist- and shear-mediated activation of eNOS. Phosphorylation at Y83 (bovine equivalent of Y81) has been shown to correlate with an increase in eNOS activity. For example, Fulton *et al* (2008) indicated that bradykinin- and VEGF-stimulated Y83 phosphorylation was associated with NO release. Moreover, they showed that expression of eNOS Y83 nonphosphorylatable mutant (tyrosine to phenylalanine substitution) in eNOS knockdown ECs attenuated agonist-stimulated NO release compared to expression of wildtype eNOS (Fulton *et al.*, 2008). On the other hand, phosphorylation at Y657 by proline-rich tyrosine kinase 2 was associated with an attenuation of eNOS activity (Fisslthaler *et al.*, 2008). Specifically, measuring L-citrulline production as an indicator of eNOS activity, eNOS Y657-phosphomutants were inactive compared to wildtype controls, when overexpressed in HEK cells. (Fisslthaler *et al.*, 2008).

Phosphorylation of S617 and S635 has been reported to occur with agonist stimulation but the contribution of these two residues to eNOS regulation is less well defined (Fulton *et al.*, 2001). However, phosphorylation of these two residues by PKA is thought to be associated with eNOS activation (Fulton *et al.*, 2001; Dudzinski & Michel, 2007). Thus, the regulation of eNOS by phosphorylation is complex and activation of eNOS is often accompanied by alteration in the phosphorylation levels of different residues.

1.8 Mechanisms of Ca^{2+} influx

1.8.1 Ionic mechanisms of ECs

As mentioned in Chapter 1.7.2.1, Ca^{2+} entry occurs downstream of agonist stimulation and is important in the activation of eNOS. The molecular entities underlying Ca^{2+} influx will be discussed in Chapter 1.8.2-1.8.6. In addition to ion channels that mediate Ca^{2+} entry, E_m, which provides the electrochemical gradient across the PM, indirectly influences Ca^{2+} influx.

E_m of ECs is determined by complex regulation of outward and inward currents, which include K^+ and Cl^- currents, in addition to Ca^{2+} currents (Nilius & Droogmans, 2001). Volume-regulated Cl^- and K_{ir} currents have been suggested to establish resting E_m (Nilius & Droogmans, 2001). Upon agonist (e.g acetylcholine) stimulation, the release of Ca^{2+} from the store is thought to activate IK_{Ca} and SK_{Ca}, leading to E_m hyperpolarization, which is thought to facilitate Ca^{2+} influx and subsequent NO production (Luckhoff & Busse, 1990a, b; Sheng & Braun, 2007). Ca^{2+} influx has also been shown to be necessary for the sustained activation of K_{Ca}s and maintenance of agonist-induced E_m

hyperpolarization (Busse *et al.*, 1988; Chen & Suzuki, 1990). However, a role for E_m in the regulation of Ca^{2+} influx is not consistent. Muscarinic agonist-induced sustained increase in $[Ca^{2+}]_i$ in ECs from hamster cremaster arterioles and rat mesenteric arteries was unaffected by inhibition of E_m hyperpolarization (Cohen & Jackson, 2005; McSherry *et al.*, 2005).

The hyperpolarization of ECs during activation, combined with the observation that basal Ca^{2+} influx in ECs is decreased, not increased, by E_m depolarization suggests the presence of a Ca^{2+} entry pathway distinct from the VGCC-mediated Ca^{2+} entry in SMCs (Johns *et al.*, 1987). Sustained Ca^{2+} influx in ECs has been widely assumed to be due to the presence of transient receptor potential (TRP) protein-containing NSCCs in the PM. However, findings in the last few years also suggest roles for NCX and Orai1 as alternative mechanisms underlying Ca^{2+} influx in ECs.

1.8.2 TRP superfamily of proteins

1.8.2.1 Overview

The *trp* gene was first identified by Hardie and Minke, which manifested as a Ca^{2+}-permeable channel involved in the phototransduction signaling pathway in fruit flies (Hardie & Minke, 1992). The TRP superfamily of proteins are grouped into six subfamilies based on DNA and protein sequence identity: TRPC (canonical), TRPV (vanilloid), TRPM (melastatin), TRPA (ankyrin), TRPP (polycystin), and TRPML (mucolipin). They are a large and functionally versatile group of proteins that form cationic channels. TRP channels are thought to consist of 6 transmembrane (TM) regions with cytosolic amino and carboxyl

termini; the intracellular termini vary in length depending on the TRP subfamily. Functional TRP channels are thought to be comprised of homo- or hetero-multimers of four subunits, with TM5 and TM6 believed to be the pore region (Pedersen *et al.*, 2005; Owsianik *et al.*, 2006).

In vascular ECs, expression of TRPC1-7 (with the exception of C2), TRPA1, TRPM2 and M7, TRPV3 and V4 has been reported (Vennekens, 2011). These TRPs have been shown to be involved in endothelial physiological functions such as endothelium permeability, cell migration, tubular formation, angiogenesis, and vasodilation (Abdullaev *et al.*, 2008; Li *et al.*, 2011a; Wu *et al.*, 2011; Antigny *et al.*, 2012; Senadheera *et al.*, 2012).

TRP channels are unique in that they do not discriminate between the passage of monovalent and divalent cations. With the exception of TRPV5 and TRPV6, which exhibit a high degree of Ca^{2+} selectivity, and TRPM4 and M5 that are Ca^{2+} impermeant (Owsianik *et al.*, 2006), most TRP channels display a varying degree of selectivity for cations. While initially identified as a Ca^{2+} entry pathway, it has been shown that, depending on channel composition and current recording conditions, TRP channels display relative permeability of Ca^{2+}/Na^{+} (P_{Ca}:P_{Na}) in the range of <1 to ~10 (Owsianik *et al.*, 2006).

The ability of TRP subunits to form homo- and hetero-multimers further complicates the current understanding of the regulation and biophysical properties of TRP subunit-containing channels. The functional channels formed by TRP subunits can exhibit diverse biophysical properties, activation mechanisms, and varied ion permeability profiles, depending on the subunits that

are involved. For example, TRPC4 or C5, when co-expressed with TRPC1, have distinct current-voltage relationships and different single channel conductances from TRPC4 or TRPC5 homomultimeric channels (Strubing *et al.*, 2001, 2003). The wide array of possible channels that can be formed by TRP subunits, combined with a lack of specific inhibitors of TRP subunit-containing channels, limits the ability to characterize channel composition and thus function.

1.8.2.2 TRPC

TRPC proteins have emerged as the molecular entities underlying Ca^{2+} entry in a variety of cell types. Specifically, an emphasis was initially placed on their potential roles in store-operated Ca^{2+} entry (SOC), a Ca^{2+} entry mechanism that occurs subsequent to a decrease in $[Ca^{2+}]_{ER}$ downstream of PLC stimulation. However, emerging evidence indicates that TRPC can also be activated independent of store depletion in what is termed receptor-operated Ca^{2+} entry (ROC).

TRPC subunit-containing channels have been characterized in the context of store- and receptor- operated Ca^{2+} entry pathways. Depletion of ER Ca^{2+} with thapsigargin (SERCA inhibitor) and IP_3 has been shown to elicit I_{SOC} in CHO cells over-expressing TRPC1 (Liu *et al.*, 2003). TRPC3 has also been suggested as a SOC by Muallem and colleagues (1998) who showed carbachol and IP_3 both activated I_{SOC} in HEK cells co-expressing muscarinic receptors and TRPC3 (Kiselyov *et al.*, 1998). Yet, DAG stimulated TRPC3 and TRPC6 activity independent of store depletion (Hofmann *et al.*, 1999). TRPC4 has been shown to contribute to SOC in the endothelium (Tiruppathi *et al.*, 2002). TRPC5 is

closely related to TRPC4 based on sequence identity, and has been shown to be activated by store depletion in a stimulus-dependent manner. However, co-expression of TRPC4/C5 revealed TRPC5 can be activated downstream of phospholipase-C activation independent of store depletion (Parekh & Putney, 2005). Although, in stably transfected cell lines, TRPC7 exhibited both store-dependent and -independent Ca^{2+} entry (Lievremont *et al.*, 2004), TRPC6 and TRPC7 are generally accepted to be receptor activated (Trebak *et al.*, 2003).

Studies involving TRPC-containing channels are often hampered by several factors. Firstly, TRPC-containing channels can form homo- and hetero-multimers, adding complexity to the molecular identification of the pore forming subunits of SOC/ROC. Secondly, not all TRPCs exhibit store-dependency and are activated by a wide array of stimuli (Strubing *et al.*, 2003). Lastly, while the classical view maintains that TRPC1/4/5 and TRPC3/6/7 subunits form distinct SOC- and ROC-channels, respectively (Kiselyov *et al.*, 1998), other data suggest this may not be a clear classification (Strubing *et al.*, 2003; Lievremont *et al.*, 2004). Stimulation with GPCR-linked agonist often results in activation of both store-dependent and -independent pathways making it difficult to classify whether a TRPC-mediated Ca^{2+} entry is ROC or SOC. Despite these discrepancies, TRPC channels have been shown to play a role in Ca^{2+} entry in ECs following stimulation by GPCR-linked agonists. For example, TRPC1 and C4 as homo- and/or heterotetrameric channels alone, or associated with STIM1 and/or Orai1, have been implicated as potential SOCs in ECs (Tiruppathi *et al.*, 2002; Ahmmed *et al.*, 2004; Kwiatek *et al.*, 2006; Singh *et al.*, 2007; Pani *et al.*,

2009; Sundivakkam *et al.*, 2009; Sundivakkam *et al.*, 2012). On the other hand, TRPC6 (Hicks *et al.*, 2010; Singh *et al.*, 2007) has been suggested to form ROCs.

1.8.2.3 TRPV4

The TRPV (V1-V6) subfamily is composed of six members with different functional properties. TRPV1–4 are Ca^{2+}-permeable, nonselective cation channels that are activated by a variety of stimuli, with a common sensitivity to heat. Unlike TRPV1–4, TRPV5 and TRPV6 are highly Ca^{2+}-permeable channels and have been reported to be involved in epithelial Ca^{2+} transport (Wu *et al.*, 2011). TRPV4 has also been implicated in sensing osmolality, nociception, and mechanical stressors (Zhang *et al.*, 2009; Wu *et al.*, 2011; Zhang & Gutterman, 2011). In ECs, TRPV4 has recently been elucidated as an important Ca^{2+} entry pathway that mediates shear-induced, mechanosensitive Ca^{2+} influx and contributes to the regulation of basal, agonist-induced, and shear-induced changes in vascular tone (Earley *et al.*, 2009; Zhang *et al.*, 2009; Ma *et al.*, 2010; Dekker *et al.*, 2011; Li *et al.*, 2011b; Bagher *et al.*, 2012; Bubolz *et al.*, 2012; Sullivan *et al.*, 2012).

Although the traditional view maintains that TRP proteins form homo- and hetero-multimeric channels within members of their subfamily, recent studies have shown that being members of the same TRP subfamily is not a requirement for formation of functional channels. TRPV4 has been reported to form homomultimeric channels with itself and heteromultimeric channels with TRPC1

in cultured ECs and in heterologous overexpression systems (Ma *et al.*, 2010; Dekker *et al.*, 2011; Li *et al.*, 2011b).

TRPV4 activity is associated with shear-induced increase in endothelial $[Ca^{2+}]_i$ and flow-mediated dilation (FMD). Shear stress has been shown to increase $[Ca^{2+}]_i$ in HEK cells overexpressing TRPV4 (Kohler *et al.*, 2006). Stimulation of cultured human aortic ECs with GSK1016790A (GSK, 5 nM), a TRPV4 agonist, and shear stress increased $[Ca^{2+}]_i$, which was blocked by the putative TRPV4 antagonist, ruthenium red (Mendoza *et al.*, 2010). Additionally, the dilatory response to shear stress was effectively abolished in mesenteric arteries obtained from TRPV4-/- mice compared to that of wildtype mice (Mendoza *et al.*, 2010). These data indicate that TRPV4-mediated Ca^{2+} entry plays an important role in the physiological regulation of EC function in response to shear stimulation.

1.8.3 NCX as a Ca^{2+} influx pathway

1.8.3.1 Overview

The observation that some TRP channels display minimal Ca^{2+} permeation and carry a predominantly Na^+ inward current raises the possibility that other channels/transporters may be involved in mediating Ca^{2+} entry if TRPC is not the main Ca^{2+} carrier. NCX, as a modulator of both $[Na^+]_i$ and $[Ca^{2+}]_i$ appears to be a candidate in bridging this gap.

1.8.3.2 NCX protein

NCX transporters belong to the gene family *SLC8*. Three isoforms of NCX have been identified, NCX1, NCX2, and NCX3. ECs predominantly express

NCX1. Due to its electrogenic nature, the NCX is able to operate in a bidirectional manner that is dependent on Na^+ and Ca^{2+} gradients across the membrane and E_m; it is capable of both Ca^{2+} extrusion (forward) and Ca^{2+} influx (reverse) (Ruknudin *et al.*, 2007). NCX brings in Na^+ and extrudes Ca^{2+} from the cell at a ratio of 3:1. NCX is an important Ca^{2+} extrusion mechanism along with the PMCA, with the former being a low affinity-high capacity mechanism and the latter being high affinity-low capacity. Structurally, NCX consists of two hydrophobic clusters with 5 and 4 TM helices in the first and second cluster, respectively (Lytton, 2007). NCX activity is regulated by the large cytoplasmic loop between TM5 and TM6. Within the cytosolic loop, the exchanger inhibitory peptide (XIP) region and Ca^{2+}-binding sites are important for NCX regulation. Specifically, they are involved in Ca^{2+}-dependent activation and Na^+-dependent inactivation of the NCX.

1.8.3.3 Ultrastructural basis in support of reversal of NCX activity

Due to its electrogenic nature and its dependence on both Na^+ and Ca^{2+} gradients and E_m, NCX activity can either extrude or import Ca^{2+}. However, whether reversal of NCX activity can occur in a physiological setting is debated. On one hand, it has been argued that reversal of NCX is theoretically unlikely to occur in a physiological setting because of the high $[Na^+]_i$ required for its activation (Lyu *et al.*, 1992). On the other hand, reverse NCX has been shown to play an important role in the regulation of $[Ca^{2+}]_i$ in SMCs (Dai *et al.*, 2007; Hirota *et al.*, 2007a; Hirota *et al.*, 2007b; Poburko *et al.*, 2007; Syyong *et al.*, 2007). This is most likely due to the unique cellular ultrastructure observed in some SMC

types that could facilitate the reversal of NCX (Dai *et al.*, 2005). In SMCs of rabbit inferior vena cava (IVC), electron microscopy revealed that the peripheral or superficial sarcoplasmic reticulum (SR) is often within 20 nm of the PM; these areas of close apposition span up to 400 nm along the membranes (Dai *et al.*, 2005). This creates narrow spaces sandwiched between two membranes referred to as PM-SR junctions. This spatially restricted region allows for generation of local ion concentrations that are orders of magnitude higher than in the bulk cytosol and provides a structural foundation for NCX reversal. Similar cellular architectures have also been speculated in cardiomyocytes, where a restricted space of 15 nm between junctional SR and PM is also thought to facilitate localized subspace [Ca^{2+}] elevation (Sobie *et al.*, 2002)

A similar PM-ER junction in EC has not been characterized using electron microscopy, but has been speculated from indirect evidence obtained from functional studies and co-localization investigations. Simultaneous measurements of $[Ca^{2+}]_{ER}$ and $[Ca^{2+}]_i$ revealed that refilling of the ER store occurred without bulk cytosolic [Ca^{2+}] changes, implying close apposition of PM and ER (Jousset *et al.*, 2008). Moreover, biochemical and immunohistochemical approaches have been employed to elucidate interactions between PM and ER proteins, which provide indirect evidence that the two membranes are in close proximity to each other. Specifically, interaction between TRPC1 and IP_3R has been documented in cultured ECs (Mehta *et al.*, 2003). Moreover, co-immunoprecipitation of STIM1 (See chapter 1.8.5), which is thought to be present in the ER membrane, with TRPC4 has been reported in ECs (Sundivakkam *et*

al., 2009; Sundivakkam *et al.*, 2012). The co-immunoprecipitation and co-localization of PM and ER-spanning proteins provide indirect evidence for physical proximity between the two membranes in ECs.

1.8.3.4 Evidence in support of NCX as a Ca^{2+} influx pathway

In SMCs, the functional linked effect of KB-R7943 (KBR, inhibitor of reverse NCX) and SKF-96365 (SKF, inhibitor of NSCC) lead to the hypothesis that Ca^{2+} influx is partially mediated by reverse NCX activity. Specifically, the opening of NSCCs allows for Na^+ influx and this ultimately leads to a sufficient localized increase in $[Na^+]_i$ in the PM-SR junction that provokes reversal of NCX activity (Poburko *et al.*, 2007). Arnon and Blaustein (Arnon *et al.*, 2000b, a) have demonstrated that 5HT-stimulated increase in $[Na^+]_i$ in arterial SMCs was sensitive to La^{3+} and Gd^{3+}, blockers of NSCC, suggesting a role for NSCC in this rise in $[Na^+]_i$. More recently, a localized increase in $[Na^+]_i$ due to agonist stimulation in rat aortic SMCs was observed. Occurrence of these Na^+ transients was inhibited by SKF and expression of a dominant-negative TRPC6 construct, and they increased in frequency and duration when reverse NCX was inhibited with KBR (Poburko *et al.*, 2007). *In situ* calibration provides estimates of $[Na^+]_i$ within this region to be ~25-30 mM (Poburko *et al.*, 2007). This localized elevation in rat aortic SMC was hypothesized to be sufficient to trigger reverse-mode NCX activity. Pharmacological modulation of these transient Na^+ responses functionally demonstrates the presence of a PM-SR junction microdomain and that both TRPC subunits- containing NSCCs and reverse NCX are involved in the dynamic ionic regulation in SMCs.

In ECs, a role for reverse NCX in the maintenance of agonist-induced $[Ca^{2+}]_i$ is less well defined. Agonist stimulation of EC has been shown to increase $[Na^+]_i$ (Paltauf-Doburzynska *et al.*, 2000). Manipulating the Na^+ gradient across the PM, either by Na^+ loading the cells with Na^+ ionophore (monensin) or transiently reduced extracellular $[Na^+]$, has been shown to influence eNOS activity (Sedova & Blatter, 1999; Teubl *et al.*, 1999). For instance, Na^+ loading with monensin was found to enhance NO production as measured by L-citrulline formation (Teubl *et al.*, 1999). Moreover, bradykinin-induced NO production was inhibited by dichlorobenzamil, a non-specific inhibitor of NCX (Schneider *et al.*, 2002). Although further characterization is required to better understand the regulation of NCX in ECs, these functional studies suggest that NCX could have a physiological function in the regulation of EC $[Ca^{2+}]_i$.

1.8.4 Orai1

Genome-wide RNAi screening of *Drosophila* genes resulted in the identification of Orai1 (Vig *et al.*, 2006), which was later identified as the pore-forming unit mediating Ca^{2+} release-activated Ca^{2+} current (I_{CRAC}) in T-lymphocytes. I_{CRAC} is analogous to SOC as I_{CRAC} is also dependent on $[Ca^{2+}]_{ER}$ (Prakriya *et al.*, 2006; Yeromin *et al.*, 2006). The current-voltage relationship of Orai1 exhibits the inward-rectifying characteristics of I_{CRAC}. The mechanisms underlying the activation of Orai1 are poorly understood. Li *et al.* showed that Orai1 can form puncta in the PM following store depletion, indicating Orai1 proteins assemble post-stimulation to mediate store-dependent Ca^{2+} entry (Li *et al.*, 2007; Li *et al.*, 2008). However, Gwack *et al.* showed Orai1 exists as a dimer

or multimer in both basal and store-depleted states, suggesting that store-depletion does not induce clustering of Orai1 (Gwack *et al.*, 2007).

There is some evidence suggesting Orai1 is a Ca^{2+} influx pathway in ECs. RNA silencing of Orai1 significantly reduced VEGF-induced $[Ca^{2+}]_i$ elevation in human umbilical vein endothelial cells (Li *et al.*, 2011a). Similarly, Orai1 was shown to mediate thrombin-induced Ca^{2+} entry since silencing of TRPC1 and C4 had no effect on the thrombin-induced increase in $[Ca^{2+}]_i$ in pulmonary arterial ECs (Abdullaev *et al.*, 2008). Orai1 has also been reported to alter ion selectivity of TRPC-containing channels in ECs. Specifically, Orai1 knockdown reduced TRPC1/4 channel activation and converted channel phenotype from one that is Ca^{2+}-selective to one that is non-selective for cations (Cioffi *et al.*, 2012). Despite recent findings that implicate Orai1 in the regulation of EC $[Ca^{2+}]_i$, the contribution of Orai1-mediated Ca^{2+} entry to overall $[Ca^{2+}]_i$ dynamics in ECs remains to be defined with certainty.

1.8.5 T-type voltage-dependent Ca^{2+} channels

Given the resting and activated range of E_m in ECs, a possible role for T-type VGCC as a Ca^{2+} entry pathway has been suggested (Kuo *et al.*, 2011). T-type VGCCs are low voltage-activated Ca^{2+} channels that exhibit a window current within the physiological range of the endothelial E_m (-60 mV to -30 mV). Yet, the involvement of T-type channels in ECs is controversial because documentation of its expression in ECs is limited. Immunostaining with T-type channel antibodies revealed the presence of immunoreactivity in ECs of intact mesenteric and cerebral arteries (Braunstein *et al.*, 2009; Kuo *et al.*, 2011), but

functional characterization of T-type channel activity has been mostly limited to pulmonary arterial ECs (Wu *et al.*, 2003; Zhou *et al.*, 2010), and the identity of the immunoreactive protein has been debated.

1.8.6 Stromal interaction molecule protein 1 (STIM1)

The activation of SOC requires communication between the $[Ca^{2+}]_{ER}$ and PM channel. STIM1 was identified as a $[Ca^{2+}]_{ER}$-sensitive protein and provided a link between ER-depletion and the activation of SOC (Liou *et al.*, 2005). STIM1 is an ER membrane protein with a single membrane-spanning domain with Ca^{2+} sensor inside the ER. The regulation of STIM1 by $[Ca^{2+}]_{ER}$ is a dynamic process. ER Ca^{2+} depletion results in the unbinding of Ca^{2+} from the Ca^{2+} sensor and leads to STIM1 oligomerization (Liou *et al.*, 2007). Subsequent to oligomerization, STIM1 proteins form puncta, which are believed to be involved in the translocation of STIM1 toward the PM. The termination of STIM1 puncta formation is associated with both the termination of the stimulus and a refilled ER (Varnai *et al.*, 2007).

Protein interactions between STIM1 and TRPCs are well documented, and these interactions are thought to be important in the activation of SOC. Initial experiments assessing the role of STIM1 in store-operated entry have revealed the C-terminus of STIM1 to be important in SOC activation and that over-expression experiments in HEK cells revealed STIM1 to co-immunoprecipitate with TRPC1, C2, C4 and C5 (Huang *et al.*, 2006a). Moreover, upon activation of SOC, TRPC1 has been documented to form puncta, which co-localize with STIM1 (Pani *et al.*, 2009). While physical interactions between Orai1 and STIM1

are not well-documented, a polybasic region of STIM1 (K384-86) has been implicated in Orai1 gating through interaction with the Orai1 C-terminus (Calloway *et al.*, 2009). A correlation between STIM1 expression and NCX1-mediated currents has also been reported. It was shown in pulmonary arterial SMCs that STIM1 knockdown significantly reduced NCX-mediated current (Liu *et al.*, 2010). While the study did not provide direct evidence showing physical interaction between the two proteins, it showed a functional relationship exists between the STIM1 and NCX1.

STIM1 has been shown to regulate endothelial $[Ca^{2+}]_i$ downstream of agonist stimulation. STIM1 knockdown and expression of a dominant-negative STIM1 construct inhibited thrombin-induced Ca^{2+} entry in human and murine pulmonary ECs (Sundivakkam *et al.*, 2012). Using type 1 diabetic mouse models, reduced Ca^{2+} release from the ER was associated with downregulation of STIM1 protein expression in mouse coronary artery ECs (Estrada *et al.*, 2012). While detection of $[Ca^{2+}]_{ER}$ by STIM1 is thought to mediate activation of agonist-induced Ca^{2+} entry, the precise mechanism by which STIM1 activates EC Ca^{2+} entry is still under investigation.

1.9 Summary and rationale for our study

Coordination of $[Ca^{2+}]_i$ is important in the regulation of endothelial function. The ability of Ca^{2+} to elicit a plethora of downstream physiological activities has been attributed to tight spatial and temporal control of dynamic $[Ca^{2+}]_i$ events. Localized Ca^{2+} events have been reported in several vascular beds and under different stimulating conditions. The strategic locations of signaling proteins and

membranes have been attributed as the underlying cause for the generation of these Ca^{2+} events. Although in the last few years a role for NCX as a Ca^{2+} influx pathway has come to prominence, based on an argument for its role in localized signaling, the data that support this view are largely circumstantial.

Firstly, although there is functional evidence for a role of NCX as a $[Ca^{2+}]_i$ regulatory pathway in ECs, the use of nonspecific pharmacological tools and non-physiological manipulation of the $[Na^+]$ gradient prevents any concrete conclusions regarding the physiological contribution of reverse mode activity to Ca^{2+} influx. Moreover, even if the presence of TRPC-NCX signaling complexes has been tentatively identified in other cell types, evidence showing their presence in ECs is lacking.

Secondly, most of the studies regarding the role of NCX have been focused on its role downstream of agonist stimulation. However, constant flow is an important regulator of endothelial function and vascular tone in physiological conditions. Although shear-induced TRPV4-mediated increase in $[Ca^{2+}]_i$ is thought to be important in the initiation of endothelium-dependent dilation, this view largely dismisses the relatively non-selective nature of TRP channels for monovalent and divalent cations.

The work presented in this thesis aims to expand on the current understanding of how endothelial function is controlled by NCX-mediated regulation of $[Ca^{2+}]_i$ through examination of the molecular entities in the NCX-containing macromolecular signaling complex, and investigation of NCX-

mediated regulation of agonist-induced changes in $[Ca^{2+}]_i$ and shear-induced dilation of pressurized resistance arteries.

1.10 Hypothesis

The central hypothesis of this thesis is that NCX facilitates Ca^{2+} entry in ECs in response to agonist- and shear-stimulation and that the activation of reverse-mode NCX is dependent on its close proximity to and functional interaction with TRP-containing NSCCs.

1.11 Major objectives

The major objectives of this thesis were two-fold:

(1) To determine whether a TRPC-NCX signaling complex contributes to agonist-evoked increases in endothelial $[Ca^{2+}]_i$;

(2) To identify a role for NCX in the regulation of shear-induced vasodilation in rat intact cerebral artery.

1.12 Significance

The findings of this thesis will provide a novel and important contribution to our understanding of the underlying molecular basis of Ca^{2+} signaling in endothelial cells. Such information is important not only for our understanding of the molecular mechanisms that might be involved in the generation of localized Ca^{2+} signals and their role in endothelial function, but it will provide a basis for understanding the generation of abnormal Ca^{2+} signals and associated endothelial dysfunction.

Chapter 2: Methods

2.1 Cell culture and transfection

Human umbilical vein endothelial cells (Ea.Hy926 cell-line) were cultured in low-glucose Dulbecco's Modified Eagle's Medium (DMEM) with 10% fetal bovine serum (FBS), penicillin, streptomycin and sodium hypoxanthine (10 mM) and thymidine (1.6 mM) supplement. Cells were maintained at 37 °C at 5% CO_2.

For Fura-2 imaging experiments, cells were plated on glass coverslips 1-3 days before experiments. For siRNA experiments, cells were plated onto 12 mm glass coverslips and transfected 1 day after seeding. Cells were either transfected with control scrambled siRNA or siRNA targeted against NCX1 or TRPC1 (Santa Cruz); green fluorescent protein (GFP) was utilized as a marker for successful transfection. For each coverslip, transfection reagents were premade in the following volume: 125 μl of opti-MEM with 3 μl of siRNA and 0.5 μg of GFP followed by incubation at room temperature for 20 min. Transfection reagent, Lipofectamine 2000 (Invitrogen, Oakville, ON), was added to cells after washing the cells first with antibiotic-free medium. The final concentration of the siRNA in the cultured media was 15 nM. Media containing transfection reagents were removed 5 hours later. Cells were used two days post-transfection.

2.2 Cytosolic calcium measurements

Intracellular calcium concentration was measured with fura-2 acetoxymethyl ester (fura-2/AM, Invitrogen, Burlington, ON). Cells were grown on glass coverslips and incubated for 20 min at room temperature in 5 μM fura-2AM

in HEPES-buffered saline solution (physiological saline solution (PSS), composition in mM: 135 NaCl, 5 KCl, 1 $MgCl_2$, 1.5 $CaCl_2$, and 10 HEPES, pH 7.4 with 1M NaOH) and 0.1 mg/ml bovine serum albumin. Cells were washed twice with PSS. Coverslips were mounted in a perfusion chamber (Warner Instruments, Hamden, CT, U.S.A.) on an inverted microscope (Nikon TE2000-S) equipped with an S-Fluor ×20/0.75 objective and a Chroma filter set using the ImageMaster System and the DeltaRAM rapid wavelength-switching illuminator and FURA-2 loaded cells were excited at 340 nm and 387 nm. Emission intensity was collected at 510 nm. The ratio of emission intensity at 360 nm and 380 nm was used to to indicate relative changes in intracellular Ca^{2+} levels. Images were acquired once every 4 s and analyzed with the Compix Simple PCI 6 software. Specifically, areas of interest were drawn around each cell of interest. The average fluorescent intensity of the cells was determined for continuous recordings and used to generate Ca^{2+} fluorescence versus time relations . Ca^{2+} imaging experiments were carried out in the laboratory of Dr. Wayne Chen.

2.3 RT-PCR

Total RNA was extracted from Ea.Hy926 cells using the RNeasy Kit (Qiagen). cDNA was prepared from the RNA preparation using the Sensiscript kit and oligo(dT) primers via reverse transcription. The reverse transcripts were amplified with the following primer sets as previously described for TRPC and actin (Yip *et al.*, 2004):

hTRPC1: Forward 5’ CTTCCTCTCCATCCTCTTCC 3’

Reverse 5’ GTTTCTGACACCCGTAGTCC 3’

hTRPC3: Forward 5’ GACATATTCAAGTTCATGGTCCTC 3’

Reverse 5’ ACATCACTGTCATCCTCAATTTCT 3’

hTRPC4: Forward 5’ GGCGGACTTCAGGACTACAT 3’

Reverse 5’ GCTGTGCTTTGACATTGGTC 3’

hTRPC5: Forward 5’ TCAAGTTTATCTGCCACACAGC 3’

Reverse 5’ TAGGCTCATCGATAGCTCTGGT 3’

hTRPC6: Forward 5’ TTGGAAGAACAGTCAAAGACATCT 3’

Reverse 5’ CAATTTCCTGGAATGAACTGTTGA 3’

hTRPC7: Forward 5’ GTCCGAATGCAAGGAAATCT 3’

Reverse 5’ TGGGTTGTATTTGGCACCTC 3’

Actin: Forward 5’ CAGAGCAAGAGAGGCATCCT 3’

Reverse 5’ GTTGAAGGTCTCAAACATGAT 3’

NCX1: Forward 5’ CTACCACGCAGCCAATGGGG 3’

Reverse 5’ TGCAAAGATGGCCCTGCCTC 3’

PCR reactions were initiated with a hot start at 95 °C for 15 min followed by 40 cycles of 94°C for 15 s, 59 °C for 30 s and 72 °C for 45 s. Amplicons were separated by electrophoresis on a 1% agarose/1X TAE gel and DNA bands were visualized with ethidium bromide. Resolved amplicons were cut out and extracted using the Qiagen gel extraction kit (Qiagen, Toronto, Ontario). Extracted amplicons were sequenced at the University of Calgary sequencing facility.

2.4 Co-immunoprecipitation and western blotting

Ea.Hy926 cell lysates were collected in lysis buffer (containing in mM: 20 Tris-HCl (pH 7.5), 138 NaCl, 3 KCl, 1 EGTA, 2 EDTA, 1 benzamidine, and 5 μg/mL aprotinin, 5 μg/mL leupeptin, 5 μg/mL pepstatin) containing 1% (v/v) Triton-X100. The crude lysates were centrifuged at 13,000 rpm for 10 minutes to remove insoluble material. Cell lysates undergoing co-immunoprecipation were incubated in 5 μg of R3F1 or caveolin-1 antibody for each mg of protein overnight at 4 °C. Protein G- Sepharose beads (Amersham, Mississauga, ON, Canada) were washed 2x in lysis buffer and re-suspended in lysis buffer in 50:50 proportion. 100 μL of the bead slurry were added to each immunoprecipitation reaction. After 8 h of incubation at 4 °C, beads were spun down at 13,000 rpm for 10 minutes, and washed 2x with lysis buffer. Beads bound with immunoprecipitates were heated for 10 min at 95 °C in 2x SDS sample buffer (124 mM Tris-HCl pH 6.8, 20% glycerol, 4% SDS, 0.005% Bromophenol Blue) containing dithiothretol DTT (2.5 mM) prior to separation by sodium dodecyl sulfate-polyacrylamide gel electrophoresis (SDS-PAGE; 10%). Proteins were transferred to 0.2 μm nitrocellulose membranes (BioRad) at 100 V at 4 °C for 1.5 h in transfer buffer containing in mM: 25 Tris-HCl, 192 glycine, 1% SDS and 20% methanol. Nitrocellulose membrane was blocked with 5% non-fat dry milk (NFDM) in 0.1% Tween-20 PBS (PBST; composition in mM: 137 NaCl, 3 KCl, 10 Na_2HPO_4, 1.73 NaH_2PO_4, 0.1% Tween v/v) prior to incubation with primary antibody in 1% NFDM overnight at 4 °C (rabbit anti-TRPC1: 1:500, rabbit anti-TRPC4: 1:500, mouse anti-caveolin1: 1:1000, mouse R3F1 anti-NCX: 1:5000).

TRPC1 and C4 proteins were detected by standard western blotting; membranes were washed with PBST after primary antibody treatment, and then treated with secondary antibodies for 1 h at 20-22 °C (goat anti-rabbit HRP, 1:20,000). Caveolin-1 and NCX1 proteins were detected using a high-sensitivity three-step western blotting method, as described previously (Takeya *et al.*, 2008; Johnson *et al.*, 2009). In this case, membranes were washed after primary antibody treatment and then treated with biotin-conjugated anti-mouse antibody (1:40,000) followed by strepavidin-HRP treatment (1:100,000) for 30 min at 20-22 °C. Membranes were then treated with the Amersham ECL advanced western blotting detection kit (GE Healthcare, Mississauga, ON, Canada). The emitted light was detected and quantified with a chemiluminescence imaging analyzer (LAS3000 Mini; Fujifilm Canada, Mississauga, ON, Canada) and images were analyzed with MultiGauge v3.0 software (Fujifilm Canada).

2.5 Phospho-eNOS analysis of Ea.Hy926 cells

Ea.Hy926 cells were washed 2X in PSS, and subjected to six different treatments: 1) PSS treatment, 2) 10 μM histamine, 3) 10 μM histamine + 0 Ca^{2+}, 4) 1 μM A23187, 5) 30 μM SKF + 10 μM histamine and 6) 10 μM KBR+10 μM histamine. Lysis buffer was added to treated cells (containing in mM: 20 Tris-HCl (pH 7.5), 138 NaCl, 3 KCl, 1 EGTA, 2 EDTA, 1 benzamidine, 1 DTT, and 5 μg/mL aprotinin, 5 μg/mL leupeptin, 5 μg/mL pepstatin) containing 1% Triton-X100. Protein samples were prepared by combining cell lysates with 4X SDS sample buffer containing DTT and β-mercaptoethanol and heated for 1 h at 50 °C. Samples were loaded onto an 8 % SDS-PAGE gel and electrophoresed

initially at 70 V and then resolved at 170 V. Proteins were transferred to 0.2 μm nitrocellulose membranes (BioRad) at 100 V at 4 °C for 2 h in transfer buffer containing in mM: 25 Tris-HCl, 192 glycine, 1% SDS and 20% methanol. Nitrocellulose membranes were blocked with 5% NFDM in 0.1% Tween-20 TBST (TBST; composition in mM: 137 NaCl, 3 KCl, 20 Tris-HCl pH 7.5, 0.1% Tween v/v) followed by incubation with primary antibody in 0.1% TBST overnight at 4 °C (mouse anti-eNOS: 1:500, mouse anti-phospho S1177-eNOS: 1:1000, rabbit anti-actin 1:2000). Membranes were washed with 0.1% TBST + 1% NFDM after primary antibody treatment, and then treated with secondary antibodies for 1 h at 20-22 °C (for eNOS and phospho S1177-eNOS detection: goat anti-mouse HRP, 1:10,000; for actin detection: goat anti-rabbit HRP, 1:40,000). Signal detection was carried out as described in the previous section.

2.6 Immunocytochemistry and proximity ligation assay

Ea.Hy926 cells were washed 3x with PBS and fixed with 3% paraformaldehyde (in PBS) for 10 min. 100 mM glycine treatment of 5 min quenched the fixative. Permeabilization was carried out in PBS solution containing 0.1% Triton-X100 for 15 min. Cells were subjected to 45 min block in TBST containing 4% NFDM and then incubated with primary antibodies in pairing of interest for 2 h at room temperature (1:50 rabbit anti-TRPC1 and 1:150 mouse anti-NCX1 or 1:100 rabbit anti-STIM1 and 1:150 mouse anti-NCX1).

Proximity ligation assay was carried out following 2 h primary antibody incubation at room temperature. Cells were incubated in blocking solution containing a pair of mouse anti-PLUS and rabbit anti-MINUS oligonucleotide-

tagged secondary antibodies (1:5 dilution) for 2 h at 37 °C. The hybridized oligonucleotides were then ligated prior to rolling circle amplification. The concatemeric amplification products extending from the oligonucleotide arm of the PLA probes were then detected using red fluorescent fluorophore-tagged complementary oligonucleotide sequences. Images were taken at 0.25 μm intervals in the z-plane to sample the distribution of the PLA products. In experiments where comparisons in signal between two parallel PLA experiments were carried out, puncta were counted manually.

2.7 Immunohistochemistry and proximity ligation assay (PLA)

Rat middle cerebral arteries from Sprague-Dawley rats were fixed in 4% PFA in 0.1 M phosphate buffer (PB) for 1.5 hours, washed 2 x 10 minutes in PB containing 0.5% Triton-X100 then permeabilized for 1.5 h in PB containing 0.5% Triton-X100. Blocking step was carried out with the Duolink custom blocking solution with 0.5% Triton-X100 for 1 h, then incubated overnight at 4 °C in primary antibody in 0.2% Tween in PB (1:100 goat anti-PECAM with 1:50 rabbit anti-TRPC1 and 1:150 mouse anti-NCX1; 1:100 rabbit TRPV4 and 1:150 mouse anti-NCX1; 1:100 mouse anti-caveolin1 and 1:100 rabbit anti-eNOS). This was followed by proximity ligation assay using a pair of mouse anti-PLUS and rabbit anti-MINUS oligonucleotide-tagged secondary antibodies using the protocol outlined by the manufacturer and described in Chapter 2.6. Following PLA assay, RMCAs were incubated in a donkey anti-goat Alexa fluor-488 for 1 h at room temperature in 0.2% Tween in PB for detection of PECAM-1. Subsequent detection of PLA products was carried out on Zeiss Axioimager with attached

apotome in the laboratory of Dr. Ray Turner (Hotchkiss Brain Institute, University of Calgary) with the assistance of Ms. Mirna Kruskic. An Apotome microscope was equipped with LED modules (Colibri): 365, 470 and 590 nm; and a white light source Illuminator HXP120 and filtersets equipped to image DAPI, GFP and Cy3. Cy3-based dye (PLA signal) was excited at 545/25 nm and emission was collected at 605/70 nm, Alexa-488 was excited at 470/40 nm and emission was collected at 525/50 nm, and DAPI was excited at 365 nm and emission was collected at 445/450 nm. Images were taken with a 63x oil immersion lens with numerical aperture of 1.4. PLA experiments utilizing caveolin-1 and eNOS primary antibody pairs (mouse anti-caveolin-1 1:100 and 1:100 rabbit anti-eNOS) were carried out as a positive control. As a negative control, single NCX1 primary antibody (1:150) was employed followed by PLA. Image slices of 0.25 μm in the z-plane were taken and exposure was limited to reduce photo-bleaching.

2.8 Intact arterial vessel pressure myography

Male Sprague-Dawley rats (250-300g, Charles River) were maintained and killed by halothane inhalation and exsanguination according to the standards of the Canadian Council on Animal Care and the Animal Care Committee of the Faculty of Medicine, University of Calgary. Whole brain was carefully removed and placed in cold Krebs' buffer (in mM: NaCl 120, $NaHCO_3$ 25, KCl 4.8, NaH_2PO_4 1.2, glucose 11, $CaCl_2$ 1.8) bubbled with 95% air and 5% CO2. Subcerebellar and posterior cerebral arteries from left and right hemispheres were dissected and used for pressure myography. After mounting on a pressure myograph, vessels were allowed to equilibrate for 15 min and then the

temperature was raised to 37 °C. After 30 min temperature equilibration, vessels were subjected to a pressure step from 0 to 60 mmHg. Only leak-free vessels that exhibited active constriction of > 40 μm due to spontaneous tone development within 30 min at 60 mmHg were used. Tissues were further primed with 2 x 5-min 80 mmHg steps to ensure stable development of a myogenic response.

2.9 Measurement of flow-mediated dilation

An open-system pressure myography was used to ensure maintenance of luminal pressure while changing flow rate. Two pressure transducers were connected to the pressure servo control and the flow pump, respectively, measuring the pressure on either side of the artery. The flow pump was calibrated manually by measuring the amount of liquid that passed through the pump in 10 min at the highest flow rate and back-calculated for each incremental increase in flow rate. The luminal pressure was approximated as the mean pressure between the two pressure transducers. Flow rate for the pump was manually calculated, and the optimal flow rate for our tissue was calculated using the following equation:

$$SS = \frac{4 \times \eta \times Q \times 10^9}{\pi r^3}$$

where SS is shear stress, η is viscosity in Poise (dyne s/cm^2) at 37 °C, Q is flow rate (μL/s), and *r* is artery radius (μm) (Kang *et al.*, 2008; Luksha *et al.*, 2011). Viscosity of the physiologic NaCl solution was 0.7 cP (Kang *et al.*, 2008). The factor of 10^9 in the equation is to correct for the use of both μL/s for flow and μm for arterial radius (1 μL is equivalent to 10^9 μm^3). Flow-induced changes in

arterial diameter were calculated from the established baseline diameter in the presence of intraluminal pressure of either 60 or 80 mmHg. Differences between the diameter before and after application of flow represented the magnitude of flow-mediated dilation.

2.10 Protein densitometric measurement from tissue samples

Rat cerebral arteries (RCA) were subjected to 60 mmHg of pressure until tone development. Two 5-min 80 mmHg-priming steps were evoked to ensure robust contractile response of the vessel. Only vessels exhibiting greater than 40 μm of constriction were collected for biochemical analysis to reduce variability. Arteries were collected in 5 conditions: 60 mmHg + no flow, 60 mmHg + flow, 60 mmHg + flow + C2C12 anti-NCX1 antibody, 60 mmHg + flow + KBR, and 60 mmH + flow + 6H2 anti-NCX1. Arteries were flash-frozen in an ice-cold mixture of 10% trichloroacetic acid (TCA) and 10 mM dithiothreitol (DTT) in acetone for 15 min. Arteries were washed in ice-cold acetone containing 10 mM DTT and lyophilized overnight. Prior to protein extraction, the cannulated ends of the vessels were dissected from the lyophilized vessel segment and discarded to eliminate tissue that was not subjected to the test pressures. For protein extraction, 35 μl of sample buffer (4% SDS, 100 mM DTT, 10% glycerol, 0.01% bromophenol blue, 60 mM Tris-HCl, pH 6.8) was added to 5 pooled cerebral vessels (~0.5 mm each in length) per experimental group. Samples were heated at 95 °C for 10 min and rotated end-over-end overnight at 4°C prior to electrophoresis.

2.11 Detection of phospho-S1177 and pan eNOS in RCA

Eight percent SDS-PAGE gels were used to resolve protein samples. Proteins were transferred to nitrocellulose membranes (0.2 μm pore size, Bio-Rad) at 100 V for 2 h at 4 °C in transfer buffer containing in mM: 25 Tris-HCl, 192 glycine, 1% SDS and 20% methanol. Membranes were stained with Ponceau-S for 5 min to ensure successful transfer of protein and then washed with water to remove the Ponceau stain. Membranes were blocked in 3% BSA in 0.05% TBST for 2 hours. Membranes were first probed with mouse monoclonal phospho-S1177 eNOS antibody (1:1000 dilution in 0.05% TBST, overnight at 4 °C). After 2 x TBST washes, membranes were incubated in 1:20,000 goat anti-mouse biotin for 1 h at room temperature. Secondary antibody was washed out with 2 x 5 minutes TBST and membrane was incubated in streptavidin-linked HRP (1:100,000). Membranes were washed twice more prior to development with ECL detection reagent (Amersham). Membrane was washed in water and re-blocked with 3% BSA prior to re-probing with monoclonal mouse pan-eNOS antibody (1:500 in TBST overnight at 4 °C). After 2 x TBST washes membranes were incubated in 1:20,000 goat anti-mouse biotin for 1 h at room temperature. Secondary antibody was washed out with 2 x 5 min TBST and membrane was incubated in streptavidin-linked HRP (1:100,000). Membranes were washed twice more prior to development with ECL detection reagent (Amersham). The emitted light was detected and quantified with a chemiluminescence imaging analyzer (LAS3000 Mini; Fujifilm Canada, Mississauga, ON, Canada) and images were analyzed with MultiGauge v3.0 software (Fujifilm Canada).

2.12 Materials

All drugs were obtained from Sigma Aldrich (St. Louis, MO) with the exception of KB-R7943 and RN1734 (Tocris, Ellisville, MO). Biochemical reagents were obtained from BioRad (Mississauga, Ontario, Canada). Rabbit TRPC1 and TRPC4 antibodies were from Alomone (Jerusalem, Israel), mouse monoclonal caveolin-1 antibody, eNOS antibody, phospho S1177-eNOS antibody were from BD Biosciences (Mississauga, Ontario, Canada), PECAM1 antibody was from Santa Cruz **(**Dallas, Texas**),** mouse 6H2 NCX1 antibody was from Novusbio (Oakville, Ontario), mouse C2C12 NCX1 antibody was from Abcam (Toronto, Canada) and mouse R3F1 monoclonal NCX1 antibody was generously provided by Dr. Jonathan Lytton (University of Calgary).

2.13 Data Analysis

Data are shown as mean ± SEM. Statistical analysis was carried out using Prism4 software. Statistical significance of differences in mean values was assessed by unpaired Student's t-test for single comparisons and ANOVA followed by Bonferroni's post-hoc test for multiple comparisons.

Chapter 3: Presence of a TRPC1-NCX1 signaling complex in cultured ECs

3.1 Introduction

3.1.1 Overview

The endothelium is considered to be a key determinant of vascular health. Appropriate release of NO from ECs is critical for normal physiological functioning of the cardiovascular system. NO is a principal mediator of all endothelial protective effects and contributes to blood pressure regulation through its ability to induce smooth muscle relaxation and arterial dilation. While the mechanisms that regulate NO production and release are not clearly understood, some aspects of the mechanisms are clearly established, such as the role played by increased $[Ca^{2+}]_i$ in the activation of eNOS (Singer & Peach, 1982; Luckhoff *et al.*, 1988; Forstermann *et al.*, 1991; Kruse *et al.*, 1994).

3.1.2 Molecular entity underlying Ca^{2+} influx in ECs

Early experiments carried out in cultured ECs showed that bradykinin, acetylcholine, and purinergic stimulation leads to a rapid, transient increase in $[Ca^{2+}]_i$ followed by a sustained plateau response; the sustained $[Ca^{2+}]_i$ was inhibited in the absence of extracellular Ca^{2+} and in the presence of lanthanum, a putative blocker of SOC (Colden-Stanfield *et al.*, 1987; Viana *et al.*, 1998). These data suggest Ca^{2+} influx occurs downstream of agonist stimulation and contributes to the resulting increase in $[Ca^{2+}]_i$. Agonist-induced Ca^{2+} influx in ECs has been largely attributed to ROC and SOC mechanisms since ECs do not consistently express VGCC as detected in excitable cells (Chapter 1.8.4).

Although Ca^{2+} influx has been shown to play an important role in the regulation of EC functions, the molecular identity of the Ca^{2+} entry channel has remained elusive. It was not until the identification of transient receptor potential (TRP) channel proteins in the phototransduction pathway of *Drosophila* that TRP channels became widely viewed as molecular candidates for facilitating Ca^{2+} entry in ECs (Nilius & Droogmans, 2001; Dietrich & Gudermann, 2011; Vennekens, 2011). Both native and cultured ECs express a range of TRP channel proteins, including TRPCs, TRPVs, TRPA1 and TRPMs (Vennekens, 2011). Some of these proteins have been implicated in SOC- and ROC-mediated Ca^{2+} entry. For example, TRPC1 and C4 as homo- and/or heterotetrameric channels alone, or associated with STIM1 and/or Orai1, have been implicated as potential SOCs in ECs (Tiruppathi *et al.*, 2002; Ahmmed *et al.*, 2004; Kwiatek *et al.*, 2006; Singh *et al.*, 2007; Pani *et al.*, 2009; Sundivakkam *et al.*, 2009; Sundivakkam *et al.*, 2012). On the other hand, TRPC1 (Mehta *et al.*, 2003; Ahmmed *et al.*, 2004; Hicks *et al.*, 2010) and TRPC6 (Hicks *et al.*, 2010; Singh *et al.*, 2007) have been reported to be putative ROCs.

With the exception of TRPV5 and V6, that are highly Ca^{2+} selective, and TRPM4 and M5 that are Ca^{2+}-impermeant, TRP channels are non-selective for mono- and divalent cations with permeability ratios for Ca^{2+} and Na^{+} varying from 1 to 5 when expressed as either homo- or heteromultimeric channels (Owsianik *et al.*, 2006). Several labs have shown activation of NSCC current (I_{NSCC}), attributed to TRP subunit-containing channels, occurs downstream of agonist stimulation (e.g. bradykinin, histamine, ATP, acetylcholine and thrombin)

(reviewed in Nilius *et al.*, 2001; Girardin *et al.*, 2010; Ma *et al.*, 2011b). These currents were inhibited by removal of external Na^+ (Girardin *et al.*, 2010; Ma *et al.*, 2011b), indicating a significant contribution of Na^+ in mediating this inward current.

3.1.3 Localized Ca^{2+} signaling and microdomains

Ca^{2+} is an ubiquitous, multi-functional signaling ion in the cell that is tightly regulated, both spatially and temporally. The precise spatial locations of Ca^{2+} signals have been suggested to facilitate localized increase in $[Ca^{2+}]_i$ in signaling microdomains within the cell without bulk increase in cytosolic $[Ca^{2+}]_i$. These Ca^{2+} "hotspots" have been shown to be present in ECs (Isshiki *et al.*, 1998; Isshiki *et al.*, 2002a; Isshiki *et al.*, 2004; Murata *et al.*, 2007; Bagher *et al.*, 2012; Senadheera *et al.*, 2012; Sonkusare *et al.*, 2012) and are associated with the appropriate regulation of NO synthesis and coordination of endothelium-dependent vasodilation.

Caveolae are omega-shaped invaginations of the plasma membrane that are rich in cholesterol and sphingolipids and have been shown to play an important role in the regulation of Ca^{2+} entry in ECs (Isshiki *et al.*, 2002a; Isshiki *et al.*, 2004; Murata *et al.*, 2007). Using a caveolae-targeted protein Ca^{2+} sensor, $[Ca^{2+}]_i$ within the caveolar region was measured to be higher than the bulk $[Ca^{2+}]_i$ in response to ATP stimulation. Moreover, Ca^{2+} entry in this domain was associated with the activation of eNOS (Isshiki *et al.*, 2002a). The generation of localized Ca^{2+} signaling within the caveolae is likely due to strategic positioning of Ca^{2+} channels and transporters in this region. For example, TRPC1 and 4

subunit-containing channels have been shown to localize within caveolae (Murata *et al.*, 2007). TRPC1 and C3 have also been suggested to be targeted to caveolae, and TRPC1- and C3-mediated Ca^{2+} entry was disrupted upon membrane cholesterol depletion by cyclodextrin (Lockwich *et al.*, 2001; Bergdahl *et al.*, 2003). These findings suggest TRPC channels are located within the caveolar signaling hotspots. Moreover, as alluded to in Chapter 1.7.1, targeting of eNOS to caveolae is important for its functionality. For instance, eNOS localization in ECs was evaluated by a subcellular fractionation technique and eNOS was found to be located in the same fraction as caveolin-1, indicating its presence in caveolae (Shaul *et al.*, 1996). In the same study, this group showed that eNOS activity was 7-fold greater in the PM fraction than in cytosol, and eNOS activity was 9- to 10-fold greater in caveolae membranes compared to the whole PM (Shaul *et al.*, 1996). Thus, caveolae are not only important sites for Ca^{2+} signaling, but also functionally important in the regulation of eNOS activity.

Certain proteins in the caveolar hotspot have been reported to directly interact (protein-protein interaction) with each other, such as interaction of eNOS with caveolin-1, and caveolin-1 with TRPC1, through functional mapping using recombinant proteins and yeast 2-hybrid analysis (Tiruppathi *et al.*, 2002; Ahmmed *et al.*, 2004; Kwiatek *et al.*, 2006; Singh *et al.*, 2007; Pani *et al.*, 2009; Sundivakkam *et al.*, 2009; Sundivakkam *et al.*, 2012). However, direct protein-protein interaction is not a pre-requisite for the generation of signaling microdomains and localized Ca^{2+} responses. Two proteins can interact spatially, as indicated by co-localization, without directly interacting or binding to each

other. For example, IP_3R and IK_{Ca}, which are not known to directly interact with each other, have been reported to be co-localized within the IEL of intact mesenteric arteries; the spatial proximity between these two proteins is believed to facilitate activation of IK_{Ca} through IP_3R-mediated generation of localized Ca^{2+} signals (Ledoux *et al.*, 2008). Microdomain signaling can thus be viewed as a method by which the cell concentrates signaling molecules within a confined space to facilitate efficient transduction of extracellular signals into cellular responses.

3.1.4 NCX activity reversal

As mentioned in Chapter 1.8.2, the view that NCX is an important Ca^{2+} entry pathway is substantiated by findings from SMCs where the unique ultrastructure of the PM and ER membranes and measurement of localized $[Na^+]_i$ owing to TRPC6-mediated Na^+ entry provided a functional basis for NCX activity reversal leading to Ca^{2+} influx and a rise in $[Ca^{2+}]_i$ (Dai *et al.*, 2005; Lemos *et al.*, 2007; Poburko *et al.*, 2007). A similar functional link between TRPC subunit-containing channels and NCX was observed in HEK cells over-expressing TRPC3; carbachol-induced Ca^{2+} influx in TRPC3 over-expressing HEK cells was inhibited by KBR, a reverse-mode NCX blocker (Rosker *et al.*, 2004). Moreover, sucrose fractionation experiments revealed NCX1 to be present in the same fraction as caveolin-1 and TRPC3, and further analysis indicated TRPC3 and NCX1 co-immunoprecipitate (Rosker *et al.*, 2004). A similar observation was made using cardiomyocytes, where NCX-mediated Ca^{2+} entry depended on TRPC3-induced $[Na^+]_i$ elevation (Rosker *et al.*, 2004; Eder *et al.*, 2007). Co-

localization and co-immunoprecipitation of TRPC3 and NCX1 was also detected in protein lysates of cardiomyocytes (Rosker *et al.*, 2004; Eder *et al.*, 2007). These data combined suggest close apposition of TRPC subunit- containing channels and NCX1 within the same signaling complex is necessary to facilitate activation of reverse NCX.

3.1.5 Evidence of Na^+ entry and reversal of NCX activity in ECs

While the NCX-mediated Ca^{2+} entry has not been extensively studied in ECs, reports of increased Ca^{2+} entry in ECs maintained in conditions of reduced extracellular Na^+ concentration ($[Na^+]_o$), or cytosolic Na^+-loading due to monensin or ouabain treatment, have fostered the view that Na^+ influx through TRP channels may indirectly contribute to sustained elevations in $[Ca^{2+}]_i$ by influencing NCX activity (Sedova & Blatter, 1999; Teubl *et al.*, 1999; Schneider *et al.*, 2002). KBR and Ni^{2+}, putative blockers of NCX, have also been shown to selectively inhibit the outward component of the histamine-induced I_{NSCC} in human umbilical vein ECs, which suggests that NCX is activated during histamine stimulation (Girardin *et al.*, 2010). These data are consistent with the view that NCX can function as a Ca^{2+} influx mechanism. However, evidence that a TRPC-NCX signaling complex is present in EC, where it contributes to the regulation of Ca^{2+}, is lacking.

3.1.6 Hypothesis

We hypothesize that NCX-mediated Ca^{2+} entry during agonist stimulation contributes to maintenance of $[Ca^{2+}]_i$ in ECs and that the activation of reverse-mode NCX depends on the presence of a TRPC-NCX signaling complex.

3.1.7 Objective of the Study

The three main objectives in this chapter are:

1) To examine the contribution of NSCC and NCX to agonist-evoked $[Ca^{2+}]_i$ elevation and/or Ca^{2+}-dependent eNOS phosphorylation in cultured human umbilical Ea.Hy926 cells.

2) To test for the presence of TRPC-NCX1 interaction through co-immunoprecipitation of NCX with TRPC1 and TRPC4, as well as NCX, TRPC1 and TRPC4 with caveolin-1, and NCX with STIM1 from Ea.Hy926 cell lysates

3) To evaluate spatial co-localization of TRPC1 and NCX, and STIM1 and NCX in Ea.Hy926 cells by proximity ligation *in situ* localization assay.

3.2 Methods

The details of the methodology employed in this chapter are detailed in Chapter 2. Briefly, Ea.Hy926 cells were loaded with fura-2 and measurement of $[Ca^{2+}]_i$ was carried out on a Nikon inverted microscope. RT-PCR was used for evaluating the presence of mRNA transcripts. The presence of a TRPC-NCX1 signaling complex was evaluated by co-immunoprecipitation and proximity ligation assay (PLA).

3.3 Results

3.3.1 Modulation of histamine-induced $[Ca^{2+}]_i$ response by SKF and KBR

Stimulation of cultured Ea.Hy926 cells with histamine (10 μM) elicited a sustained increase in $[Ca^{2+}]_i$ of consistent magnitude during repeated agonist exposure (Figure 3.1A). When SKF (30 μM), an inhibitor of NSCC, was applied prior to a second application of histamine in a double histamine stimulation

experiment, histamine-induced $[Ca^{2+}]_i$ was reduced by 61 ± 5% at 6 min post-stimulation compared to the initial agonist stimulation ($p < 0.05$; Figure 3.1B). In the presence of KBR (10 μM), an inhibitor of reverse-mode NCX, the $[Ca^{2+}]_i$ response to histamine was similarly suppressed, but the magnitude of reduction at 27 ± 3% was significantly smaller than that of SKF ($p < 0.05$; Figure 3.1C). The magnitude of reduction in the $[Ca^{2+}]_i$ response to histamine in the presence of SKF plus KBR at 76 ± 1% (Figure 3.1D) was not significantly different from that in SKF alone;

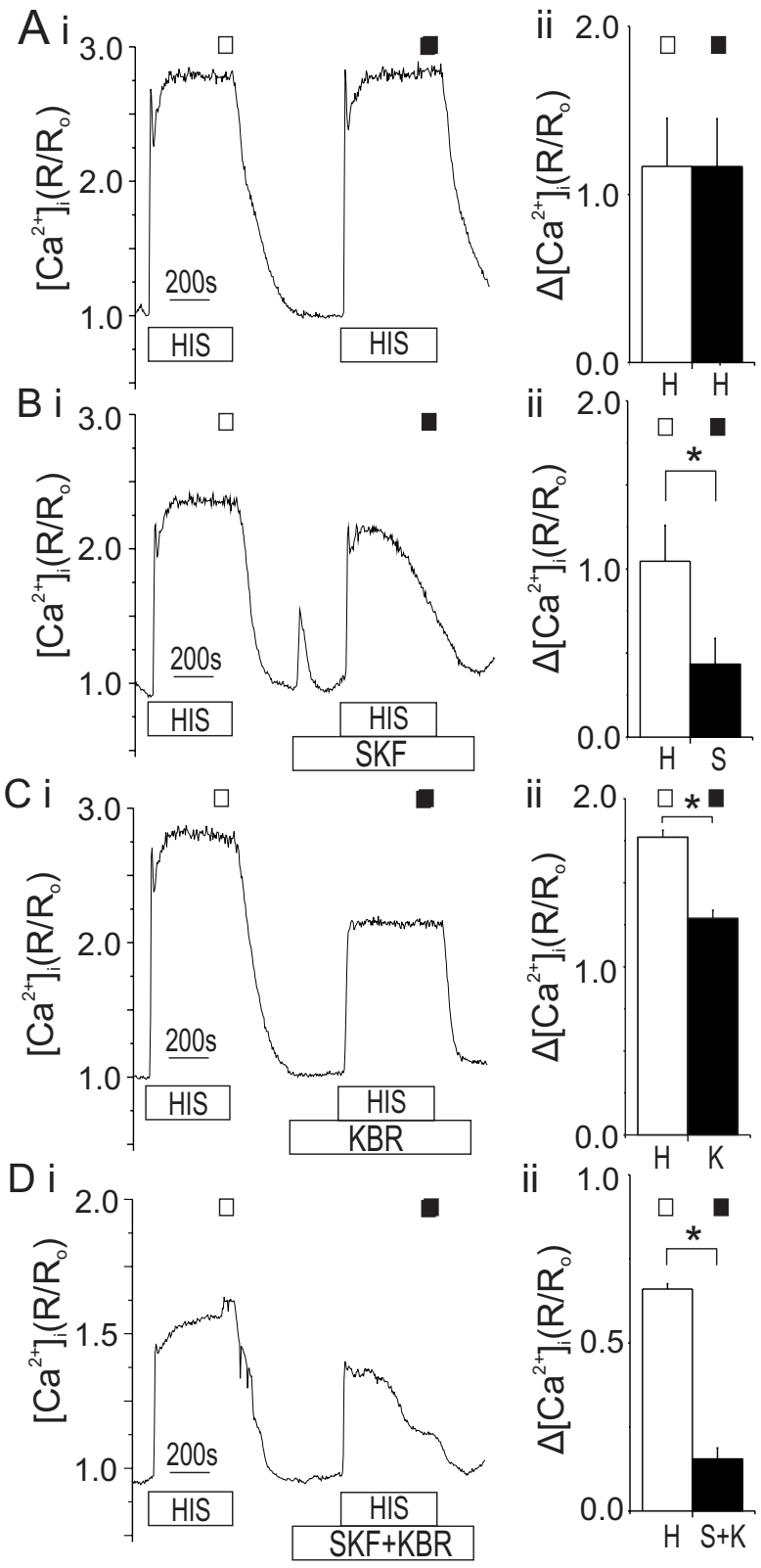
A i
ii
B i
ii
C i
ii
D i
ii
[Ca2+]i(R/Ro)
Δ[Ca2+]i(R/Ro)
200s
HIS
HIS
SKF
KBR
SKF+KBR
H
S
K
S+K
*

Figure 3.1: Effects of SKF and KBR on the histamine-induced $[Ca^{2+}]_i$ increase

A, Representative recording (i) and mean values ± SEM (ii) of histamine-induced increase in fluorescence associated with an increase in $[Ca^{2+}]_i$ measured from Ea.Hy926 cells under control condition of double stimulation with histamine (10 μM, n = 6 experiments). Here and in subsequent panels, changes in relative $[Ca^{2+}]_i$ are represented by changes in fura-2 ratio (R/R_o). B, Representative recording and mean values ± SEM of histamine-induced increase in $[Ca^{2+}]_i$ in control conditions and in the presence of SKF (30 μM, n = 7 experiments). C, Representative recording and mean values ± SEM of histamine-induced increase in $[Ca^{2+}]_i$ following pre-treatment with KBR (10 μM, n = 4 experiments). D, Representative recording and mean values ± SEM of histamine-induced increase in $[Ca^{2+}]_i$ following pre-treatment with SKF and KBR (30 μM + 10 μM, n = 5 experiments). *, $p < 0.05$, open and closed squares indicate the time point where measurements were taken for mean value calculations in the absence and presence of inhibitors, respectively.

i.e. the effects of SKF and KBR were not additive. The distinct, non-additive effects of SKF and KBR suggested that the drugs were likely interacting with different targets in the same signaling pathway for agonist-dependent regulation of $[Ca^{2+}]_i$ in Ea.Hy296 cells.

To better assess whether the observed histamine-induced $[Ca^{2+}]_i$ response was due to ER release or Ca^{2+} influx, histamine stimulation was carried out in the absence of extracellular Ca^{2+} (0 Ca^{2+}) followed by Ca^{2+} re-addition. Application of histamine in the absence of extracellular Ca^{2+} evoked a transient increase in $[Ca^{2+}]_i$ consistent with release from internal stores (Figure 3.2A). Re-addition of 1.5 mM Ca^{2+} to bath solution in the continued presence of histamine evoked a second, larger increase in $[Ca^{2+}]_i$ that was of similar magnitude during repeated applications of histamine (Figure 3.2A). Using the 0 Ca^{2+}-Ca^{2+} re-addition protocol, the increase in $[Ca^{2+}]_i$ on re-exposure to 1.5 mM Ca^{2+} was slightly reduced by SKF (19 ± 3%, Figure 3.2B), but in this case, KBR caused a significantly larger reduction in $[Ca^{2+}]_i$ during re-addition of 1.5 mM Ca^{2+} at 33 ± 3% of the initial histamine response compared to the effect of SKF ($p < 0.05$; Figure 3.2C). These data suggest that Na^+ loading during the 0 Ca^{2+} incubation reduced the impact of SKF, but not KBR, on Ca^{2+} influx. These data are consistent with the view that an increase in $[Ca^{2+}]_i$ in response to histamine was due in part to KBR-sensitive reverse-mode NCX activity facilitated by increased $[Na^+]_i$ owing to influx through SKF-sensitive TRP channels.

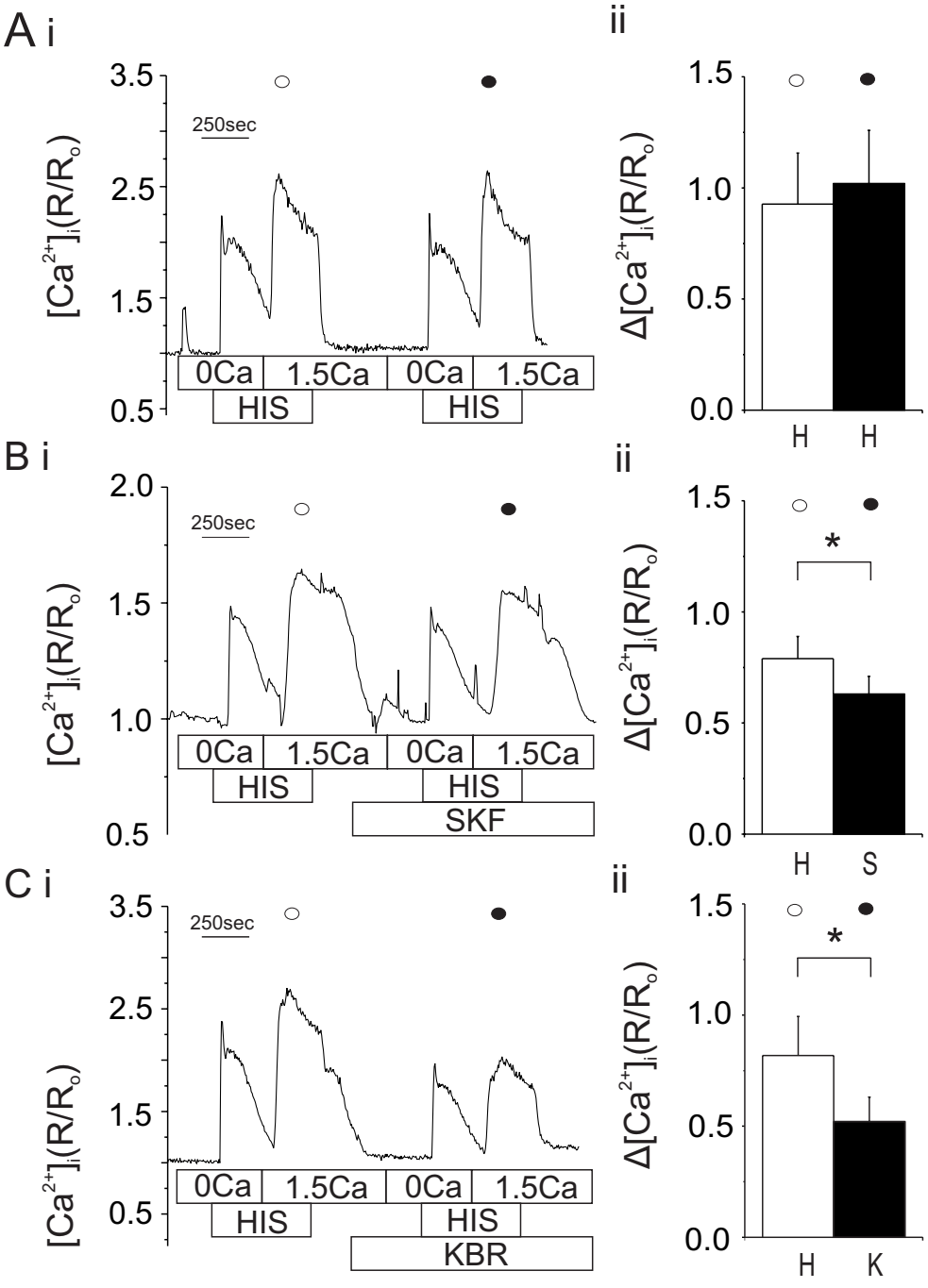

Figure 3.2: Effects of SKF and KBR on the histamine-induced $[Ca^{2+}]_i$ increase in 0 Ca^{2+}-Ca^{2+} re-addition protocol

A, Representative recording and mean values ± SEM of histamine-induced increase in fluorescence associated with an increase in $[Ca^{2+}]_i$ in Ea.hy926 cells

in 0 Ca^{2+} followed by Ca^{2+} re-addition, n = 5 experiments. B + C, Representative recording and mean values ± SEM showing the effect of SKF (30 μM, n = 9 experiments) and KBR (10 μM, n = 5 experiments) on histamine-induced increase in $[Ca^{2+}]_i$ in Ea.Hy926 cells using 0 Ca^{2+}-Ca^{2+} re-addition protocol. Paired-wise t-test was utilized (*, $p < 0.05$), open and closed circles indicate the time point where measurements were taken for mean value calculations in the absence and presence of inhibitors, respectively.

A difference in the response to SKF and KBR was also observed when the blockers were applied after the increase in $[Ca^{2+}]_i$ reached a stable maximum in histamine. SKF and KBR were perfused into the bath in the continued presence of histamine, 2 minutes after the initial application of histamine. In this case KBR treatment caused a significant, reversible decrease in $[Ca^{2+}]_i$ compared to the steady-state plateau level in control experiments (Figure 3.3A and 3.3B), whereas SKF had no effect when applied during histamine stimulation (Figure 3.3C).

3.3.2 Modulation of agonist-induced $[Ca^{2+}]_i$ response by NCX inhibition

KBR has been reported to exhibit non-specific interaction with other cellular proteins, including inhibition of TRPC channels (Kraft, 2007; Liang *et al.*, 2009). Although SEA0400 has been proposed to be a more selective and potent inhibitor for NCX, at the time of the present study, it was not commercially available. For this reason, an siRNA approach was employed to test the involvement of NCX in the histamine-induced $[Ca^{2+}]_i$ response. All the siRNAs used in the present study were confirmed to mediate knockdown by direct measurement of reduced protein content (Figure 3.4). Figure 3.5 shows that the $[Ca^{2+}]_i$ response to histamine was significantly reduced by suppression of NCX1-protein expression. Ea.hy926 cells were co-transfected with either scrambled control siRNA, or siRNA targeted against NCX1, and cDNA encoding GFP to allow for positive selection of transfected cells. The histamine-induced $[Ca^{2+}]_i$ response of GFP-positive cells transfected with NCX1 siRNA was sustained, but significantly reduced in amplitude compared to GFP-positive cells transfected

with scrambled siRNAs (Figure 3.5). Note the similar appearance of the $[Ca^{2+}]_i$ response in the presence of molecular NCX1 suppression versus pharmacological inhibition with KBR (Figure 3.1C) compared to control recordings.

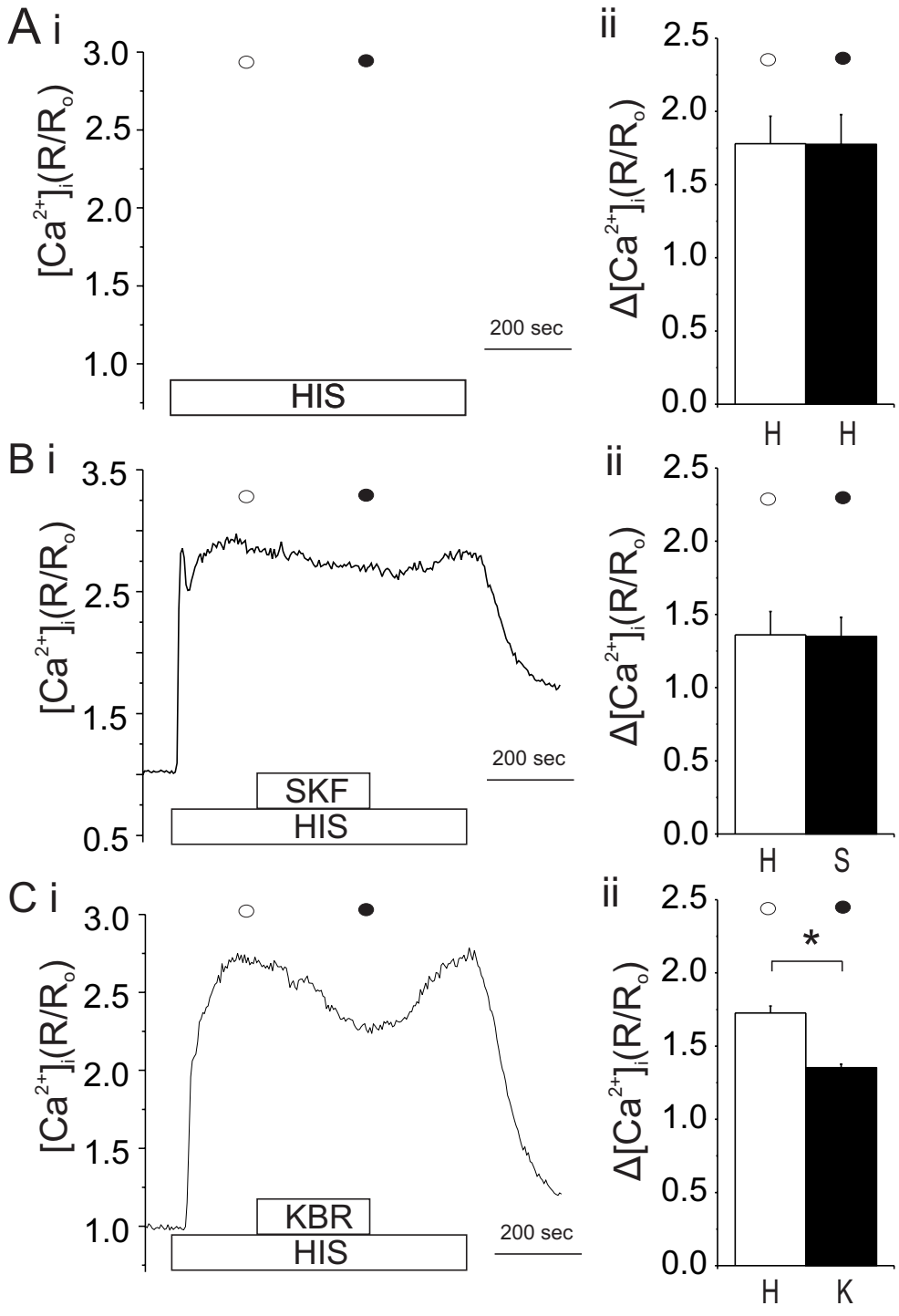
A i
ii
B i
ii
C i
ii
[Ca2+]i(R/Ro)
Δ[Ca2+]i(R/Ro)
200 sec
HIS
SKF
KBR
H
S
K
*

Figure 3.3: Effects of SKF and KBR on $[Ca^{2+}]_i$ when applied during histamine stimulation

A, Representative trace (i) and mean values ± SEM (ii) of histamine-induced increase in fluorescence associated with an increase in $[Ca^{2+}]_i$ measured from Ea.Hy926 cells in control condition, n = 4 experiments. B+C, Representative recording and mean values ± SEM of histamine-induced increase in $[Ca^{2+}]_i$ followed by application of SKF (30 μM, n = 4 experiments) and KBR (10 μM, n = 4 experiments) and subsequent drug washout after histamine-induced increase in $[Ca^{2+}]$ response reached a steady-state plateau. *, $p < 0.05$, open and closed circles indicate the time point where measurements were taken for calculation of mean value calculations in the absence and presence of inhibitors, respectively.

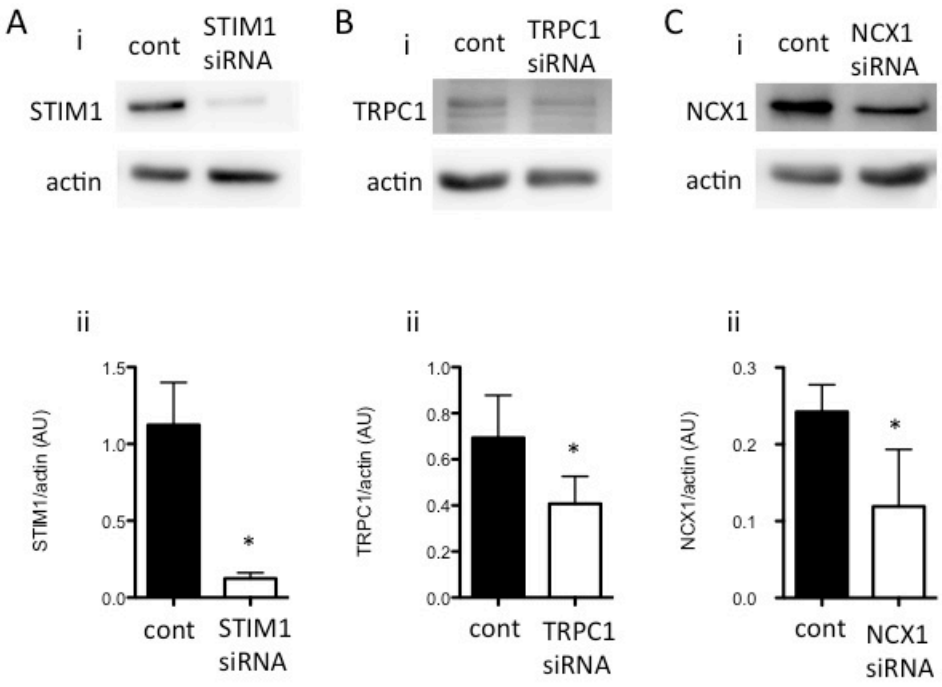

Figure 3.4: Protein expression is decreased by siRNA treatment.

Representative blots (i) and mean band intensity (ii) showing the effect of STIM1 siRNA (A), TRPC1 siRNA (B), and NCX1 siRNA (C). (*, $p<0.05$)

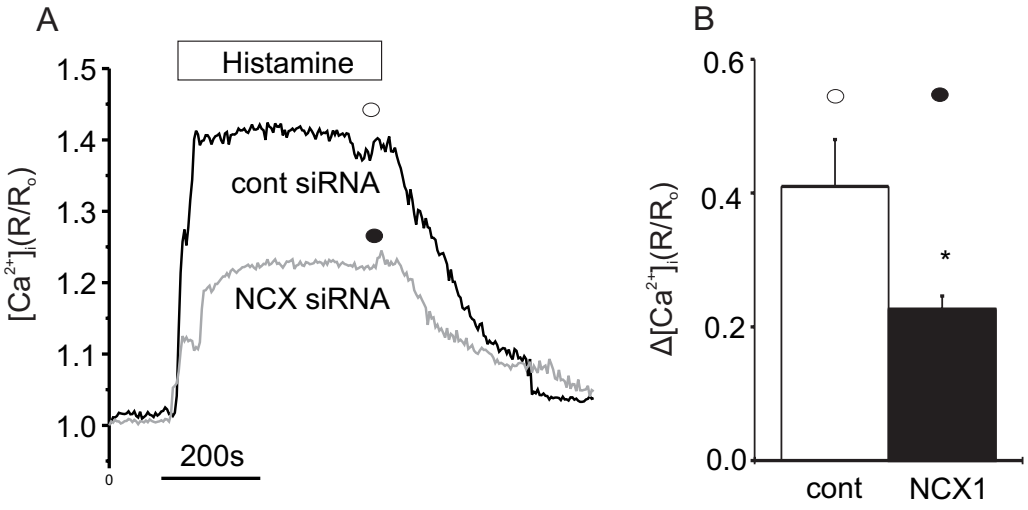

Figure 3.5: Effect of NCX siRNA on the histamine-induced $[Ca^{2+}]_i$ increase

A, Representative recording of single cell measurement of histamine-induced increase in fluorescence associated with an increase in $[Ca^{2+}]_i$ measured in GFP-positive Ea.Hy926 cells that were co-transfected with GFP and either scrambled control siRNA (black trace, n = 3 experiments) or NCX1 siRNA (gray trace, n = 5 experiments). B, Mean values ± SEM of $[Ca^{2+}]_i$ response indicate a significant reduction of histamine-induced $[Ca^{2+}]_i$ with NCX1 knockdown. *, $p < 0.05$, open and closed circles indicate the time point where measurements were taken for mean value calculations in control siRNA and NCX1 siRNA-treated cells, respectively.

To determine if the involvement of NCX in the regulation of $[Ca^{2+}]_i$ was limited to histamine, or a common signaling pathway for control of $[Ca^{2+}]_i$ by agonists in general, the effects of KBR and NCX knockdown on thrombin-induced changes in $[Ca^{2+}]_i$ were investigated. Thrombin at 1 U/ml was found to elicit a robust increase in $[Ca^{2+}]_i$, which was significantly reduced by KBR treatment (Figure 3.6A). Unlike histamine stimulation, the thrombin-induced $[Ca^{2+}]_i$ response did not reach a steady plateau, rather, thrombin induced a transient increase in $[Ca^{2+}]_i$, followed by an elevated, but slowly declining increase in $[Ca^{2+}]_i$ above the un-stimulated baseline (Figure 3.6A). For this reason, mean values for thrombin-induced $[Ca^{2+}]_i$ response were calculated based on the measurements taken at peak response value. Moreover, compared to control scrambled siRNA-transfected cells, the thrombin-induced increase in $[Ca^{2+}]_i$ was significantly reduced in NCX1 siRNA-transfected cells (Figure 3.6B).

To study the underlying mechanism involved in the activation of NCX in the regulation of agonist-evoked calcium responses, we hypothesized that STIM1 protein may be involved in the recruitment and activation of NCX. To first evaluate whether STIM1 is a likely candidate involved in the histamine-induced $[Ca^{2+}]_i$ response, STIM1 siRNA-transfected cells were used to assess the effect of STIM1 knockdown on histamine-induced changes in $[Ca^{2+}]_i$. Histamine-induced $[Ca^{2+}]_i$ response was measured from GFP-positive cells that were co-transfected with GFP and either STIM1 or control scrambled siRNAs. Significantly, a decrease in the magnitude of histamine-induced $[Ca^{2+}]_i$ was only detected in STIM1-knockdown cells (Figure 3.7).

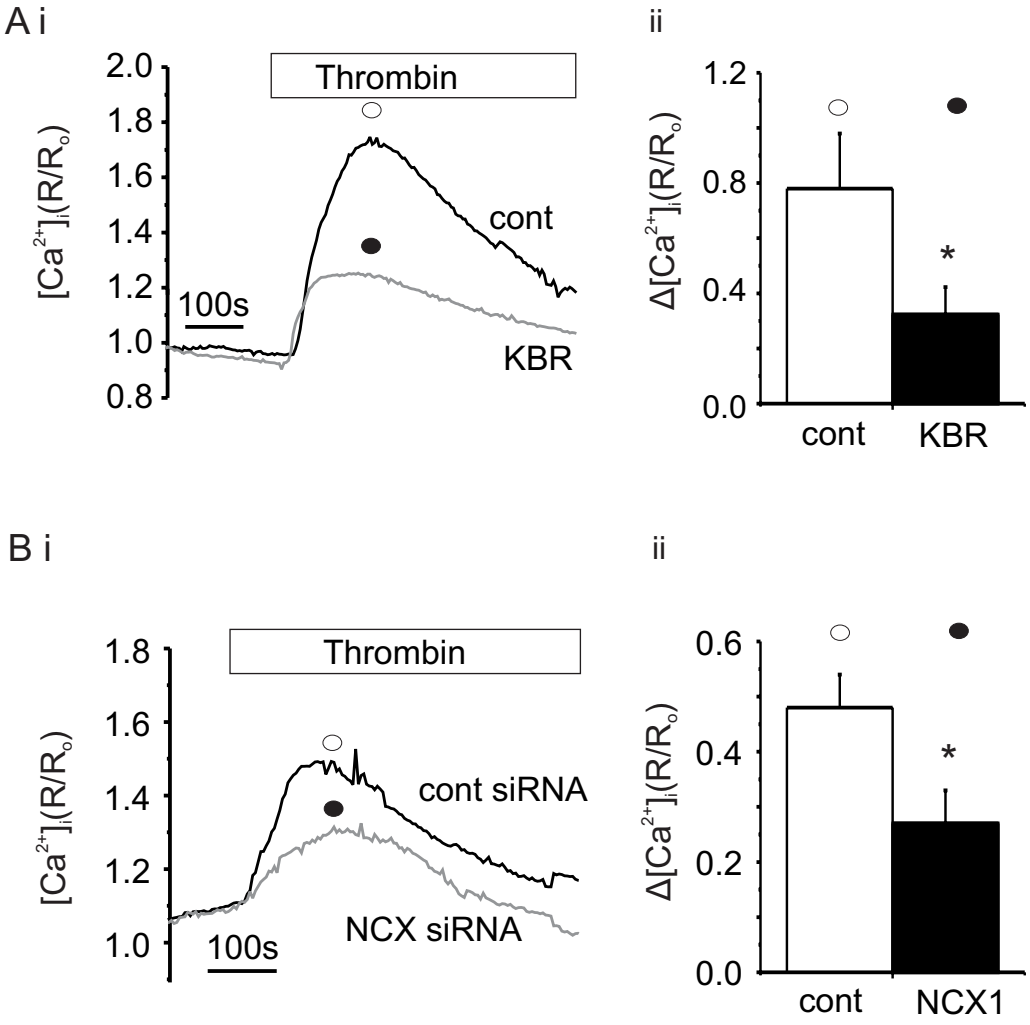

Figure 3.6: Effects of KBR and NCX siRNA on the thrombin-induced $[Ca^{2+}]_i$ increase

Representative trace (i) and mean data ± SEM (ii) showing the effect of thrombin-induced $[Ca^{2+}]_i$ elevation in the presence of (A) KBR treatment 5 min prior to addition of thrombin (n = 5 and 8 experiments for control and treated groups, respectively) and (B) siRNA silencing of NCX1 (n = 8 and 7 experiments for control and treated groups, respectively). Experiments were done in unpaired fashion with same day control. *, $p<0.05$, open and closed circles indicate the

time point where measurements were taken for statistics in control and KBR/NCX1 siRNA-treated cells, respectively.

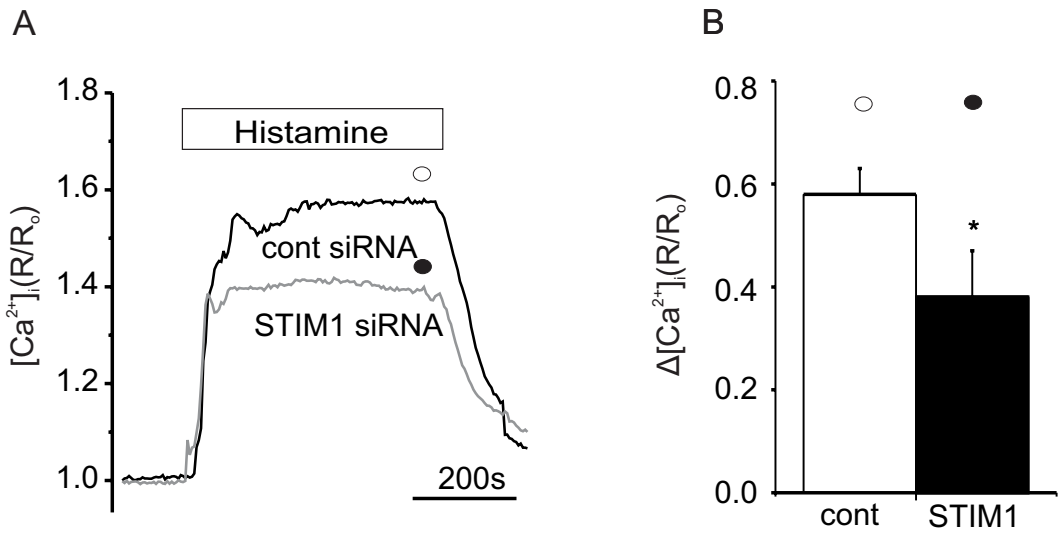

Figure 3.7: Effect of STIM1 siRNA on the histamine-induced $[Ca^{2+}]_i$ increase

A, Representative recording of single cell measurement of histamine-induced increase in fluorescence associated with an increase in $[Ca^{2+}]_i$ measured in GFP-positive Ea.Hy926 cells that were co-transfected with either scrambled control siRNA (black trace, n = 6 experiments) or STIM1 siRNA (gray trace, n = 6 experiments). B, Mean values ± SEM of $[Ca^{2+}]_i$ response indicate a significant reduction of histamine-induced $[Ca^{2+}]_i$ with STIM1 silencing. *, $p<0.05$, open and closed circles indicate the time point where measurements were taken for mean value calculations in control siRNA and STIM1 siRNA-treated cells, respectively.

3.3.3 Effects of KBR and SKF on the phosphorylation of eNOS at S1177

Phosphorylation of S1177 of eNOS (S1177-eNOS) has been extensively studied and shown to be sensitive to trans-membrane Ca^{2+} flux and $[Ca^{2+}]_i$ elevation (Fulton *et al.*, 2004). By detecting changes in the phosphorylation of S1177-eNOS, we aimed to evaluate if SKF- and KBR-sensitive Ca^{2+} pathways were important to the regulation of eNOS activity. Cultured ECs were incubated in either 1.8 mM Ca^{2+} PSS, zero Ca^{2+} PSS, SKF (30 μM), or KBR (10 μM) for 5 min prior to application of histamine (10 μM). Cell lysates were collected 5 min post-histamine stimulation. Stimulation of cultured ECs with histamine was associated with increased phosphorylation of S1177-eNOS. S1177-eNOS phosphorylation was 1.7-fold greater in the histamine-treated cells compared to the basal phosphorylation level detected in untreated cells (Figure 3.8). Histamine-induced phosphorylation at S1177-eNOS was completely inhibited by removal of extracellular Ca^{2+}. SKF and KBR both significantly reduced histamine-induced phosphorylation of S1177-eNOS. To further test the Ca^{2+}-dependency of phosphorylation of S1177, a Ca^{2+} ionophore, A23197, was used as a positive control and was shown to elicit a significant 2.1-fold increase in the phosphorylation at S1177-eNOS.

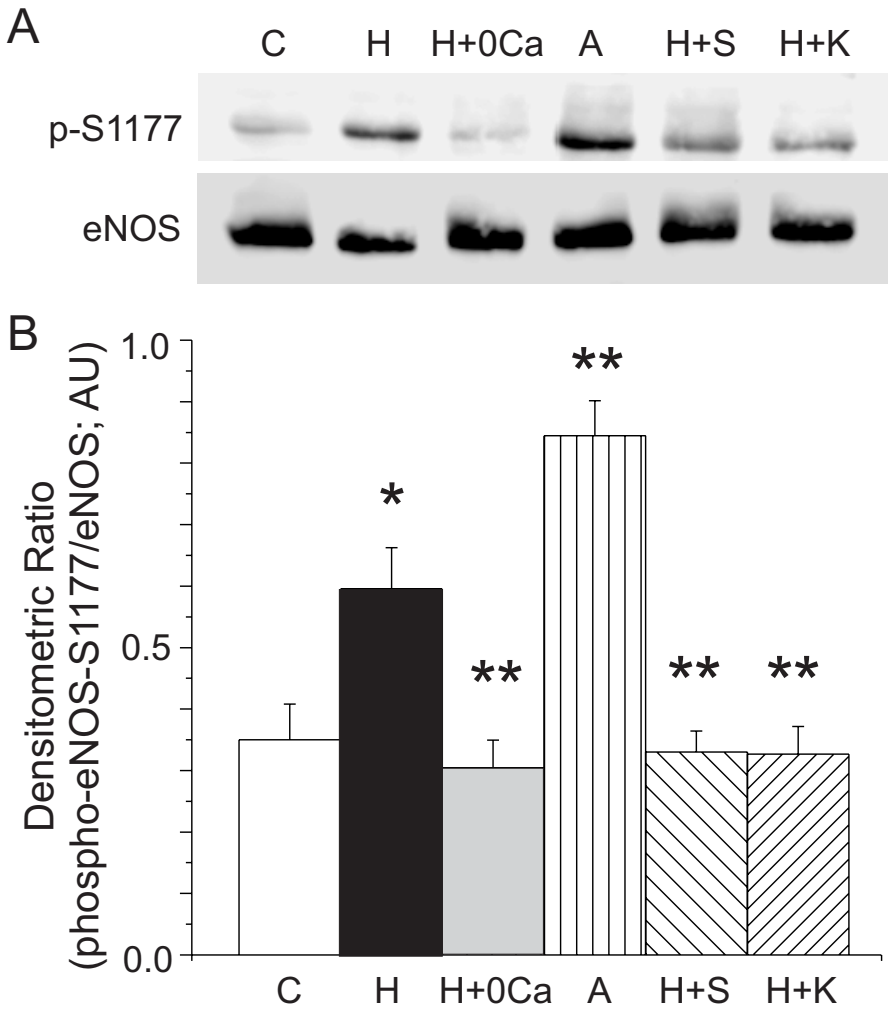

Figure 3.8: Histamine-induced phosphorylation of S1177-eNOS

A, Representative western blot of phospho S1177-eNOS (top panel) and eNOS (bottom panel) in control and in the presence of histamine (10 μM), 0 Ca^{2+} + histamine (10 μM), A23187 (1 μM), SKF + histamine (30 μM and 10 μM) or KBR + histamine (10 μM and 10 μM). B, Mean densiometric ratio values ± SEM of phospho S1177-eNOS normalized to eNOS (AU) in control, histamine alone, histamine + 0 Ca^{2+}, A23187, SKF + histamine or KBR + histamine. (n = 9 blots)

3.3.4 Detection of TRPC-NCX association via co-immunoprecipitation

Previous findings indicated that a close spatial association of TRP subunit-containing channels and NCX must be present in order to facilitate local elevations in $[Na^+]_i$ owing to Na^+ influx through TRP-containing non-selective cation channels and the activation of reverse-mode NCX (Paltauf-Doburzynska *et al.*, 2000; Fulton *et al.*, 2004; Rosker *et al.*, 2004; Poburko *et al.*, 2007). To evaluate if TRPC and NCX are closely associated with each other, co-immunoprecipitation and PLA experiments were performed to test for the presence of a physical and co-localization of TRPC and NCX proteins in ECs.

TRPC1-7 and NCX1-3 isoform specific expression in Ea.Hy926 cells was first characterized by RT-PCR. The utility of all primers was validated using human TRPC as positive controls. RT-PCR revealed the expression of mRNAs encoding TRPC1, 4, 5, 6, 7 and NCX1 (Figure 3.9A). TRPC1 and 4 were consistently detected in all replicates of the experiments, but variability in the expression of the other TRPCs was evident, with TRPC5, 6, and 7 mRNA detected in less than 50% of experiments. Western blotting confirmed the presence of immunoreactive bands of appropriate molecular size for TRPC1, TRPC4 and NCX1 in Ea.Hy296 cells.

Direct biochemical evidence in support of NCX1-TRPC association was obtained in co-immunoprecipitation experiments using NCX1-, TRPC1-, TRPC4- and caveolin1-specific antibodies and protein lysates derived from control (C) or histamine-treated (H) Ea.Hy296 cells. Anti-TRPC1 immunoreactive bands of appropriate molecular mass were detected in immunoprecipitates of control (C)

and histamine-treated (H) cells that were generated using two different NCX1 antibodies (6H2 and R3F1) and a caveolin-1 antibody (Figure 3.9B). TRPC4 immunoreactive bands were also detected in anti-NCX1 immunoprecipitates, but not consistently; i.e. in 3 out of 6 replicates (Figure 3.9C). NCX1 immunoreactive bands were apparent in NCX1 and caveolin-1 immunoprecipitates (Figure 3.9D). Moreover, STIM1 (Figure 3.8E) protein was also detected in NCX1 immunoprecipitates, the input lysates of which were obtained from control (C) histamine (H), or 0 Ca^{2+} + histamine (0 + H)-treated Ea.Hy296 cells. These data suggest the presence of a STIM1-TRPC1-NCX1 signaling complex within the caveolae in Ea.Hy926 cells.

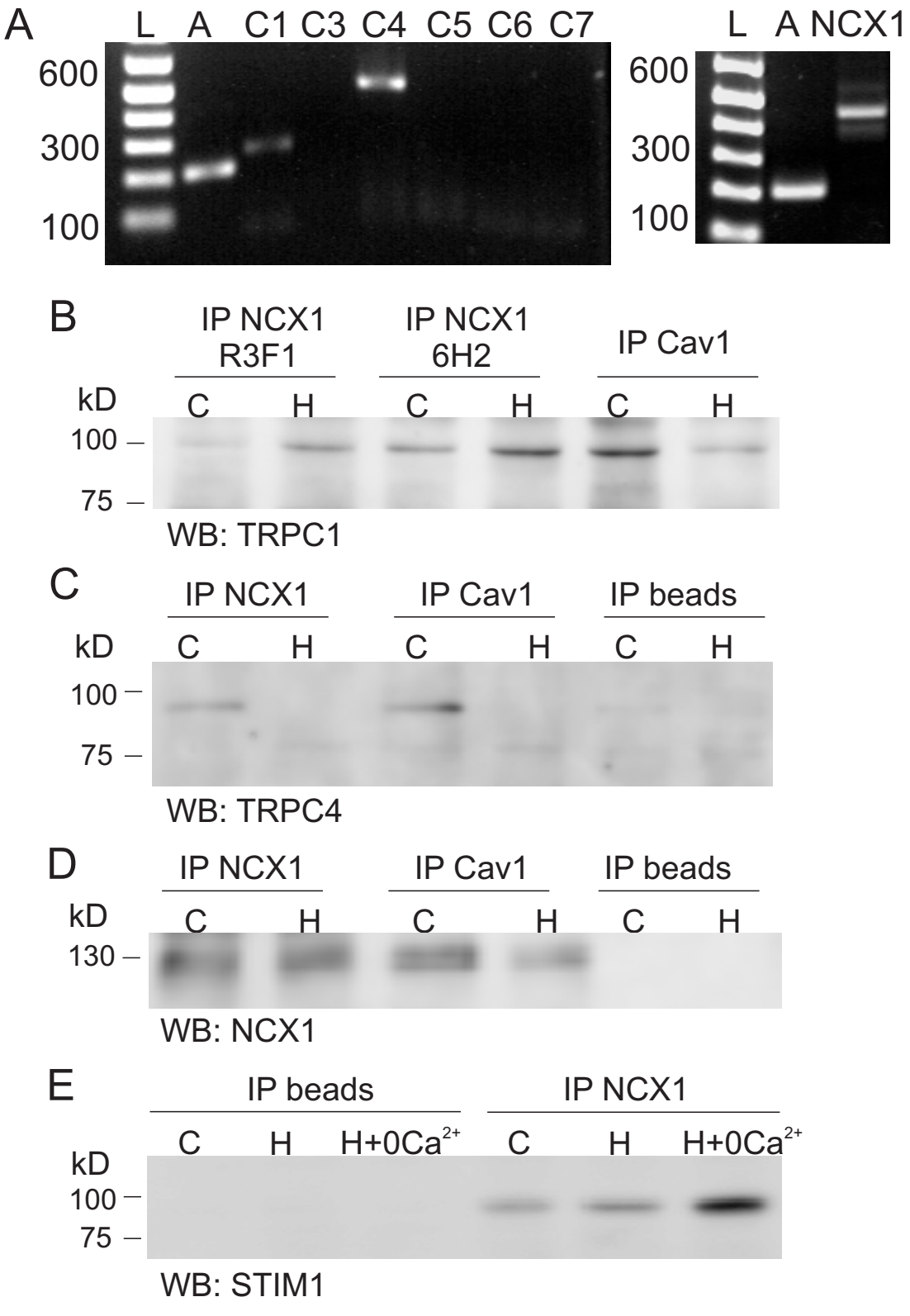
A
L A C1 C3 C4 C5 C6 C7
600
300
100
L A NCX1
600
300
100
B
IP NCX1 R3F1
IP NCX1 6H2
IP Cav1
kD
C H C H C H
100
75
WB: TRPC1
C
IP NCX1
IP Cav1
IP beads
kD
C H C H C H
100
75
WB: TRPC4
D
IP NCX1
IP Cav1
IP beads
kD
C H C H C H
130
WB: NCX1
E
IP beads
IP NCX1
C H H+0Ca2+ C H H+0Ca2+
kD
100
75
WB: STIM1

Figure 3.9: mRNA and protein detection of TRPCs and NCX

A, Representative gels indicating generation of amplicons of appropriate sizes using PCR primer pairs for actin (A), TRPC1, C3-7 and NCX1 from mRNA extracted from Ea.Hy926 cells. For TRPCs, primers were validated against pcDNA constructs of the genes. Similar results were obtained from 11 additional experiments. B, Representative western blot of TRPC1 in NCX1 (6H2 and R3F1) and caveolin-1 immunoprecipates in lysates obtained from control (C) and histamine-treated (H) cells. Protein G-Sepharose beads were used as an input control (IP beads). All blots are representative of at least n = 3. C, Representative western blot of NCX1 in NCX1 and caveolin-1 immunoprecipitates in both control- and histamine-treated conditions. D, Representative western blot of TRPC4 detection in NCX1 and caveolin-1 immunoprecipitates. E, Representative western blot of STIM1 in NCX1 immunoprecipitates in control (C), histamine (H) or histamine and 0 Ca^{2+} (0+H) conditions.

3.3.5 Direct detection of a STIM1-TRPC1-NCX1 signaling complex

3.3.5.1 Visualization of TRPC1-NCX1 co-localization

TRPC1 and NCX1 co-localization in Ea.Hy926 cells was visualized by proximity ligation assay. Briefly, this technique employs protein specific primary antibodies from two different species, and PLUS and MINUS secondary antibody probes conjugated to synthetic oligonucleotides that hybridize when in close proximity (< 40 nm). Following ligation of the hybridized oligonucleotides, and rolling circle amplification, the amplification product was detected using red fluorescent fluorophore-tagged, complementary oligonucleotides. The validity of PLA was first verified by determining whether the technique could detect the co-localization of $K_v1.2$ and $K_v1.5$ subunits within the heteromultimeric $K_v1.2/1.5$ channels (Zhong *et al.*, 2010). HEK cells overexpressing $K_v1.2/K_v1.5$ were treated with $K_v1.2$ and $K_v1.5$ primary antibody, followed by appropriately matched PLA PLUS and MINUS probes. PLA signals were consistently detected in Kv1.2/Kv1.5-transfected cells (Figure 3.10A). In contrast, PLA signals were not detected in cells expressing only Kv1.2 (B), Kv1.5 (C), or untransfected (D).

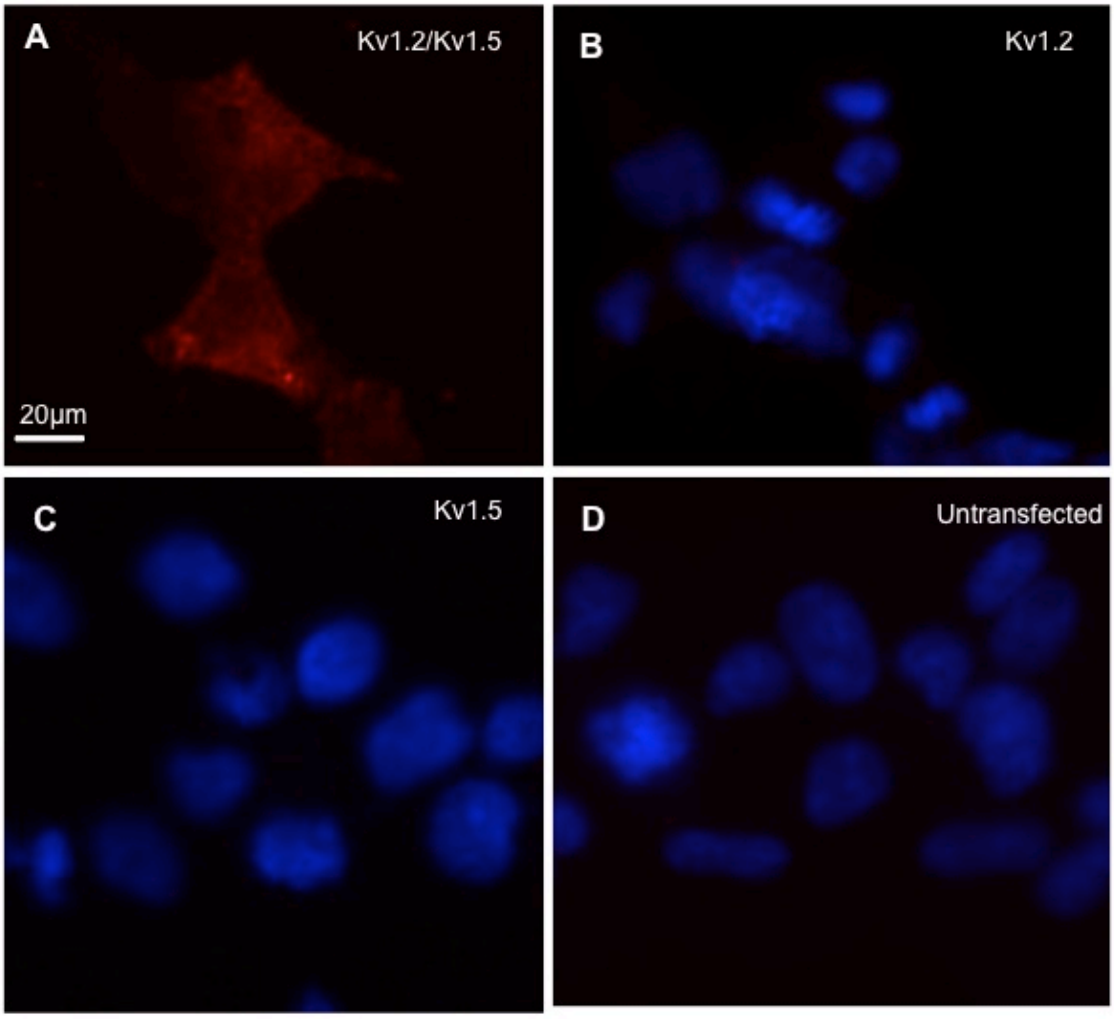

Figure 3.10: Assessing validity of the proximity ligation assay using $K_v1.2/K_v1.5$-overexpressing HEK cells

Representative images of PLA reaction product indicated by red fluorescent dots were detected in $K_v1.2/K_v1.5$-overexpressing HEK cells (A) but absent from Kv1.2-overexpressing (B), $K_v1.5$-overexpressing (C), and untransfected HEK cells (D) probed with $K_v1.2$ and $K_v1.5$ primary antibodies.

Figure 3.11 shows representative fluorescence images of Ea.Hy926 cells transfected with cDNAs encoding GFP and control (scrambled) or NCX1 siRNAs, and subsequently exposed to TRPC1 and NCX1 primary antibodies, and PLA PLUS and MINUS probes. Red fluorescent dots corresponding to sites of TRPC1 and NCX1 co-localization were detected in GFP-positive and -negative cells in cultures transfected with scrambled siRNA (Figure 3.10Ai). Fewer fluorescent dots were detected in GFP-positive cells transfected with NCX1 siRNAs compared to GFP-negative, non-transfected cells in the same culture dishes (Figure 3.11Aii), and GFP-positive cells in sister dishes transfected with scrambled siRNAs (Figure 3.11Ai). In the latter, the number of dots per GFP-positive cell was reduced by 80 ± 10% in cells transfected with NCX1 siRNA compared to scrambled siRNA (Figure 3.11B). These data indicate that TRPC1 and NCX1 are located within 40 nm of each other in Ea.Hy296 cells, and that the frequency of this association was reduced by suppression of NCX1 protein expression. Negative control experiments were carried out by exposing Ea.Hy926 cells to NCX1 primary antibody alone followed by PLA PLUS and MINUS probes. An absence of PLA products was observed compared to cells exposed to TRPC1 and NCX1 primary antibody pair (Figure 3.12A + B).

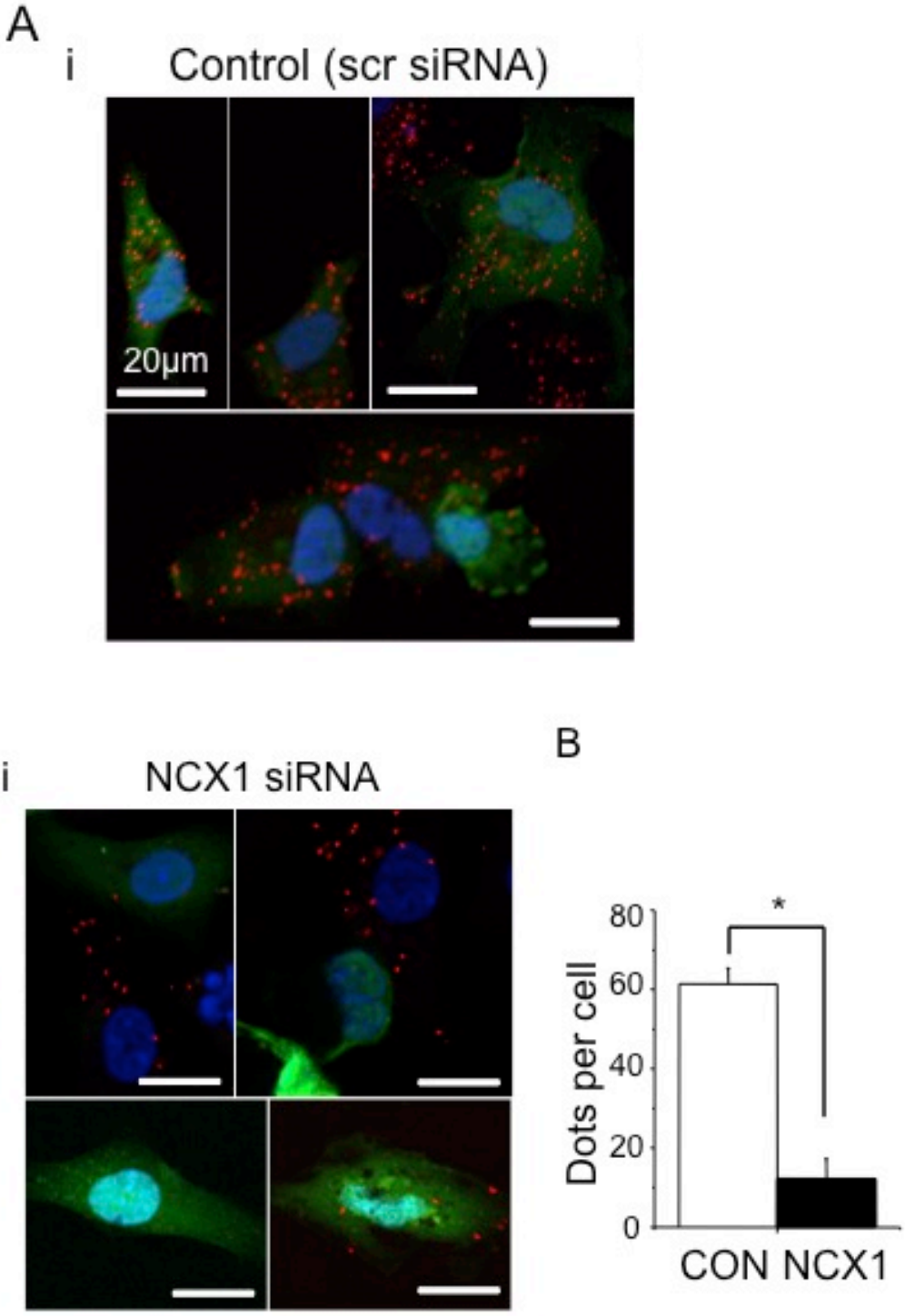
A
i
Control (scr siRNA)
20μm
ii
NCX1 siRNA
B
Dots per cell
80
60
40
20
0
*
CON NCX1

Figure 3.11: Presence of positive PLA signals in Ea.Hy926 cells when probed with TRPC1 and NCX1 primary antibodies

A, Representative images of PLA reaction product indicated by red fluorescent dots were detected in GFP-positive Ea.Hy926 cells transfected with scrambled control siRNA (i) and cDNA encoding GFP, but not in GFP-positive cells that were co-transfected with NCX1 siRNA (ii) probed with NCX1 and TRPC1 primary antibodies. B, Mean number of red fluorescent dots ± SEM in GFP-positive cells from control and NCX1 siRNA-treated cells (n = 29 and 27 cells for control and NCX1 siRNA, respectively; *, $p<0.05$). Here and in subsequent panels, the nuclei of cells are indicated by blue Hoechst 33342 stain.

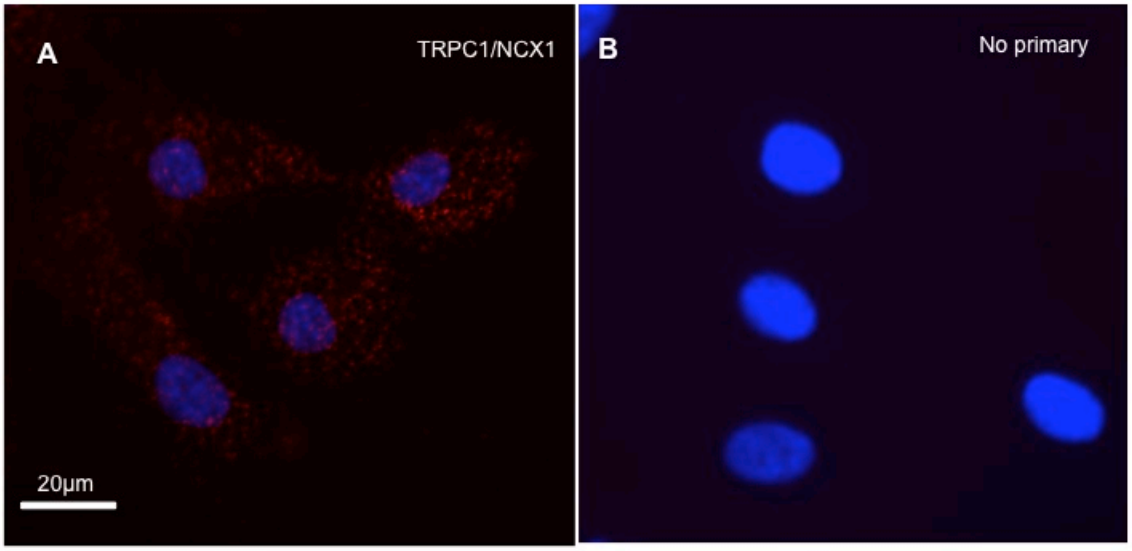

Figure 3.12: Negative control for PLA experiment with single NCX antibody probe

A, Representative image of PLA reaction product indicated by red fluorescent dots in the presence of TRPC1 and NCX1 primary probing antibodies. B, Representative image of PLA reaction product in the absence of probing primary antibodies.

3.3.5.2 Visualization of STIM1-NCX1 co-localization

STIM1 is a trans-ER membrane protein that detects changes in $[Ca^{2+}]_{ER}$. When ER $[Ca^{2+}]$ is depleted, STIM1 oligomerizes and migrates to ER regions that are in close proximity to the PM. STIM1 then interacts with proteins, such as TRPC-containing channels, and activates Ca^{2+} entry (Liou *et al.*, 2007; Pani *et al.*, 2009). Although co-localization of TRPC channels and STIM1 is well-established, the involvement of STIM1 in the regulation of NCX1 activity has not been extensively characterized. PLA experiments were carried out employing primary antibodies that recognized a cytosolic N-terminal epitope on STIM1 and a cytosolic epitope on NCX1. Ea.Hy926 cells were first treated with 0 Ca^{2+}-containing PSS and stimulated with histamine to ensure maximal depletion of the ER Ca^{2+} and facilitate translocation of STIM1 to regions in the ER in close proximity to the PM. Red fluorescent dots corresponding to sites of STIM1 and NCX1 co-localization were detected in cultured ECs transfected with scrambled siRNA (Figure 3.13A). Interestingly, fewer fluorescent dots were detected in GFP-positive cells transfected with TRPC1 siRNAs compared to scrambled control siRNA (Figure 3.13B), suggesting that the association of STIM1-NCX1 may require the presence of TRPC1.

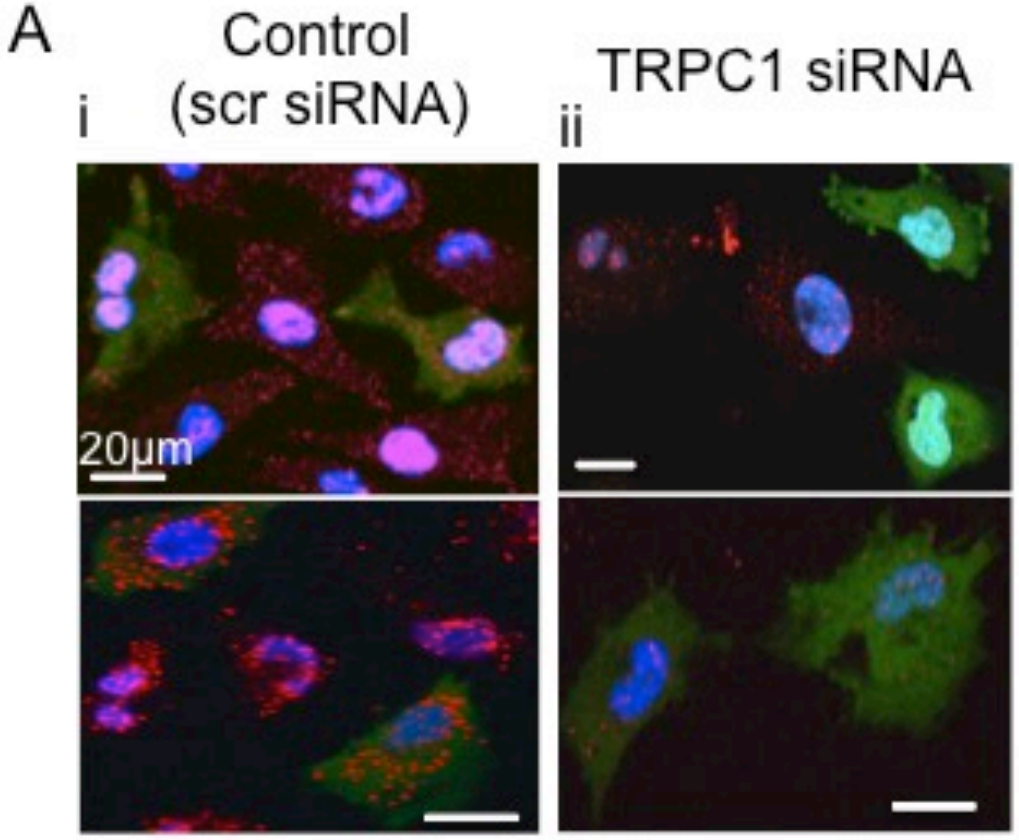
A
Control
(scr siRNA)
i
TRPC1 siRNA
ii
20μm

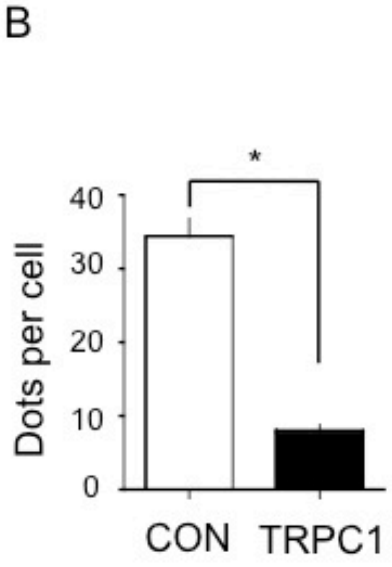
B
*
40
30
20
10
0
Dots per cell
CON
TRPC1

Figure 3.13: STIM1-NCX1 interaction requires TRPC1 expression

A, Representative images of PLA reaction product indicated by red fluorescent dots were detected in GFP-positive Ea.Hy926 cells transfected with scrambled control siRNA (i) and cDNA encoding GFP, but not in GFP-positive cells that were co-transfected with TRPC1 siRNA (ii) probed with NCX1 and STIM1 primary antibodies. B, Mean number red fluorescent dots ± SEM (n = 58 and 87 cells for control and TRPC1 siRNA; *, $p<0.05$) in GFP-positive cells from control and STIM1 siRNA-treated cells.

3.4 Discussion

3.4.1 Summary of findings

This chapter provides evidence that NCX activity contributes to the regulation of agonist-induced elevation of $[Ca^{2+}]_i$ and S1177-eNOS phosphorylation, and that the activation of NCX in cultured ECs is dependent on the presence of a macromolecular signaling complex consisting of STIM1, TRPC1/4, and NCX1. Specifically, we found that the histamine-induced increase in $[Ca^{2+}]_i$ and phosphorylation of S1177-eNOS in ECs were significantly reduced by inhibition of NSCC and NCX by SKF and KBR or specific siRNA-mediated knockdown of NCX, respectively. The notion that NCX-mediated Ca^{2+} entry is functionally linked to NSCC gating was supported by co-immunoprecipitation and co-localization of TRPC1-NCX1, NCX1-STIM1, and NCX1-caveolin1. Significantly, NCX co-localization with STIM1 was dependent on TRPC1 expression. These findings indicate the presence of macromolecular signaling complexes consisting of STIM1, TRPC1, and NCX1 perhaps within or adjacent to caveolae of EC that facilitates agonist-induced Ca^{2+} entry.

3.4.2 Modulation of $[Ca^{2+}]_i$ by NCX

3.4.2.1 Involvement of TRP channels in histamine-induced $[Ca^{2+}]_I$ increase

TRPC-containing channels have long been implicated as an important Ca^{2+} entry pathway in ECs (Nilius & Droogmans, 2001; Dietrich & Gudermann, 2011; Vennekens, 2011). Here, we showed that SKF, a prototypical TRPC-blocker, decreased histamine-induced $[Ca^{2+}]_i$ elevation, providing pharmacological evidence for a role of NSCC in the histamine-induced $[Ca^{2+}]_i$

increase. These findings are consistent with the view that TRPC subunit-containing channels contribute to Ca^{2+} influx. For example, in pulmonary arterial ECs, histamine- and thrombin-stimulated $[Ca^{2+}]_i$ increases were reduced by TRPC1 and C4 knockdown, either alone or together (Tiruppathi *et al.*, 2002; Paria *et al.*, 2004; Jho *et al.*, 2005; Antigny *et al.*, 2012; Cioffi *et al.*, 2012). TRPC3 silencing with siRNA also diminished store-dependent Ca^{2+} entry in human umbilical ECs (Antigny *et al.*, 2012). Although the identities of TRPCs that may be involved in Ca^{2+} entry were not elucidated in our study, our data are consistent with the notion that a strong association exists between TRPC channel expression and/or activity and Ca^{2+} influx in ECs.

3.4.2.2 Evidence for NCX reversal

Our data, which reported an inhibition of the histamine-induced Ca^{2+} response by both SKF and KBR, are consistent with the view that NSCC and NCX both play a role in regulation of endothelial $[Ca^{2+}]_i$ during histamine stimulation. Results obtained from 0 Ca^{2+} re-addition protocol showed that the histamine-induced increase in $[Ca^{2+}]_i$ upon Ca^{2+} re-addition was inhibited by KBR, which supports the notion that NCX serves as a Ca^{2+} influx pathway that contributes to modulation of $[Ca^{2+}]_i$. Interestingly, inhibition of NCX reduced the histamine-induced peak $[Ca^{2+}]_i$ response, suggesting NCX activity may contribute to refilling of store and consequent agonist-induced store release as was suggested for SMCs (Fameli *et al.*, 2006).

The study of NCX activity has been limited by the lack of specific blockers. Specifically, KBR has been reported to inhibit TRPC6 proteins in heterologous

overexpression systems and activate BK_{Ca} channels in cultured ECs (Kraft, 2007; Liang *et al.*, 2009). Despite the relative non-selectivity of KBR, measurement of I_{NSCC} in cultured ECs using the perforated patch, whole cell configuration of the patch-clamp technique revealed KBR selectively inhibited the outward component of I_{NSCC}, which was attributed to inhibition of reverse-mode NCX (Girardin *et al.*, 2010). Moreover, an siRNA approach was employed in the present study to specifically silence the expression of NCX in order to better understand the role of NCX in regulating endothelial $[Ca^{2+}]_i$ homeostasis. Interestingly, both siRNA NCX and KBR inhibited the entire histamine-induced Ca^{2+} response regardless of the time point during stimulation, suggesting that they are likely acting on a common target.

3.4.2.3 Discrepancies between observed and hypothesized SKF/KBR effects

In our study, we hypothesized that NCX reversal occurs downstream of TRP-containing NSCC activation; specifically, that Na^+ entry through NSCC is driving reverse-mode NCX activity. Due to the proposed functional link between NSCC and NCX, it was expected that inhibition of NSCC would functionally block reverse-mode NCX activity because of an absence of NSCC-dependent Na^+ entry to drive reverse-mode NCX activity. However, when NCX is inhibited by KBR, Ca^{2+}/Na^+ entry can still occur through NSCC, thus having a lesser effect than NSCC inhibition. This notion is supported by our double histamine challenge experiments (Figure 3.1), which showed that SKF exerted a greater inhibitory effect than that of KBR on the histamine-induced $[Ca^{2+}]_i$ increase, suggesting that

SKF and KBR were likely interacting with different targets in the same signaling pathway for agonist-dependent regulation of $[Ca^{2+}]_i$ in Ea.Hy296 cells.

Unexpectedly, KBR exerted a greater inhibitory effect than SKF on the histamine-induced increase in $[Ca^{2+}]_i$ following Ca^{2+} re-exposure in the 0 Ca^{2+}-Ca^{2+} re-addition protocol (Figure 3.2), and in conditions where the inhibitors were applied during sustained histamine exposure (Figure 3.3). However, it needs to be considered that these experimental manipulations can contribute to intracellular Na^+ loading. Intracellular Na^+ loading would have a greater functional effect on NCX activity than NSCC and could explain the reduced effect of SKF on histamine-induced $[Ca^{2+}]_i$ responses compared to KBR in these experimental conditions.

Firstly, while the 0 Ca^{2+}-Ca^{2+} re-addition protocol is typically used to assess the contribution of Ca^{2+} influx versus Ca^{2+} release to overall changes in $[Ca^{2+}]_i$, exposing cells to agonists in the absence of extracellular Ca^{2+} has been shown to induce Na^+-loading owing to forward-mode NCX extrusion of Ca^{2+} released from internal stores prior to re-exposure to Ca^{2+}-containing solution (Huang *et al.*, 2006b). Moreover, divalent-free external solution has also been found to enhance Na^+ entry through NSCC and increase $[Na^+]_i$ (Bosteels *et al.*, 1999). Although our 0 Ca^{2+} solution contains Mg^{2+}, and is therefore not divalent free, it is unclear whether Mg^{2+} can alter Na^+ entry through NSCCs as most permeability experiments have focused mainly on Ca^{2+}/Na^+ permeability. We found that the increase in $[Ca^{2+}]_i$ on re-exposure to 1.5 mM Ca^{2+}-containing solution was inhibited to a greater extent by KBR than by SKF, which is

consistent with the notion that removal of extracellular Ca^{2+} likely contributes to intracellular Na^+-loading.

Secondly, when inhibitors were applied during sustained exposure to histamine, sufficient Na^+ loading could have already occurred at the time of inhibitor application. In SMCs, agonist-induced Na^+ entry reached a steady plateau within the first 2 min of stimulation and $[Na^+]$ remained elevated even after agonist wash-out (Poburko *et al.*, 2007). Thus, at 2 min post-histamine stimulation, inhibition of NSCC would have minimal effect on $[Ca^{2+}]_i$, if sufficient accumulation of Na^+ in ECs had already occurred to drive reverse-mode NCX. Histamine-stimulated Na^+-loading could therefore explain why KBR exerted a greater inhibitory effect than SKF when applied during histamine stimulation.

3.4.2.4 Theoretical argument for NCX reversal

The magnitude of the agonist-stimulated increase in $[Na^+]_i$ has been approximated to be ~ 5-15 mM, with localized $[Na^+]_i$ elevation reported to be ~ 30 mM in SMCs (Arnon *et al.*, 2000b, a; Poburko *et al.*, 2007). Based on the principles of thermodynamics, there is a strong basis for reversal of NCX in ECs under physiological conditions. Calculation of the reversal potential for NCX (E_{NCX}; $E_{NCX} = 3\ E_{Na} - 2\ E_{Ca}$) in ECs places E_{NCX} at +20 mV at rest (T = 25 ° C, $[Na^+]_i$ = 5 mM, $[Ca^{2+}]_i$ = 100 nM, $[Na^+]_o$ = 145 mM, $[Ca^{2+}]_i$ =1.5 mM). Upon stimulation, with the approximation of $[Na^+]_i$ = 30 mM and $[Ca^{2+}]_i$ = 1 μM, E_{NCX} is calculated to be approximately = -63 mV. Based on the theoretical values of E_{NCX}, reverse NCX activity is physiologically possible given that E_m of EC during stimulation is ~ -30 mV to -50 mV (Bondarenko, 2004; Bondarenko & Sagach,

2006). However, direct visualization of changes in EC $[Na^+]_i$ in response to agonist stimulation, as previously shown for VSMCs (Poburko *et al.*, 2007), will be necessary to corroborate the role of NCX as a Ca^{2+} entry pathway in ECs.

3.4.3 Macromolecular signaling complex

3.4.3.1 Detection of TRPC and NCX mRNA and protein expression

Cultured Ea.Hy926 cells were found to express mRNA transcripts of TRPC1, 4, 5, 6 and 7 and protein expression was confirmed for TRPC1 and C4. This is in agreement with findings that TRPC1-7, with the exception of TRPC2, have been reported to be expressed in ECs from a variety of vascular beds (Vennekens, 2011). Protein and mRNA expression of NCX1 in EC lysates were also detected, which is consistent with the findings that NCX1 is expressed in most tissues and NCX2 and NCX3 are expressed in neuronal and SMCs (Lytton, 2007). Interestingly, NCX1 is the isoform detected in cell types where NCX reversal has been reported, specifically the NCX1.3 splice variant (Zhang *et al.*, 2010).

3.4.3.2 NCX1-TRPC1 signaling complex

Consistent with the view that caveolae are important in Ca^{2+} signaling, we showed that NCX1 and TRPC1 co-immunoprecipitated with each other and with caveolin-1, an important structural protein of caveolae. Moreover, PLA experiments provided support for *in situ* interaction between TRPC1-NCX1. Specifically, TRPC1 and NCX1 were shown to be located within 40 nm of each other by PLA. These data suggest that TRPC1 and NCX1 are present in the caveolae and lipid-rich domain of the cell membrane and are consistent with

previous findings of Teubl *et al.* (1999), where sucrose density gradient centrifugation revealed the presence of NCX1 in the same fraction as eNOS and caveolin-1 (Teubl *et al.*, 1999). While the interaction between the carboxyl terminus of TRPC1 and the caveolin-1 scaffolding domain have been well documented (Tiruppathi *et al.*, 2002; Ahmmed *et al.*, 2004; Kwiatek *et al.*, 2006; Singh *et al.*, 2007; Pani *et al.*, 2009; Sundivakkam *et al.*, 2009; Sundivakkam *et al.*, 2012), co-immunoprecipitation of NCX1 with caveolin-1 has only been previously shown in A6 glioma cells (Cha *et al.*, 2004). Our data indicate that TRPC1-NCX1 exists in a signaling complex in association with caveolin-1 in ECs.

3.4.3.3 NCX1-STIM1 signaling complex

In addition to TRPC1-NCX1 interaction, co-localization and co-immunoprecipitation of NCX1 and STIM1 were also detected in conditions where the ER Ca^{2+} store was depleted. Although STIM1 was detected in NCX1 immunoprecipitates in control, histamine, and 0 Ca^{2+} and histamine treated cells, quantification of STIM1 and NCX1 association in the different treatment conditions was not attempted. Interestingly, we showed that STIM1 and NCX1 were located within 40 nm of each other; however, this co-localization only occurred in the presence of TRPC1. This observation suggests that the identified interaction between STIM1 and NCX1 is likely dependent on their individual tethering to TRPC1 and is, therefore, indirect. Our findings are consistent with the well-documented physical association between TRPC1 and STIM1, as well as TRPC and NCX1, detected in other cell types using both co-immunoprecipitation and immuno-FRET approaches (Tiruppathi *et al.*, 2002;

Ahmmed *et al.*, 2004; Kwiatek *et al.*, 2006; Singh *et al.*, 2007; Pani *et al.*, 2009; Sundivakkam *et al.*, 2009; Ng *et al.*, 2012; Sundivakkam *et al.*, 2012).

Similar co-immunoprecipitation and co-localization of NCX1 and STIM1 has not been previously described, although NCX1 and STIM1 have been shown to interact functionally (Liu *et al.*, 2010). Specifically, reduced STIM1 expression with siRNA inhibited NCX-mediated current in airway SMC (Liu *et al.*, 2010). This suggests that STIM1 and NCX could be involved in the same signaling pathway. In the current study, we showed that the histamine-induced increase in $[Ca^{2+}]_i$ was inhibited by reduced expression of both STIM1 and NCX1 with siRNA treatment; however, further analysis of the histamine-induced $[Ca^{2+}]_i$ increase in treatments where STIM1 and NCX1 are sequentially inhibited will be necessary to assess whether STIM1 and NCX1 are different components of the same signaling pathway. Together, these data provide evidence supporting the presence of a STIM1-TRPC1-NCX1 macromolecular signaling complex that contributes to the agonist-induced $[Ca^{2+}]_i$ response in ECs.

As mentioned previously, STIM1 is reported to link changes in $[Ca^{2+}]_{ER}$ to activation of Ca^{2+} influx, but several studies have shown that STIM1 alone is not enough for activation of TRPC subunit-containing channels following store depletion and that the presence and recruitment of other proteins, such as Orai1, is necessary for the activation of SOC (Cheng *et al.*, 2011). While the involvement of Orai1 channels in Ca^{2+} regulation has been extensively studied in cells that are known to carry I_{CRAC}, their roles in ECs are less well defined. However, Orai1 was recently shown to interact with TRPC1 and C4 and to

contribute to the activation and Ca^{2+} selectivity of these TRPC-containing channels in ECs, which do not exhibit prototypical I_{CRAC} (Cioffi *et al.*, 2012). Although a role for Orai1 in the regulation of $[Ca^{2+}]_i$ in Ea.Hy926 cells was not investigated in the present study, its potential role in interacting with components of the STIM1-TRPC1-NCX1 macromolecular signaling complex described here would be an intriguing future area of research.

3.4.3.4 Physiological relevance of localized Ca^{2+} signaling: an emphasis on the caveolae

Our data indicate reverse-mode NCX activity contributes to endothelial Ca^{2+} homeostasis and its activation is dependent on its spatial proximity to STIM1 and TRPC1. Specifically, we showed that NCX1 and TRPC1 co-immunoprecpitated with caveolin-1, and NCX1 and TRPC1/STIM1 were located within close proximity of each other. These data suggest these STIM1-TRPC1-NCX1 macromolecular signaling complexes are present within the caveolae and could be involved in the organization and generation of localized Ca^{2+} signaling. Localization of Ca^{2+} signaling molecules has been suggested to have functional implications. For example, using Gd^{3+} and La^{3+} as pharmacological blockers to discriminate between SOC and ROC, it was suggested by several groups that the location of the TRPC channels is the predominant factor determining whether SOC- or ROC-dependent activation occurs (Strubing *et al.*, 2001, 2003; Liou *et al.*, 2007). Furthermore, measurement of sub-plasmalemmal $[Ca^{2+}]_i$ using a caveolae-targeting Ca^{2+} sensor revealed localized Ca^{2+} signals under the PM during agonist stimulation, which were initiated at caveolae (Isshiki *et al.*, 2002b),

indicating that caveolae are an important site for the generation of Ca^{2+} signals in ECs. This notion was also supported by the finding that disruption of caveolae with methyl-β-cyclodextran reduced Ca^{2+} influx in freshly isolated pulmonary arterial ECs (Paffett *et al.*, 2011). These data point to caveolae as a hot spot for Ca^{2+} signaling and our findings in this chapter place TRPC1-NCX1 signaling complexes within this signaling hotspot.

The presence of Ca^{2+} modulating proteins, such as TRPC1 and NCX1, in the caveolae is significant because eNOS is expressed predominantly in the lipid-enriched fraction of the membrane (Garcia-Cardena *et al.*, 1996a). As mentioned in Chapter 1.6, the targeting of eNOS to the PM is important for its activity, specifically its ability to produce NO in response to transmembrane Ca^{2+} flux (Fulton *et al.*, 2004). Moreover, caveolin-1 is bound to eNOS to render it inactive at rest (Garcia-Cardena *et al.*, 1996a; Garcia-Cardena *et al.*, 1997; Fulton *et al.*, 2001). Given the observations that: (1) TRPC1 and NCX1 are found in the caveolae and (2) the presence of eNOS in the cavolae, the close proximity of these proteins may allow the cell to efficiently convert Ca^{2+} signals to the activation of eNOS and production of NO.

3.4.4 Ca^{2+} dependency of S1177 eNOS phosphorylation

As mentioned previously, S1177 phosphorylation has been reported to be mediated by several kinases, such as Akt and CaMKII in both Ca^{2+}-independent and -dependent fashion (Dimmeler *et al.*, 1999; Fleming *et al.*, 2001). Our data showed histamine-induced phosphorylation of S1177-eNOS was blocked by inhibition of NSCC and NCX and removal of extracellular Ca^{2+}, and that the Ca^{2+}

ionophore, A23187, mimicked the effect of histamine. These observations suggest phosphorylation of S1177-eNOS is Ca^{2+}-dependent in our experimental conditions. Although further experiments are required to identify the specific kinase involved in the phosphorylation of S1177, our data indicate phosphorylation of S1177-eNOS is strongly associated with an elevation in $[Ca^{2+}]_i$ and Ca^{2+} influx mediated by NSCC and NCX activities.

Phosphoprotein analysis was carried out on EC lysates collected 5 min post-histamine stimulation, as others have found that stimulation of pulmonary artery ECs with bradykinin increased S1177 phosphorylation, which peaked within the first 5 min of stimulation (Fleming *et al.*, 2001). Interestingly, bradykinin-induced phosphorylation of S1177-eNOS returned to baseline within 15 min (Motley *et al.*, 2007). This is in stark contrast to our finding that the $[Ca^{2+}]_i$ response to histamine stimulation was maintained at a sustained elevated level for 7 min. Moreover, $[Ca^{2+}]_i$ has been reported to remain elevated for 20 min in response to agonist stimulation, in the presence of extracellular Ca^{2+} (Jousset *et al.*, 2008). Thus, the relationship between S1177-eNOS phosphorylation and $[Ca^{2+}]_i$ warrants further study. Specifically, the time-course of S1177-eNOS phosphorylation and $[Ca^{2+}]_i$ should be measured in a single EC in response to agonist and will be necessary to better understand the relationship between $[Ca^{2+}]_i$ and eNOS phosphorylation.

Histamine (10 μM) has been shown to stimulate production of NO in Ea.Hy926 cells (Sheng & Braun, 2007), which is consistent with our finding that histamine stimulation is associated with an increase in phosphorylation of S1177.

However, it is unclear whether S1177 phosphorylation alone is sufficient for eNOS activation and should be considered in the interpretation of our data. Future experiments, such as the effect of NCX inhibition on histamine-induced NO production, would provide a more direct endpoint in understanding the contribution of NCX-mediated Ca^{2+} entry in NO production and release.

3.4.5 Evidence for a PM-ER junction in ECs

The presence of a PM-ER region is thought to be a fundamental feature required for reverse-mode NCX-mediated Ca^{2+} entry in physiological responses. As mentioned in Chapter 1.8.3, the presence of a PM-ER junction in EC has been elucidated indirectly, based on co-localization and co-immunoprecipitation of proteins that are known to be expressed on the PM and ER, respectively. Our data provide evidence in support of a PM-ER junction in EC. Specifically, the PLA data indicate that NCX1, a PM protein, and STIM1, an ER resident protein, are located within 40 nm of each other, which places PM and ER membrane within 40 nm each other. However, this is likely an over-estimation of the width of the PM-ER junction because the spatial arrangement of NCX1 and STIM1 is unknown and 40 nm is the detection limit for the PLA technique. Other techniques, such as immuno-FRET, have been used to study TRPC1 and STIM1 co-localization and the distance between the two proteins was estimated to be ~ 7 nm (Pani *et al.*, 2009). These experimental values are comparable to the approximation of the width of the PM-ER junction in SMCs, reported to be 20 nm (Dai *et al.*, 2005) and suggest the presence of a similar junction in EC.

3.4.6 Limitations

3.4.6.1 Information gap

In this chapter, we provided evidence in support of a role for NCX in the regulation of $[Ca^{2+}]_i$ in cultured ECs. Our proposed mechanism hinges on the underlying assumption that there is Na^+ entry through TRP-containing channels in order for activation of reverse-mode NCX. However, an increase in $[Na^+]_i$ will not only activate reverse-mode NCX but it will also suppress forward-mode NCX (see Chapter 6). Moreover, although KBR has been reported to be a selective reverse-mode NCX inhibitor, there is considerable debate as to how an inhibitor can selectively block one direction of transport. It has been argued that the effectiveness of KBR to selectively block reverse-mode NCX holds true only in conditions where thermodynamics favour reverse-mode activity (Ruknudin *et al.*, 2007). Thus, understanding changes in $[Na^+]_i$, in addition to $[Ca^{2+}]_i$, in response to agonist would be necessary to better understand the functionally linked TRPC-NCX-mediated Ca^{2+} influx.

3.4.6.2 Limitations of our model system

We used a cell culture model in the present study for several reasons: (1) endothelial monolayer allows for $[Ca^{2+}]_i$ measurements independent of interfering signals from SMCs, (2) the use of cultured ECs enables study of TRPC and NCX mRNA and protein expression, as well as TRPC-NCX interactions without contamination from other cell types, such as SMCs, and (3) immunoprecipitation studies require a large amount of input protein and the use of cultured cells was necessary to generate enough lysate to detect relatively low abundance proteins

such as TRPC, NCX and STIM1. However, the use of cultured EC is not an accurate representation of native EC and protein expression is known to change with passage. For example, TRPV4 protein has been shown to be expressed in intact arteries from a variety of vascular beds, and is crucial for flow-mediated dilation (Zhang *et al.*, 2009; Mendoza *et al.*, 2010; Bubolz *et al.*, 2012). However, GSK, an agonist of TRPV4, did not elicit a Ca^{2+} response in Ea.Hy926 cells and RT-PCR did not detect TRPV4 mRNA transcripts, suggesting TRPV4 are not expressed in Ea.Hy926 cells (data not shown). Thus, in the next chapter, intact cerebral arteries were used to study the contribution of NCX to the shear-induced response.

3.4.6.3 Technical limitations

NCX-mediated Ca^{2+} influx has been inferred to be important in generating localized Ca^{2+} events. However, in this study, quantification of $[Ca^{2+}]_i$ was carried on an epifluorescence microscope, measuring bulk cytosolic $[Ca^{2+}]_i$ changes, thus the specific location of the signal (i.e. subplasmalemmal versus perinuclear) could not be discriminated given the poor spatiotemporal resolution of the technique. This does not imply that the changes in the measured $[Ca^{2+}]_i$ in response to KBR inhibition are not localized to the subplasmalemmal region, only that the actual concentration may be higher. Utilization of confocal microscopy and membrane targeted Ca^{2+} probes would assist in dissecting the Ca^{2+} signal in the subplasmalemmal area where significant Ca^{2+} flux is known to occur (Isshiki *et al.*, 2002a; Isshiki *et al.*, 2002b; Isshiki *et al.*, 2004; Earley *et al.*, 2005; Murata *et al.*, 2007; Sullivan *et al.*, 2012). Measurement of localized $[Ca^{2+}]$ would add to

our understanding of how NCX-mediated Ca^{2+} entry contributes to the regulation of endothelial $[Ca^{2+}]_i$ and subsequent function.

Co-immunoprecipitation and proximity ligation assay were employed to assess the spatial association of STIM1, TRPC1, and NCX1. Although co-immunoprecipitation approaches allow for identification of proteins in a macromolecular signaling complex, certain information, such as the presence of direct protein interactions and the spatial orientation of the proteins of interest, are not considered in this technique. The use of proximity ligation assay in our study complemented data obtained from co-immunoprecipitation experiments by allowing for the characterization of protein interaction *in situ*. However, the resolution of PLA is 40 nm, which is still a sizeable distance, considering the dimensions of the cellular environment. For example, caveolae are approximately 60 - 100 nm in diameter, while the diameters of channels are ~1 nm. Thus, the 40 nm resolution of the PLA technique needs to be critically evaluated in order to assess whether positive PLA signals are from *bona fide* co-localization between proteins or random protein distribution.

3.4.6.4 Alternative explanations

As mentioned previously, KBR is a non-selective inhibitor of NCX. It has been reported to block TRP channels at concentrations comparable to that employed in this study (10 μM) (Kraft, 2007; Liang *et al.*, 2009). Thus, KBR effects observed in our study could be due in part to TRP channel inhibition. Even in conditions where NCX is specifically inhibited (i.e. siRNA), NCX may not act as a Ca^{2+} influx pathway. Activation of reverse-mode NCX during agonist

stimulation generates a net outward, hyperpolarizing current (3 Na^+ ions out, 1 Ca^{2+} ion in). Inhibition of NCX during agonist stimulation may reduce the NCX-mediated hyperpolarizing effect and can decrease the driving force for cation influx through NSCC.

3.5 Significance

The findings in this chapter are important for understanding the basic mechanisms involved in a critical physiological process required for cardiovascular health. It also provides a novel molecular basis for NCX-mediated Ca^{2+} entry in EC, which may be relevant for subsequent investigations of the abnormalities in NO production/release that account for dysfunctional control of vascular contractility.

Chapter 4: Involvement of NCX1 in flow-mediated dilation

4.1 Introduction

4.1.1 Overview

Arterial diameter is a critical determinant of peripheral vascular resistance and is dependent on the level of VSMC activation. The contractile state of VSMCs is determined by both intrinsic and extrinsic factors that affect cross-bridge cycling and force transmission to the extracellular matrix. The interplay between these factors is important in establishing resting vascular tone, which enables arteries at rest to exist in a partially constricted state. The presence of basal vascular tone allows the arterial diameter to be increased or decreased, depending on a given stimulus in order to match blood flow to physiological demands.

4.1.2 Control of vascular resistance

4.1.2.1 Factors contributing to control of vascular resistance

In small resistance arteries, vascular tone is determined by intrinsic and extrinsic factors that affect SMC contractility. The intrinsic property of arterial smooth muscle cells to constrict/dilate in response to a(n) increase/decrease in intraluminal pressure, called the myogenic response, is a major determinant that dictates the basal tone at a given pressure. Vascular tone is also influenced and modulated by extrinsic influences, such as factors released from the endothelium in response to blood borne, neuronal, local chemical (autocrine or paracrine) and mechanical signals.

4.1.2.2 Flow-mediated dilation: shear stress and the endothelium

ECs release vasoactive factors in response to circulating agonists and changes in blood flow. As the inner lining of blood vessels, ECs are exposed to constant shear stress, which is the friction generated from fluid-surface contact between the blood and vessel wall as blood moves through the lumen. The magnitude of shear stress is determined by the rate of blood flow, blood viscosity and arterial diameter, and is described by the following equation:

$$SS = \frac{4 \times \eta \times Q \times 10^9}{\pi r^3}$$

where SS is shear stress (dyn/cm^2), η is viscosity in Poise (dyn s/cm^2) at 37 °C, Q is flow rate (μL/s), and *r* is artery radius (μm) (Kang *et al.*, 2008; Luksha *et al.*, 2011). Arteries *in vivo* experience shear stress in the range of 10 - 40 dyn/cm^2 (Silver & Vita, 2006) and the magnitude of the shear stress experienced by an artery is dependent on the arterial diameter. For example, small resistance arteries experience the highest shear stress in the vasculature at ~40-50 dyn/cm^2 compared to ~10 dyn/cm^2 experienced by the aorta (Papaioannou *et al.*, 2006).

Laminar, or streamline, flow is associated with basal release of NO, which contributes to blood pressure regulation through its ability to induce smooth muscle relaxation and arterial dilation (Vessieres *et al.*, 2012). Acute changes in blood flow/shear stress can activate ECs to produce vasoactive factors to induce immediate changes in arterial diameter and vascular tone (Vessieres *et al.*, 2012). Long-term exposure to chronic change in blood flow can also elicit adaptive response in blood vessels. For example, repetitive exercise-induced increase in blood flow can lead to adaptive mechanisms, resulting in an increase

in local arterial diameter to match blood flow to physiological demand (Vessieres *et al.*, 2012).

To date, only a limited number of studies have investigated the effects of flow and pressure concomitantly, despite the fact that they are both important physiological determinants of basal vascular tone. Pressure-mediated myogenic constriction sets basal arterial diameter, which is subsequently modulated by flow-mediated dilation (FMD). Thus, in order to better understand the regulation of arterial diameter in physiological conditions, the influences of these two factors must be studied concurrently.

4.1.3 Association between shear force and endothelial $[Ca^{2+}]_i$

Ca^{2+} is an ubiquitous intracellular signaling ion. Ca^{2+} entry downstream of agonist stimulation is thought to be important in the activation of eNOS and the release of NO from ECs. Similarly, shear stress has been shown to increase endothelial $[Ca^{2+}]_i$ in cultured ECs and endothelium of intact arteries from various vascular beds of different species (Kuo *et al.*, 1990; Pohl *et al.*, 1991; Kuo *et al.*, 1993; Corson *et al.*, 1996; Mendoza *et al.*, 2010). Shear-induced $[Ca^{2+}]_i$ responses are complex and variable. For instance, Corson and Harrison (1996) found that shear stress-induced $[Ca^{2+}]_i$ elevation was dependent on the magnitude of shear stress and the duration of the stimulus, such that a varied pattern of Ca^{2+} responses may be elicited (Corson *et al.*, 1996). Specifically, 1.5 dyn/cm^2 of shear stress evoked a transient increase in $[Ca^{2+}]_i$, while 2.5 dyn/cm^2 caused a sustained increase in $[Ca^{2+}]_i$ in rabbit coronary arteries (Corson *et al.*, 1996).

Although acute increase in shear stress is associated with increased $[Ca^{2+}]_i$, it is unclear whether a shear-mediated increase in $[Ca^{2+}]_i$ is necessary to elicit flow-mediated dilation. For example, acetylcholine and acute increase in shear stress both increased endothelial $[Ca^{2+}]_i$ and dilated rabbit coronary arteries (Muller *et al.*, 1999). However, chelation of Ca^{2+} by BAPTA inhibited only acetylcholine- but not shear-induced dilation in rabbit coronary arteries (Muller *et al.*, 1999), suggesting that increased $[Ca^{2+}]_i$ is not required for FMD. On the other hand, removal of external Ca^{2+} eliminated the initial peak of shear-induced NO production in rabbit iliac artery, while the sustained NO production was unaffected, indicating that the involvement of Ca^{2+} in NO production during FMD may be time-dependent (Ayajiki *et al.*, 1996). At the present time, the functional impact of $[Ca^{2+}]_i$ in FMD has not been fully elucidated.

4.1.4 Involvement of TRPV4

4.1.4.1 Involvement of TRPV4 in FMD

As mentioned in Chapter 1 and 3, Ca^{2+} is required for the synthesis of NO by eNOS, but the influx mechanism is a matter of debate. While several molecular candidates have been suggested to mediate Ca^{2+} influx, as discussed in Chapter 1, TRP subunit-containing channels are the most widely accepted Ca^{2+} influx pathway in ECs. Although the functional implication of Ca^{2+} in FMD is not clearly understood, reports from several labs suggest TRPV4 to be a mechano-sensitive channel that mediates EC Ca^{2+} entry in response to shear stress (Kohler *et al.*, 2006; Mendoza *et al.*, 2010; Zhang & Gutterman, 2011). Shear stress increased $[Ca^{2+}]_i$ in HEK cells overexpressing TRPV4, but not in un-

transfected HEK cells (Ma *et al.*, 2010; Ma *et al.*, 2011a; Ma *et al.*, 2011b). Stimulation of cultured human aortic ECs with GSK1016790A (100 nM), a TRPV4 agonist, and shear stress both increased $[Ca^{2+}]_i$. The observed $[Ca^{2+}]_i$ elevation was blocked by the putative TRPV4 antagonist, ruthenium red, in cultured human aortic ECs (Mendoza *et al.*, 2010). Additionally, FMD was inhibited in mesenteric arteries obtained from TRPV4-/- mice compared to that of wild types (Mendoza *et al.*, 2010). TRPV4 activities have also been reported to contribute to FMD in human coronary and rat carotid arteries (Bubolz *et al.*, 2012).

4.1.4.2 TRPV4 as a Na^+ entry pathway

Interestingly, biophysical characterization of TRPV4 subunit-containing channels revealed that TRPV4s do not discriminate between cations (Owsianik *et al.*, 2006; Ma *et al.*, 2011b). HEK cells overexpressing TRPV4 or TRPV4-C1 exhibited a non-selective cation current when stimulated with 4α-phorbol 12,13-didecanoate (4α-PDD, a TRPV4 agonist) (Ma *et al.*, 2011b). Both homomeric and heteromultimeric TRPV4 subunit-containing channels allow for Na^+ entry, with permeability ratios of Ca^{2+} to Na^+ (P_{Ca}:P_{Na}) of 7.1 and 9.2, respectively (Ma *et al.*, 2011b). Characterization of TRPV4-mediated, hypotonicity- and heat-activated currents in corneal and mouse aortic ECs, respectively, revealed an outwardly rectifying current with reversal potential of ~ 0 mV, characteristic of I_{NSCC} (Watanabe *et al.*, 2002; Mergler *et al.*, 2010).

Thus, given that TRPV4 can form channels that carry an I_{NSCC}, the potential involvement of TRPV4-mediated Na^+ entry in FMD needs to be

considered. Specifically, TRPV4 could potentially interact with NCX1 by providing the Na^+ influx to drive reverse-mode NCX activity. The observation that TRPV4 can form heteromultimeric channels with TRPC1 in both over-expression systems and native ECs and our data in Chapter 3 that elucidates the presence of a TRPC1-NCX1 signaling complex in cultured EC, suggest a potential co-localization of TRPV4 and NCX that can facilitate their functional interaction.

4.1.5 Hypothesis

To the best of our knowledge, a role for endothelial-expressed NCX in the regulation of FMD has not been studied previously. In Chapter 3, we have established NCX as a Ca^{2+} entry pathway in cultured ECs that is functionally and spatially associated with TRPC subunit-containing channels. In this chapter, we will test the hypothesis that NCX activity contributes to shear-induced changes in $[Ca^{2+}]_i$ and plays a role in FMD.

4.1.6 Objective

The main objectives of this chapter are four-fold:

(1) To evaluate if co-localization of NCX and TRPC1/TRPV4-containing channels can be detected in ECs from intact RCAs.

(2) To characterize flow-mediated dilation and flow-dependent regulation of the myogenic response in RCAs.

(3) To determine if NCX is involved in FMD using pharmacological tools.

(4) To evaluate if FMD increases phosphorylation of S1177 on eNOS in intact pressurized arteries.

4.2 Methods

Details of the methods used in this study were described in Chapter 2. Briefly, PLA was used to evaluate co-localization of proteins. FMD studies were carried out using an open system pressure myograph to allow for control of intraluminal pressure in the presence of luminal flow. Biochemical assessment of S1177 eNOS phosphorylation in endothelium of intact RCA was carried out using 3-step western blotting.

4.3 Results

4.3.1 TRPC1-NCX1 and TRPV4-NCX1 association in intact rat cerebral arteries

The PLA technique was used to investigate the co-localization of TRPC1 and NCX1 in native ECs of rat cerebral arteries (RCAs). Panels A-D of Figure 4.1 show representative serial 0.25 μm optical slices through the depth of the arterial wall (vessel is oriented vertically here and in subsequent figures), illustrating the switch in orientation of blue, Hoechst-stained nuclei from parallel to the vessel length within the endothelium (Panel A), to a perpendicular orientation within the smooth muscle layer (Panel D). To demonstrate the capability of PLA to detect proteins previously demonstrated to co-localize within native ECs, RCAs were exposed to primary antibodies recognizing eNOS and caveolin-1 (Garcia-Cardena *et al.*, 1997). Panels A-D of Figure 4.2 illustrate the presence of red PLA signals confirming the association of eNOS and caveolin-1 in ECs, with cell identity confirmed in panel A by the presence of green fluorescent co-staining for the endothelial marker, PECAM-1 (Ilan & Madri, 2003).

Figures 4.3-4.4 show ECs (confirmed by PECAM-1 staining in panels A and B in all figures and, for better visualization of PLA signals, in the absence of PECAM-1 staining in panels C and D) from PLA experiments using TRPC1 and NCX1 antibodies (Figure 4.3), and TRPV4 and NCX1 antibodies (Figure 4.4). Red fluorescent PLA signals were detected in the endothelium of RCA exposed to TRPC1 and NCX1 as well as TRPV4 and NCX1 primary antibodies (Figure 4.3 and 4.4).

Negative control experiments for PLA were carried out by exposing RCA to only NCX1 primary antibody (Figure 4.5). In the presence of only NCX1 primary antibody, PLA signals were not detected in the endothelium. Moreover, in RCAs with positive TRPC1-NCX1 PLA signals in the EC layer, PLA signals were undetected in the SMCs of the same blood vessel (Figure 4.6). These data indicate that TRPC1 and NCX1, as well as TRPV4 and NCX1, are located within 40 nm of each other in the endothelium of cerebral resistance arteries.

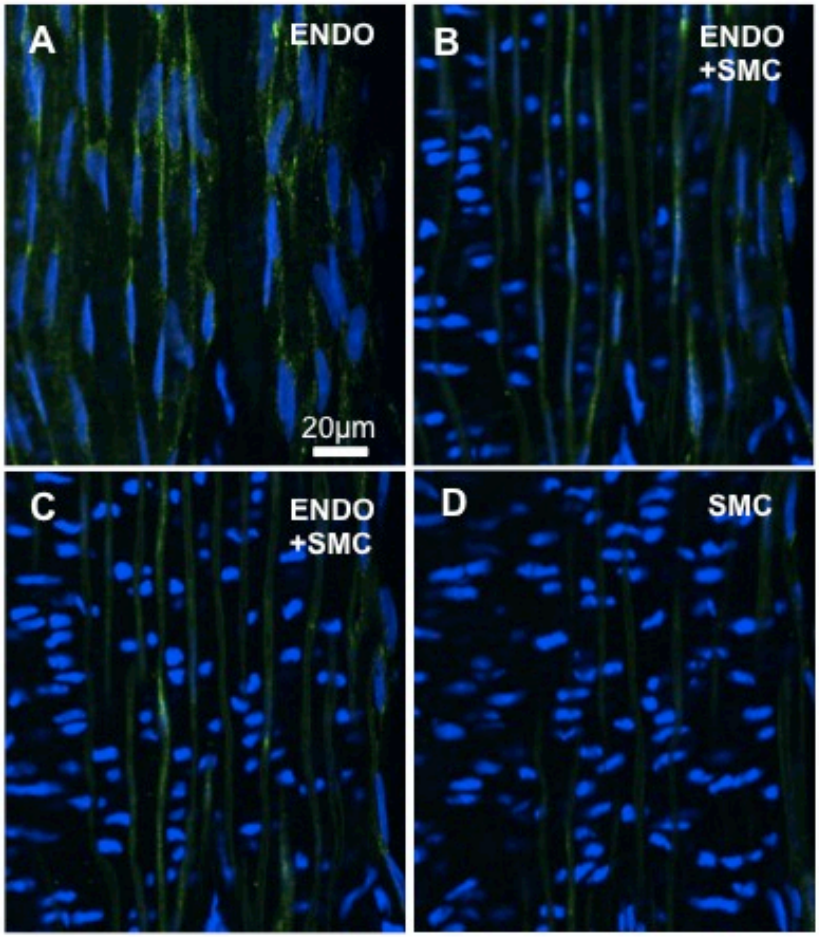

Figure 4.1: Nuclear orientation of ECs and SMCs in intact RCA

Representative images showing endothelial and smooth muscle nuclear patterns. Z-stacks of images were taken starting in the endothelial layer with long spindled shaped nuclei and positive PECAM-1 (green) staining, gradually moving into the smooth muscle layer with globular shaped nuclei and lack of PECAM-1 staining. Here and in subsequent panels, the artery is arranged with the longitudinal axis running parallel to the vertical edge of the panel and endothelial cells are identified by positive PECAM-1 (green) staining and long spindle shaped nuclei. (n = 3 experiments)

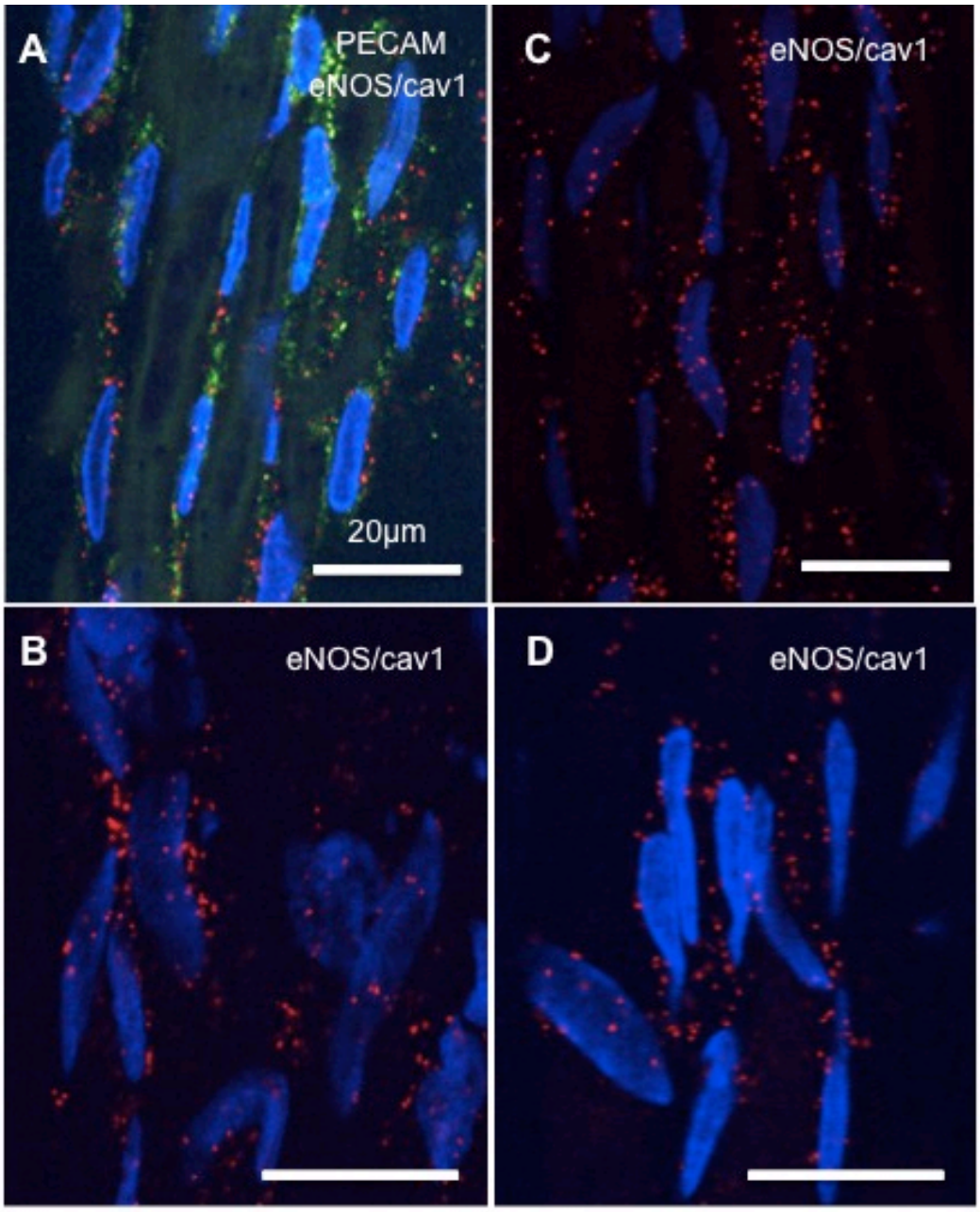

Figure 4.2: Positive caveolin-1 and eNOS PLA signals in ECs of intact RCA

Representative images of PLA reaction product, indicated by red fluorescent dots that were detected in PECAM-1-positive ECs (A) of RCA probed with caveolin-1 and eNOS primary antibodies (A-D). (n = 3 experiments)

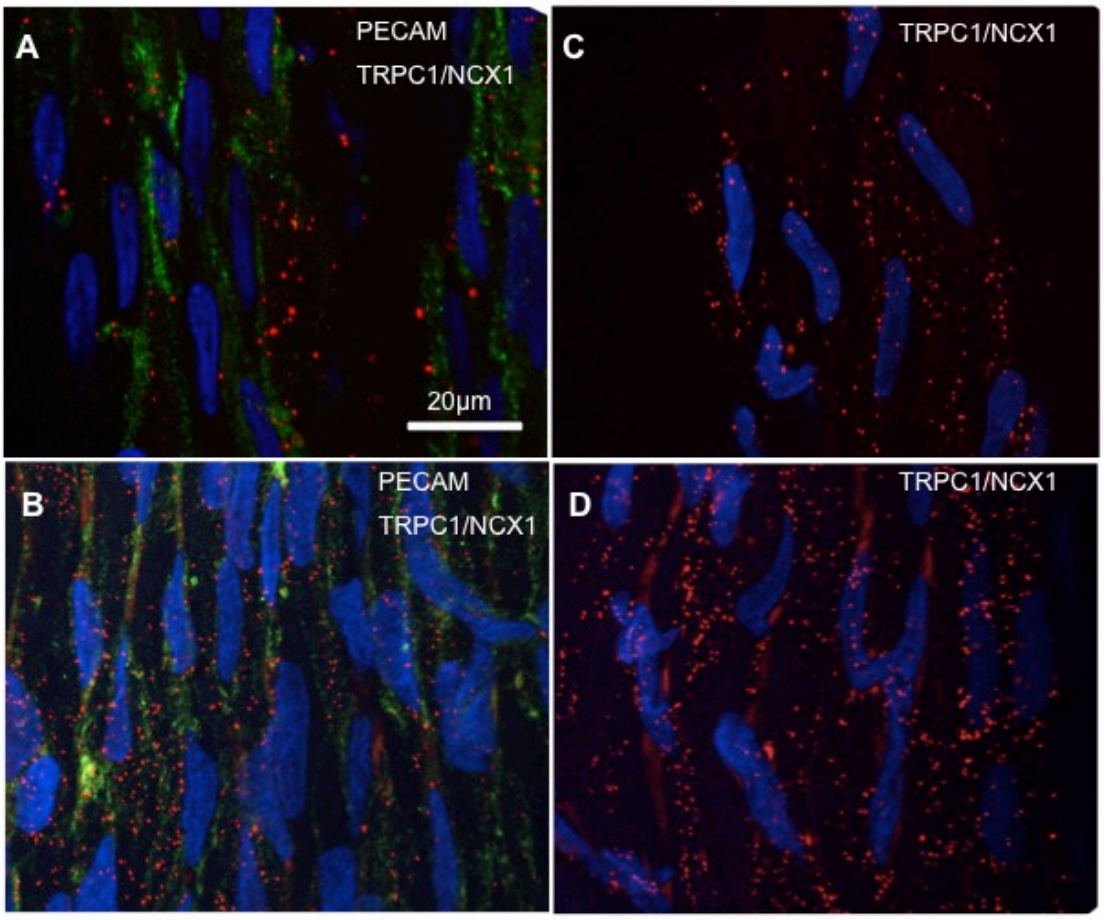

Figure 4.3: Positive TRPC1 and NCX1 PLA signals in ECs of intact RCA

Representative images of PLA reaction product, indicated by red fluorescent dots that were detected in PECAM-1-positive endothelial cells (A and B) of RCA probed with NCX1 and TRPC1 primary antibodies (A-D). (n = 5 experiments)

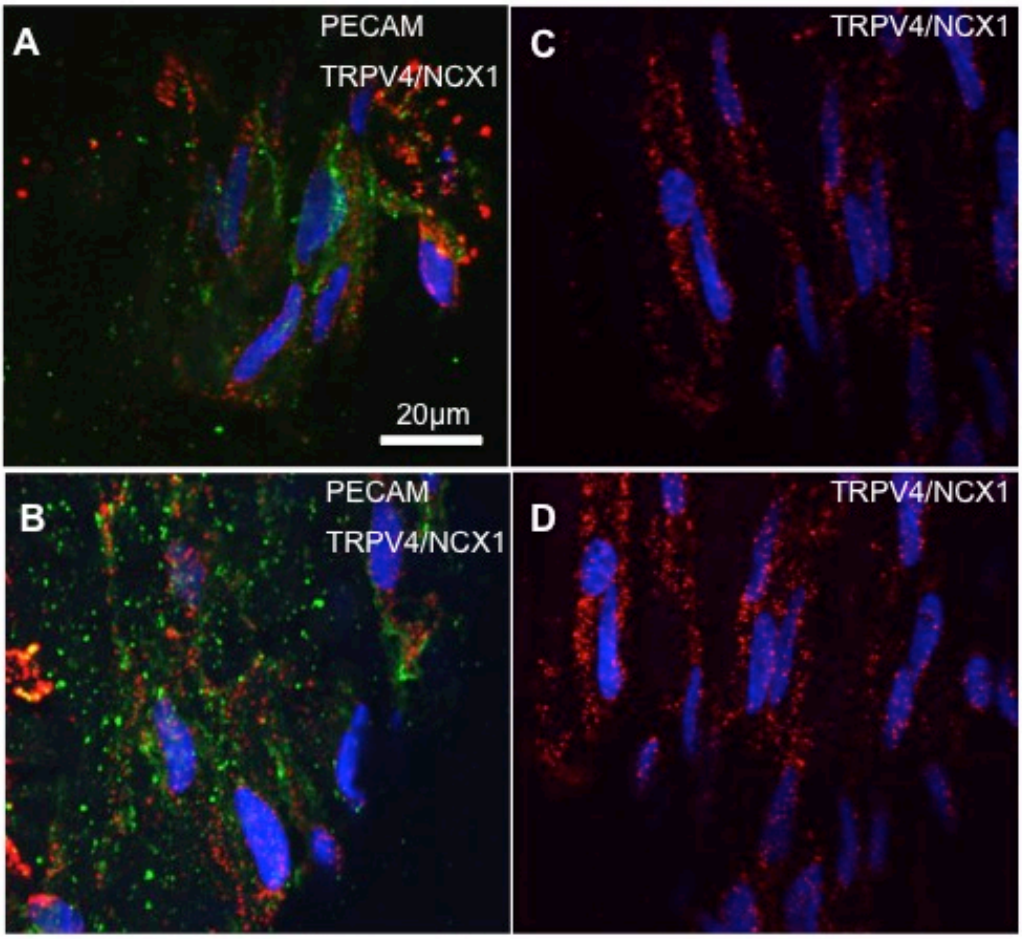

Figure 4.4: Positive TRPV4 and NCX1 PLA signals in ECs of intact RCA

Representative images of PLA reaction product, indicated by red fluorescent dots that were detected in PECAM-1-positive endothelial cells (A and B) of RCA probed with NCX1 and TRPV4 primary antibodies (A-D). (n = 4 experiments)

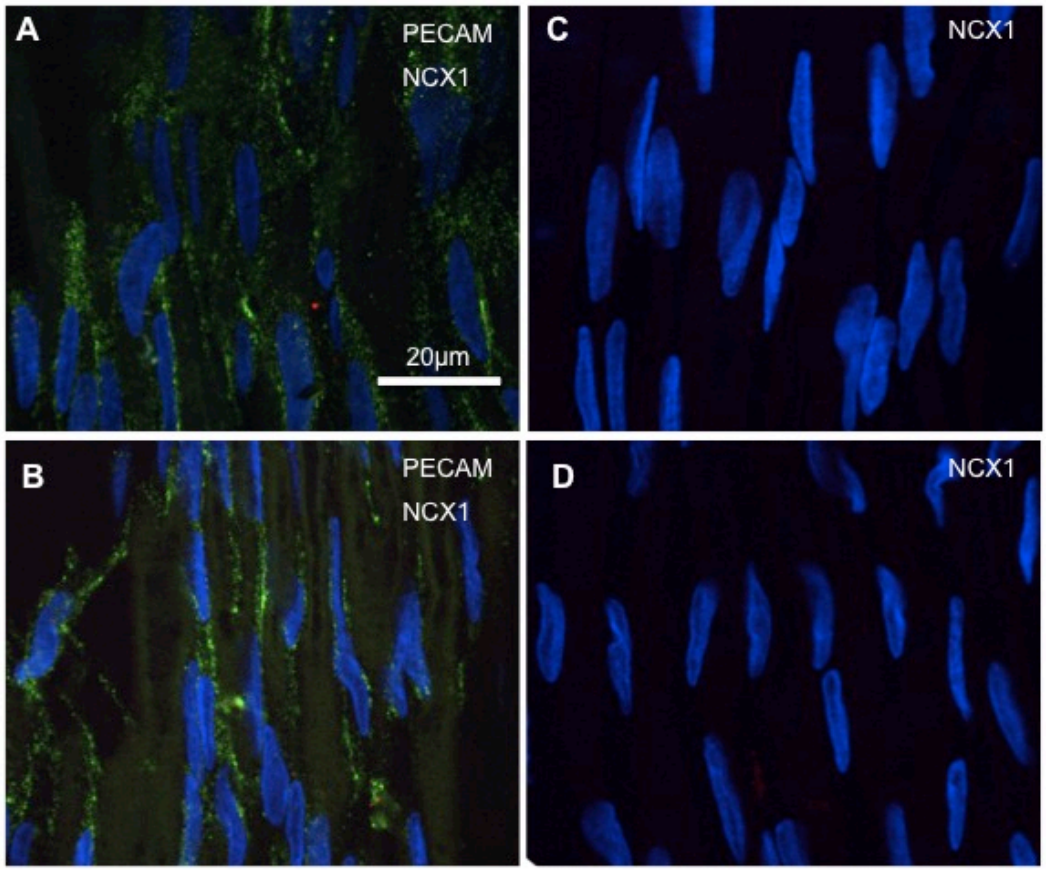

Figure 4.5: Absence of PLA signals in presence of only NCX1 primary antibody

Representative images showing negative control experiment for PLA. There was an absence of fluorescent dots detected in PECAM-1-positive endothelial cells of RCA probed with only NCX1 primary antibodies and both secondary antibodies. (n = 3 experiments)

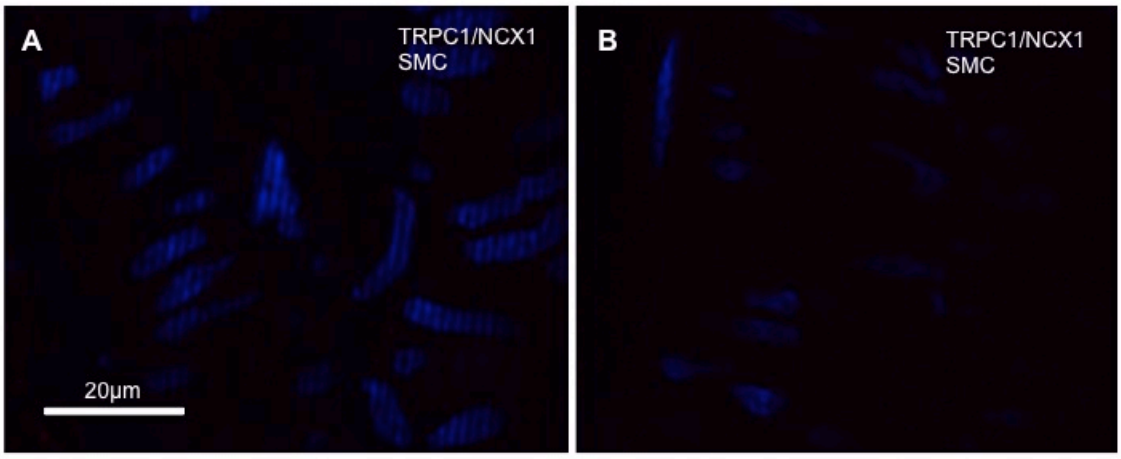

Figure 4.6: Absence of TRPC1 and NCX1 PLA signals from SMCs of intact RCA

Representative images showing an absence of TRPC1 and NCX1 PLA signals in the PECAM-1-negative smooth muscle layer of RCA. (n = 5 experiments)

4.3.2 Characterization of FMD

As this was the first study in our lab to assess the functional relationship between flow and pressure in the regulation of vascular tone in RCAs, we initially characterized flow-evoked dilation in spontaneously myogenic RCAs and determined the optimal range of flow rates for the vessels. After RCAs spontaneously developed tone at 60 mmHg, they were primed with two 5-min 80 mmHg pressure steps to ensure consistent myogenic constriction and only RCAs exhibiting acceptable functional qualities were used (> 40 μm constriction, ~ 30% of passive arterial diameter). Following tissue priming, intraluminal pressure was increased to either 60 mmHg or 80 mmHg and vessels were subjected to an increasing rate of luminal flow. Figure 4.7 shows representative traces of vasodilation evoked by increasing flow rate in RCAs pressurized to 60 (Panel Ai) and 80 mmHg (Panel Aii), with the mean flow-induced increase in diameter shown in panels Bi and Bii. We focused our attention on flow rates less than 10 μl/min; this flow rate corresponds to shear stress experienced by RCA *in vivo* and is in agreement with the flow rates that were previously used by other labs (Silver & Vita, 2006; Drouin & Thorin, 2009). The calculated shear stress for this flow rate in RCAs with a diameter 150-250 μm was 40-70 dyn/cm^2.

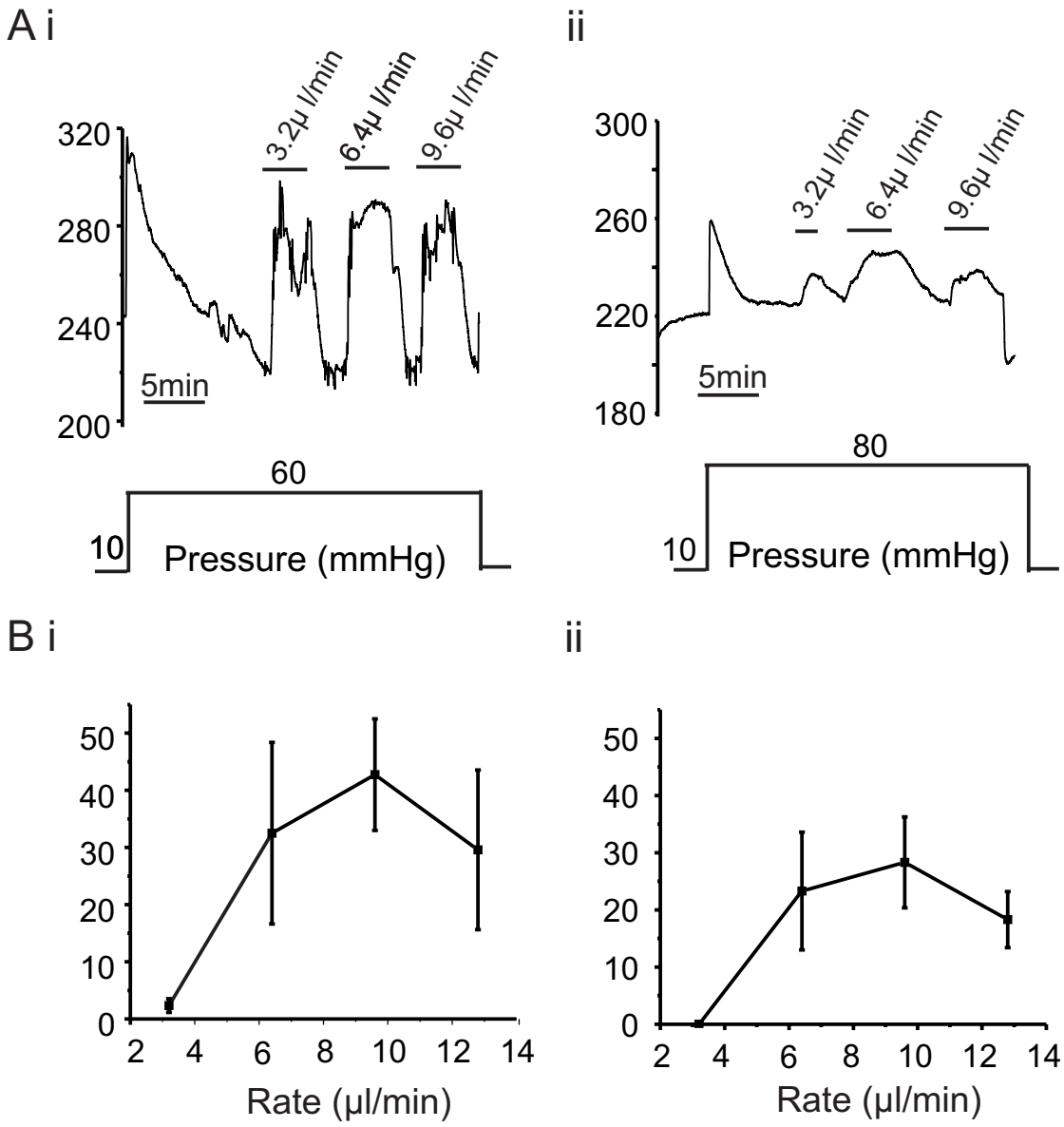

Figure 4.7: Flow-mediated dilation in RCAs

A, Representative and B, mean values ± SEM of flow-mediated dilation at increasing steps of flow rates (3.2, 6.4, 9.6 µl/min) at (i) 60 mmHg and (ii) 80 mmHg. (n = 4 for both 60 and 80 mmHg).

We observed that flow rates greater than 6.4 µl/min reliably elicited an increase in arterial diameter in RCAs and, when flow ceased, the arterial diameter returned to the baseline level. The magnitude of FMD plateaued at rates below 10 µl/min. Our goal was not to compare the effect of FMD at different intraluminal pressures but to find optimum conditions where maximal dilation in response to flow would be observed. We found that RCA at 60 mmHg exhibited greater FMD responses compared to arteries held at 80 mmHg, but this difference was not significant. Comparing the magnitude of dilation in response to a flow rate of 9.6 µl/min, at 60 mmHg and 80 mmHg, the blood vessels were dilated by 43 ± 9 µm and 28 ± 8 µm, respectively. Our observation is consistent with findings by Kuo *et al* (1990) in porcine coronary artery who showed that an increase in flow at constant intraluminal pressure resulted in increased arterial diameter (Kuo *et al.*, 1990).

To evaluate if flow-mediated dilation in RCAs was endothelium dependent, parallel experiments were conducted with endothelium-intact and endothelium-denuded vessels using the same protocol. Removal of endothelium was carried out by passing an air bubble through the lumen of the artery. Intraluminal pressure was increased to 60 mmHg and subjected to a flow rate of 9.6 µl/min. In endothelium-intact arteries, a pronounced dilation was detected (Figure 4.8A). Flow did not dilate endothelium-denuded RCAs and, in several instances, further constricted the vessel (Figure 4.8B).

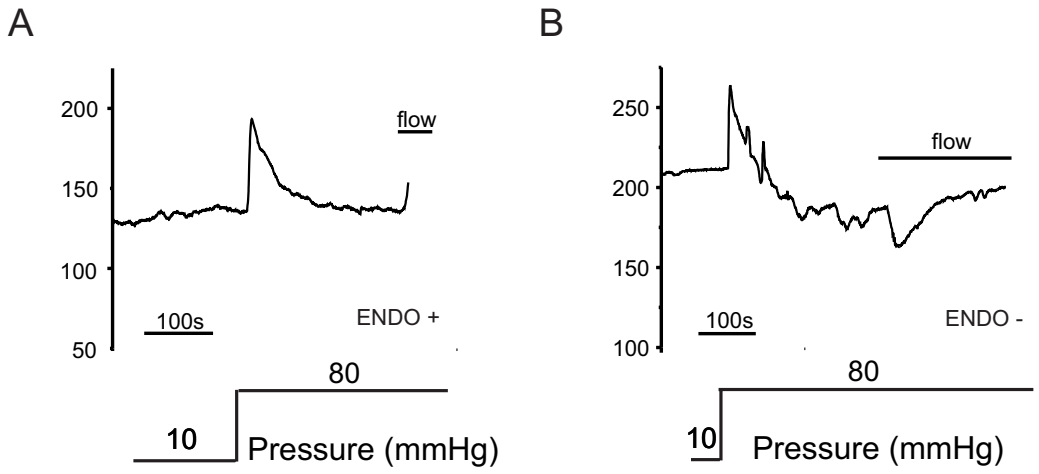

Figure 4.8: FMD requires the presence of endothelium

A, Representative recording showing the effect of flow (9.6 µl/min) in an endothelium-intact RCA. B, Representative recording of the effect of flow (9.6 µl/min) in an endothelial-denuded RCA.

4.3.3 Flow inhibits myogenic activity

The diameter responses of RCAs to sequential step increases in pressure, between 20 and 120 mmHg in 20 mmHg increments, were determined in the presence and absence of intraluminal flow and presence and absence of Ca^{2+} in the superfusate (Figure 4.9A). RCA diameter was maintained or decreased with increasing luminal pressure at pressures > ~40-60 mmHg in normal Krebs' solution whereas only passive dilation was observed in the presence of 0 Ca^{2+}-containing Krebs'. To assess the role of flow in the regulation of the myogenic response, the diameter-pressure response was repeated in the presence of intraluminal flow (9.6 µl/min). In the presence of intraluminal flow, arterial

diameters were significantly increased over the intraluminal pressure range of 60 to 120 mmHg (Figure 4.9B).

4.3.4 Pharmacological assessment of FMD

Due to variation in the magnitude of FMD in RCAs, paired experiments were conducted to assess the effects of specific inhibitors on FMD. For all experiments, we used flow rates of 6.4 and 9.6 µl/min to elicit dilations; however, FMD magnitude mean values were calculated based on data obtained at 9.6 µl/min flow rate. To ensure that repeated shear stimulation elicits a reproducible response, we carried out experiments in which RCAs were subjected to repeated periods of shear stimulation. We found that a flow rate of 9.6 µl/min elicited a comparable magnitude of dilation during repeated stimulation of the same RCA (Figure 4.11A).

Certain proteins in our study, such as TRPV4 and NCX, are expressed in both SMCs and ECs: In order to selectively inhibit the activities of these proteins in ECs, drugs were applied intraluminally. After establishing a control FMD response at intraluminal pressure of 60 mmHg, intraluminal pressure was reduced to 10 mmHg and drugs/inhibitors were applied (drug solutions were prepared in 2.5 mM Ca^{2+} Krebs' and phenol red was added to the drug solution in order to indicate the presence of the drug in the lumen). Once the drug entered the lumen, RCAs were equilibrated for 5 min to ensure sufficient incubation time for the inhibitor to take effect.

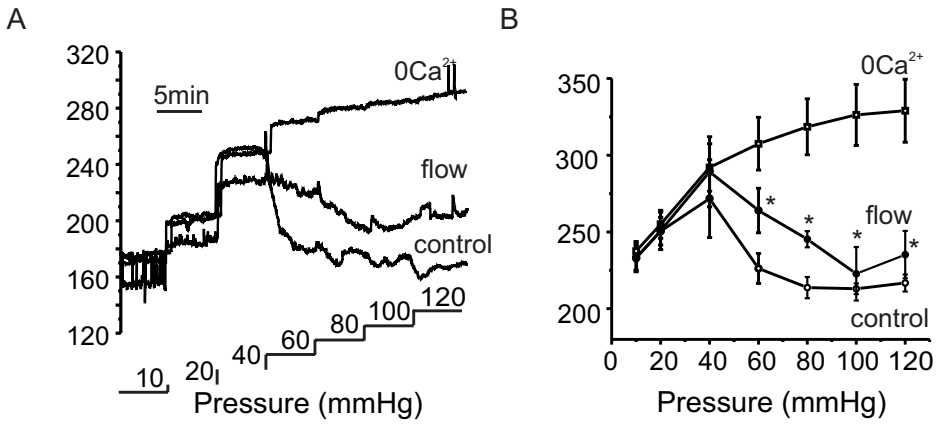

Figure 4.9: Flow opposes the myogenic response

A and B, Representative recordings and mean values ± SEM (n = 4) of RCA diameter between 10 and 120 mmHg in control conditions, at a flow rate of 9.6 µl/min flow, and in the absence of extracellular Ca^{2+} (*, $p<0.05$, paired t-test compared to control).

This standard perfusion protocol was used to assess the effects of various inhibitors on FMD unless otherwise stated.

4.3.4.1 Effects of eNOS and SK_{Ca}/IK_{Ca} inhibition on FMD

Both NO- and EDHF-mediated mechanisms have been reported to play a role in FMD (Huang *et al.*, 2001a; Huang *et al.*, 2001b; Bellien *et al.*, 2005; Watanabe *et al.*, 2005; Bellien *et al.*, 2006; Liu *et al.*, 2011), but such data are not available for RCAs. Figure 4.10A shows that the inhibition of eNOS (100 µM L-NAME) significantly reduced FMD in RCAs from 34 ± 3 µm to 9 ± 2 µm. Similarly, SK_{Ca}/IK_{Ca} inhibition by intraluminal application of 1 µM apamin + 1 µM TRAM34, (Figure 4.10C) significantly reduced FMD from 34 ± 5 µm to 13 ± 4 µm. Note that

the application of apamin and TRAM34 in the superfusate around the vessels did not affect the magnitude of FMD, as expected (Figure 4.10B).

4.3.4.2 Effects of TRPV4 antagonist, RN1734, and NCX blocker, KBR, on FMD

To evaluate if TRPV4 and NCX are involved in FMD, we investigated the effect of RN1734, a TRPV4 antagonist, and KBR on FMD. While ruthenium red has been used as the prototypical TRPV4 blocker, it has also been reported to block other channels, such as the mitochondrial Ca^{2+} uniporter (Bae *et al.*, 2003). RN1734 has been recently proposed as a selective TRPV4 antagonist (Vincent *et al.*, 2009). The effects of KBR and RN1734 were evaluated in a pair-wise fashion; the magnitude of FMD in the presence of inhibitors was compared to the control FMD response in the same artery. Intraluminal perfusion of RN1734 (1 μM) significantly reduced the magnitude of FMD from 39 ± 12 μm to 13 ± 3 μm (Figure 4.11B). A flow rate of 9.6 μl/min elicited a dilation of 20 ± 2 μm, which was significantly reduced to 2 ± 2 μm in the presence of intraluminal KBR (10 μM) (Figure 4.11C).

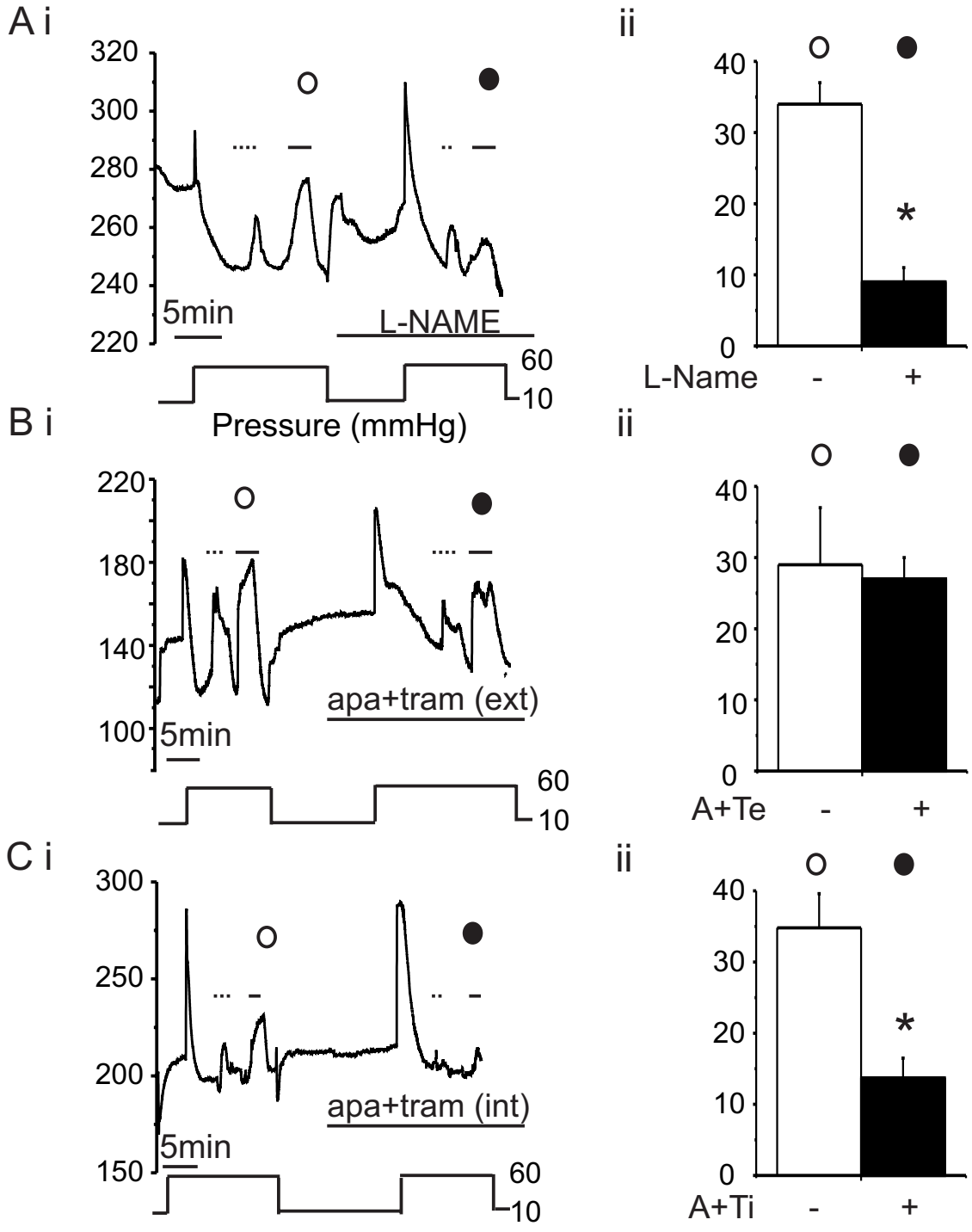

Figure 4.10: Effects of eNOS and SK_{Ca}/IK_{Ca} inhibition on FMD

Representative traces (i) and mean values ± SEM (ii) showing the effect of A, intraluminal application of L-NAME (100 μM, n = 6), B, external application of apamin and Tram-43 (1 μM and 1 μM, n = 4) and C, intraluminal application of apamin and Tram-43 (1 μM and 1 μM, n = 11) on flow-mediated dilation in a myogenic RCA held at intraluminal pressure of 60 mmHg. Dashed lines and solid lines represent flow rates of 6.4 and 9.6 μl/min, respectively. Mean values were calculated from time points indicated by circles on the representative traces at 9.6 μl/min flow rates: 1^{st} stimulus (control, open circle), 2^{nd} stimulus (treatment, closed circle) (*, $p<0.05$).

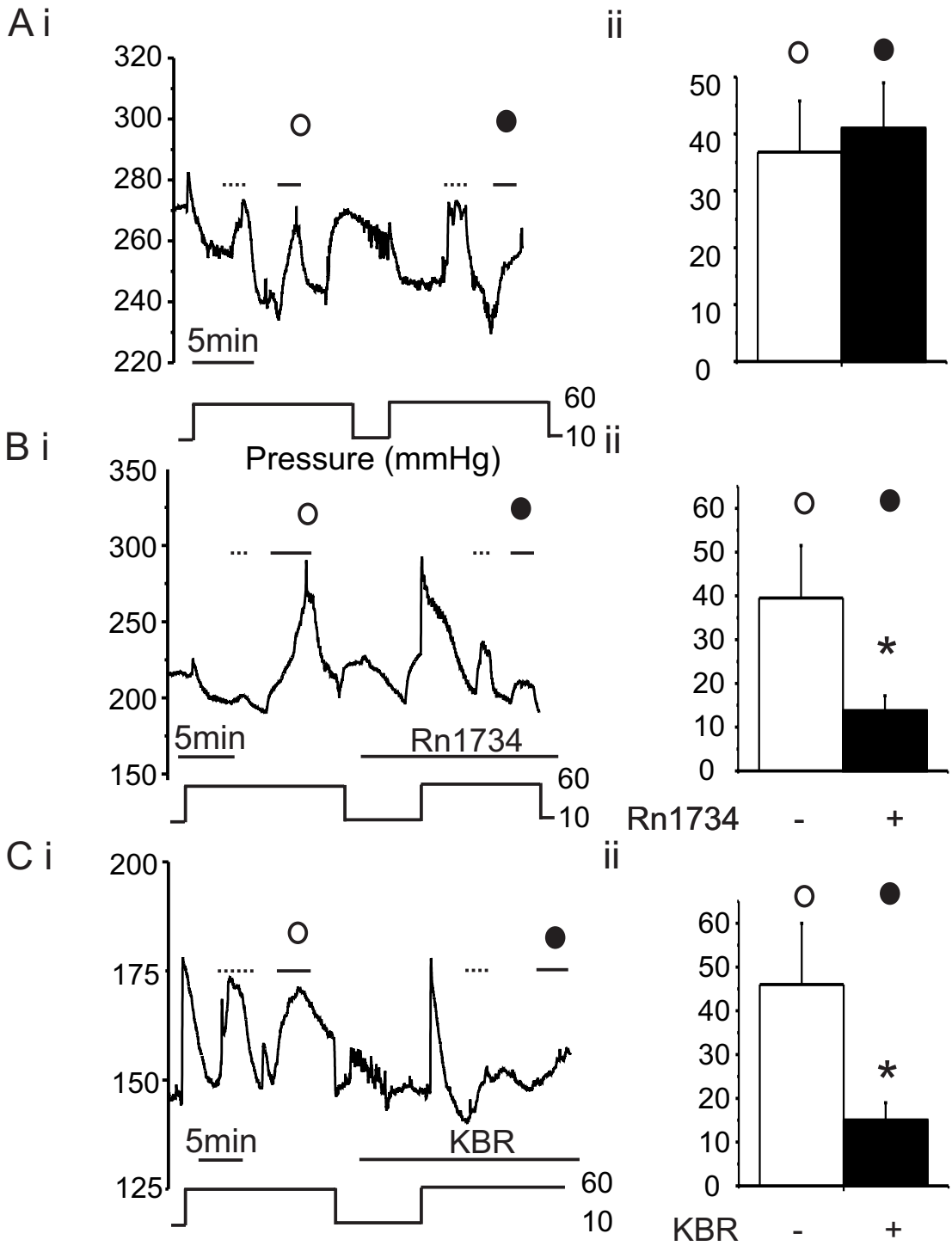

Figure 4.11 Effects of TRPV4 and NCX inhibition on FMD

A, Representative trace (i) and mean values ± SEM (n = 5) (ii) of magnitude of diameter observed at 60 mmHg elicited by flow rates of 6.4 (dashed line) and 9.6

µl/min (solid line). Repeated dilation to flow was observed in control experiments. B and C, Representative trace (i) and mean values ± SEM (ii), showing the effect of TRPV4 antagonist RN-1734 (1 µM) (B) and the NCX1 blocker KBR (10 µM) (C) on FMD at 6.4 and 9.6 µl/min. Both drugs were perfused intraluminally to limit the drug effects to the endothelium. Mean values were calculated from time points indicated by circles on the representative traces at 9.6 µl/min flow rates: 1^{st} stimulus (control, open circle), 2^{nd} stimulus (treatment, closed circle) (*, $p<0.05$).

KBR at the concentration used in this study (10 μM) has been reported to have vasomotor effects on smooth muscle as well (Dai *et al.*, 2007; Poburko *et al.*, 2007; Syyong *et al.*, 2007; Raina *et al.*, 2008). Although attempts were made to limit the effect of KBR to ECs by perfusing the drug intraluminally, it was necessary to evaluate if the observed response of intraluminal KBR was endothelium specific and not due to secondary effects on SMCs. Thus, the effect of 10 μM KBR, applied in-bath, on endothelium-intact RCAs was tested. When applied to the bath solution, KBR dilated arteries that were constricted at 60 mmHg from a diameter of 210 ± 20 μm to 244 ± 15 μm (Figure 4.12). This finding is consistent with that of Raina *et al.* (2008) where an inhibition of NCX activity reduced myogenic constriction in endothelial-denuded cremaster arteries. Since bath application of KBR increased arterial diameter, it is unlikely the observed inhibition of FMD by intraluminal KBR perfusion was due to its effect on SMC. This suggests that when perfused intraluminally, the observed KBR effects were specific to ECs.

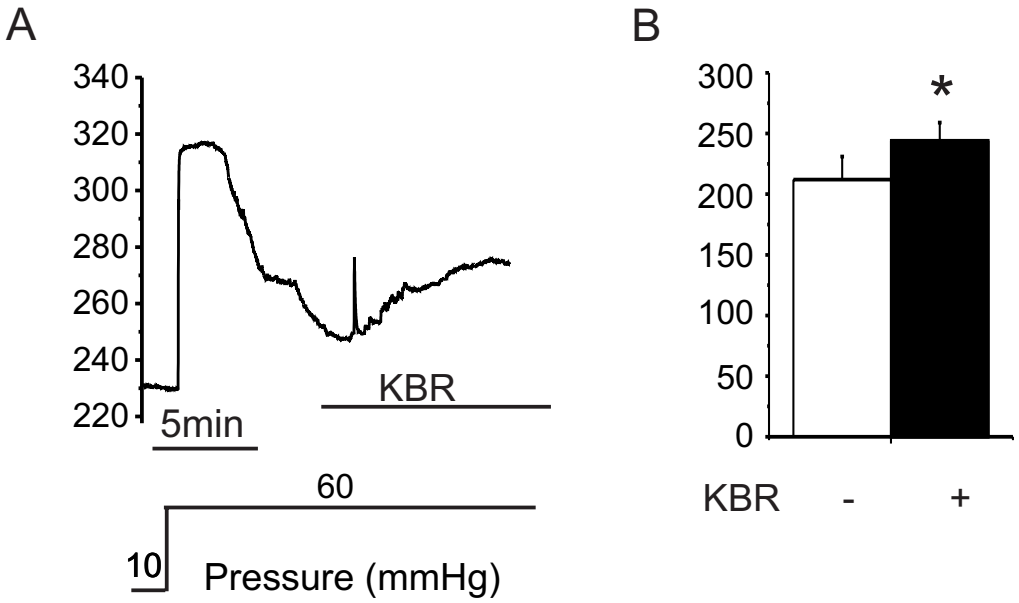

Figure 4.12: Effect of bath application of KBR on FMD

A, Representative trace and B, mean values ± SEM (n = 3) showing the effect of superfusing KBR in-bath on an endothelial-intact myogenic RCA (*, $p<0.05$, paired t-test)

4.3.4.3 Effect of NCX inhibition on FMD

As noted previously, KBR selectivity has been a source of contention and a more specific method of NCX inhibition is necessary to verify the contribution of NCX activity to FMD. XIP, a known blocking peptide of NCX, is membrane impermeable and therefore unsuitable for physiological experiments. Several other studies have used antibodies to inhibit channel activity. Specifically, antibodies against extracellular epitopes of ion channels, such as TRPC1 and C5, have been reported to inhibit channel activities (Kumar *et al.*, 2006; Xu *et al.*, 2006; Ma *et al.*, 2011a; Ma *et al.*, 2011b). To circumvent the issue of KBR

specificity, we used an NCX antibody that is generated against an extracellular epitope of NCX (6H2) as a potential NCX inhibitor. 6H2 significantly (1:500) reduced FMD from 48 ± 5 μm to 22 ± 4 μm (Figure 4.13A). As a control, we used an NCX antibody that was generated against an intracellular epitope (C2C12). C2C12 antibody (1:500 dilution) did not affect the magnitude of FMD (Figure 4.13B).

To the best of our knowledge, the use of 6H2 antibody as an inhibitor of NCX has not been reported in the literature, thus the assessment of its functional validity is crucial. The effect of 6H2 antibody on the histamine-induced $[Ca^{2+}]_i$ response in cultured ECs was investigated, since this process was shown to be dependent on NCX activity (Chapter 3). 6H2 antibody significantly inhibited the histamine-induced $[Ca^{2+}]_i$ increase, comparable to the effects of KBR and NCX siRNA transfection (Figure 4.14).

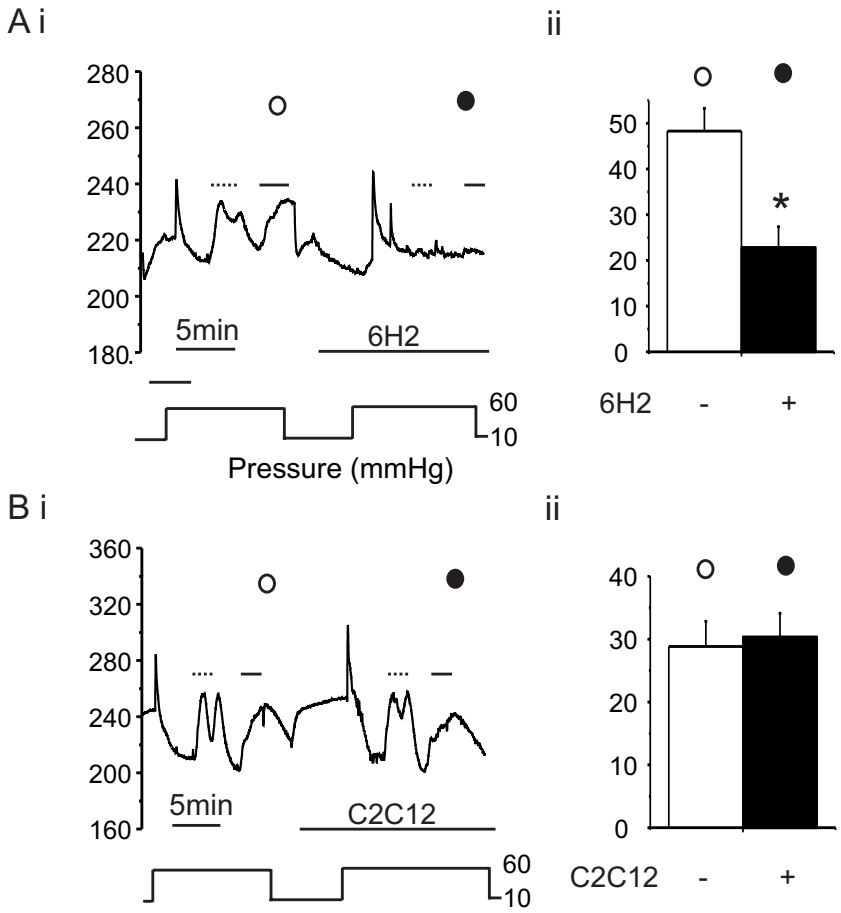

Figure 4.13: Effects of 6H2 and C2C12 NCX antibodies on FMD

A+Bi, Representative traces showing the effect of intraluminal perfusion of two NCX1 antibodies, (A) extracellular epitope-recognizing 6H2 and (B) intracellular epitope-recognizing C2C12, on FMD at 6.4 and 9.6 µl/min in intact RCAs which maintained myogenic constriction at 60 mmHg. Both antibodies were perfused intraluminally to ensure drug effects were endothelium-specific. A+Bii, Mean values ± SEM (n = 8 for 6H2, n = 6 for C2C12) of FMD were calculated from time points indicated by circles on the representative traces at 9.6 µl/min flow rates: 1st stimulus (control, open circle), 2nd stimulus (treatment, closed circle) (*, $p<0.05$).

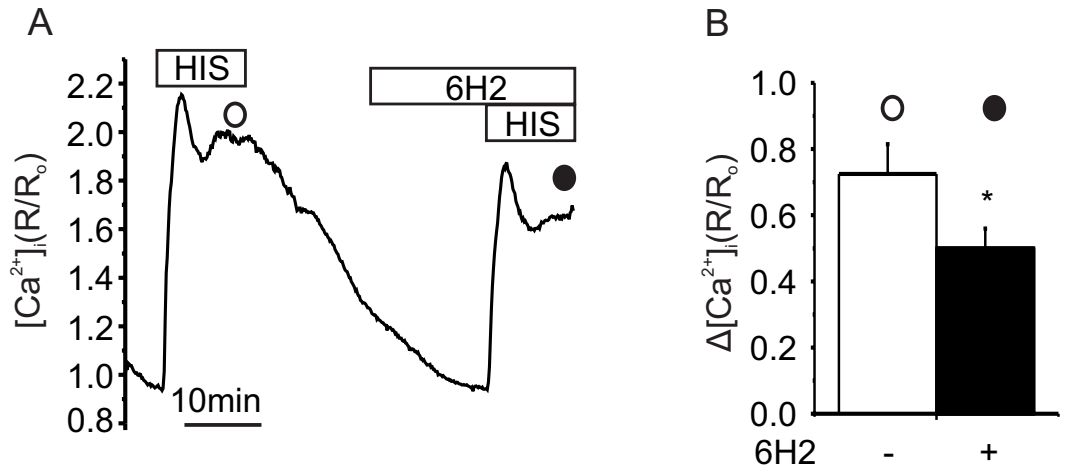

Figure 4.14: Effect of 6H2 antibody on the histamine-induced $[Ca^{2+}]_i$ increase in Ea.Hy926 cells

A, Representative trace showing the effect of the extracellular epitope-recognizing NCX1 antibody, 6H2 (1:500), on the histamine (10 μM)-induced increase in $[Ca^{2+}]_i$. B, Mean ± SEM (n=4 experiments) $[Ca^{2+}]_i$ before and after treatment with 6H2 at time points indicated by circles: control (open circle), treatment (closed circle) (*, $p<0.05$).

4.3.5 Phosphorylation of serine-1177 eNOS is dependent on NCX-mediated Ca^{2+} regulation

Data presented in Chapter 3 support the notion that agonist-induced phosphorylation of S1177-eNOS is Ca^{2+}-dependent in cultured ECs. In an analogous experiment, we aimed to test the involvement of NCX-mediated Ca^{2+} entry in shear-induced phosphorylation of S1177-eNOS in intact RCAs. Arterial segments were pressurized to 60 mmHg and subjected to the following

treatments: (1) zero flow, (2) 9.6 µl/min flow, (3) intraluminal C2C12 antibody incubation (1:500) + 9.6 µl/min flow, (4) intraluminal KBR (10 µM) + 9.6 µl/min flow, and (5) intraluminal 6H2 antibody (1:500) + 9.6 µl/min flow. Phospho-S1177 eNOS (Figure 4.15A, top panel) band intensity was normalized to pan-eNOS (Figure 4.15A, bottom panel), and each blot was normalized to the no flow pressurized treatment in the control lane to account for variability between blots.

Arteries that were subjected to 9.6 µl/min flow displayed a significant 2.6-fold increase in phosphorylation of S1177-eNOS compared to the zero-flow control. The presence of C2C12 NCX antibody did not alter the magnitude of flow-mediated phosphorylation of S1177. Flow-induced phosphorylation of S1177-eNOS was significantly inhibited in RCA samples that were treated with KBR or 6H2 antibody (Figure 4.15B). These data suggest that NCX activity is required for increased phosphorylation of S1177-eNOS during FMD.

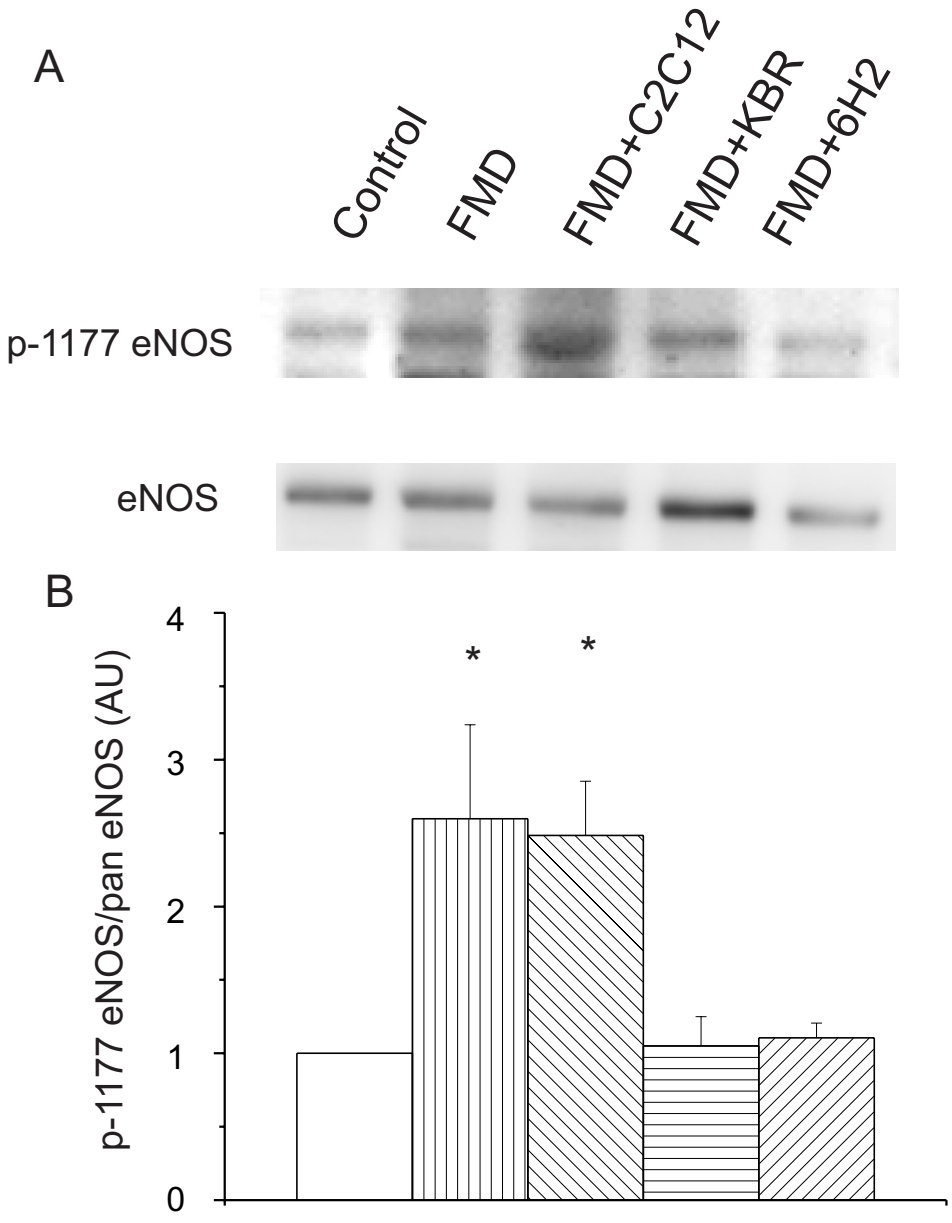

Figure 4.15: Flow-induced phosphorylation of S1177-eNOS

A, Representative western blot of phospho-eNOS-S1177 (p-1177 eNOS, top panel) and eNOS (bottom panel) in control RCAs and in RCAs stimulated by flow-mediated dilation (FMD). RCAs were either collected under control conditions (pressurized and no flow) or in the presence of flow (9.6 µl/min) with intraluminal perfusion of the following: C2C12 intracellular epitope recognizing

NCX1 antibody; KBR, 6H2 extracellular epitope-recognizing antibody. B, Mean densiometric ratio values ± SEM of phospho-eNOS-S1177 normalized to eNOS (arbitrary unit, AU) (n=4 blots, 5 RCAs per lane) in control, 9.6 µl/min flow, 9.6 µl/min flow + C2C12, 9.6 µl/min flow + KBR, 9.6 µl/min flow + 6H2 (ANOVA, followed by post-hoc test against control group, *, $p<0.05$).

4.4 Discussion

4.4.1 Summary of findings

Our observation that TRPV4/C1 co-localized with NCX1 in intact RCA endothelium provides a physical basis for the involvement of NCX in FMD. The eNOS inhibitor, L-NAME, significantly reduced the magnitude of FMD, providing evidence for the involvement of NO in FMD. Inhibition of endothelial NCX by intraluminal perfusion of KBR or 6H2 NCX antibody also significantly reduced FMD. Moreover, FMD was associated with S1177-eNOS phosphorylation, which was inhibited in the presence of NCX blockers, KBR and 6H2 NCX antibody. Thus, Na^+ entry through TRPV4/C1-containing channels was likely involved to drive reverse-mode NCX, resulting in elevation of $[Ca^{2+}]_i$ and eNOS S1177 phosphorylation, and thereby NO synthesis and vasorelaxation.

4.4.2 Interplay between TRPV4 and NCX

4.4.2.1 Implication of TRPC1-NCX1 and TRPV4-NCX1 co-localization

TRPC1-NCX1/TRPV4-NCX1 co-localization in ECs of RCA were detected by PLA, suggesting that a distance of ≤40 nm separated TRPC1 and/or V4 and NCX. Consistent with our finding in cultured cells, the occurrence of positive TRPC1-NCX1 PLA products provides the first evidence for the presence of this signaling complex in native endothelium of RCA. Although the presence of a TRPV4-NCX1 signaling complex has not been previously identified, TRPV4 has been reported to form heteromultimeric channels with TRPC1 in ECs (Ma *et al.*, 2010; Ma *et al.*, 2011a; Ma *et al.*, 2011b), suggesting TRPV4 may be a component of the TRPC1-NCX1 signaling complex. The co-localization of

TRPV4 and NCX1, and TRPC1 and NCX1, provide a physical basis for potential functional interaction between TRPC1/TRPV4 with NCX1 in endothelium of intact RCAs. No evidence of TRPC1-NCX PLA signal was detected in VSMCs of RMCAs. This result requires further confirmation as it may be an artifact arising from the inability of the PLA probes to penetrate into the SMC layer, rather than the absence of the complex in VSMCs. This view is supported by our inability to detect Kv1.2-Kv1.5 heteromultimeric channels in VSMCs within intact vessels by PLA, although they were evident in isolated myocytes (Zhong et al., 2010).

4.4.2.2 Evidence for NCX-mediated influence on FMD

TRPV4 activity has been implicated in shear and osmolality-activated Ca^{2+} influx pathways in several cell types and FMD in several vascular beds (Earley *et al.*, 2009; Mendoza *et al.*, 2010; Bubolz *et al.*, 2012) but a role for NCX in the regulation of FMD has not previously been investigated. Our data showed that KBR and 6H2 NCX antibody both significantly reduced FMD, indicating NCX activity may contribute to FMD. The use of 6H2 antibody, in addition to KBR, to inhibit NCX was a crucial experiment, allowing for the assessment of the same mechanism with a second, unrelated method for suppressing NCX activity. Moreover, the endothelium is not an impenetrable barrier and intraluminal perfusion of KBR can, with time, exert effects on SMC. For instance, it has been shown that intraluminal perfusion of KBR initially constricts RCAs, but causes dilation with prolonged exposure, suggesting intraluminal perfusion of KBR can exert effects on SMC with increased incubation time (Dr. Frances Plane, University of Alberta, unpublished observation). Specific knockdown of NCX with

siRNA is not a viable option for our study, since endothelial cells become functionally compromised during the maintenance of tissue culture. While XIP peptide has been suggested to be a specific inhibitor of NCX, its impermeability across the membrane has limited its use to whole cell patch clamping (Maack *et al.*, 2005). Here, we showed that 5 min of incubation with 6H2 (1:500) was sufficient to inhibit NCX activity. The duration of incubation is comparable to those used in functional studies employing TRPC1 antibodies, which varied from 2-30 min depending on the experimental conditions (Kumar *et al.*, 2006; Xu *et al.*, 2006).

We found that 6H2 significantly inhibited FMD while C2C12 did not exert any effect on FMD. 6H2 antibody, having been generated against an extracellular epitope of NCX, was able to exert its effect because of its access to the extracellular target. On the other hand, C2C12 did not have any effect on FMD, as it could not reach its intended target. However, this explanation for the observed effects of these two antibodies hinges on an inherent assumption that C2C12 and 6H2 have similar affinities for their respective epitopes. Although it is unlikely that C2C12 can penetrate the cell membrane and bind to the intracellular NCX epitope, the possibility that C2C12 has an extremely low affinity for NCX and therefore unable to interact with its intended target cannot be excluded. Moreover, the effect of 6H2 on FMD needs to be interpreted with caution. While there have been no reports published on the effect of 6H2 on NCX1 activity; however, given the paucity of proper NCX inhibitor, it is likely that the use of 6H2 as a NCX1 inhibitor has been studied and the lack of report may indicate no

inhibition of NCX1 activity by 6H2 is observed. Experiments are currently underway to assess the whether 6H2 specifically inhibit NCX1 in over-expression systems.

4.4.2.3 Functional interaction between TRPV4 and NCX

We found that inhibition of TRPV4 channels by RN1734 significantly reduced FMD, as did inhibition of NCX by KBR and 6H2 NCX1 antibody. These data indicate that activation of TRPV4 and NCX is associated with FMD. The reduced FMD in the presence of RN1734 and KBR is most likely due to a decrease in EC $[Ca^{2+}]_i$ in response to TRPV4 and NCX inhibition, since both RN1734 and KBR are known to block the channels/transporters directly and have not been reported to alter channel expression and/or translocation in the short term.

A proposed TRPV4/TRPC1-NCX1 linked functionality is likely since homo-multimeric TRPV4 channels and hetero-multimeric TRPC1/V4 channels have been reported to carry Na^+ influx (Watanabe *et al.*, 2002; Mergler *et al.*, 2010; Ma *et al.*, 2011b), which can activate reverse-mode NCX. Moreover, Ca^{2+} imaging experiments revealed that KBR inhibited the GSK-induced $[Ca^{2+}]_i$ increase in endothelium of intact rat heart valves (data not shown), suggesting a functional link between TRPV4 and NCX. However, functional interaction between TRPV4 and NCX in FMD has not been established within the scope of the current study. Further experiments, such as sequential inhibition of TRPV4 and NCX, would be required to determine if they overlap in function and act on the same signaling pathway.

4.4.2.4 TRPV4-mediated localized $[Ca^{2+}]_i$

Flow-induced change in EC $[Ca^{2+}]_i$ was not explicitly measured in this study but FMD was sensitive to inhibition of Ca^{2+} influx pathways (i.e. inhibition of TRPV4 and NCX activity). Other labs have demonstrated TRPV4 can generate spatially restricted Ca^{2+} signals, in conditions independent of flow, which contribute to regulation of arterial diameter (Poburko *et al.*, 2007; Bagher *et al.*, 2012; Sonkusare *et al.*, 2012). For example, TRPV4-mediated localized Ca^{2+} events were detected in the endothelium of pressurized intact rat cremaster artery. The frequency of these localized Ca^{2+} events was found to be pressure-dependent; at low luminal pressure, increased occurrence of Ca^{2+} events was observed and, at high luminal pressure, the number of Ca^{2+} events was reduced. These Ca^{2+} events were attributed to TRPV4 channel activity and occurred in discrete locations within the IEL (Bagher *et al.*, 2012). Similar localized Ca^{2+} events were observed by the Nelson group, who showed TRPV4 activation was associated with localized puncta of $[Ca^{2+}]_i$ increase, which they termed Ca^{2+} sparklets. While both groups showed these Ca^{2+} signals were effectively blocked by ruthenium red or RN1734, these data do not specifically evaluate the role of TRPV4 as the Ca^{2+} entry mechanism, they only show that TRPV4 gating is required for the generation of these Ca^{2+} events.

Several observations provide support for a potential role of NCX in mediating these localized Ca^{2+} events. Firstly, the distribution of the TRPV4-NCX1 signaling complex in the present PLA experiment resembled the cellular locations of Ca^{2+} sparklets, which were evenly distributed in the ECs with 37% of

their occurrences within the IEL (Sonkusare *et al.*, 2012). Secondly, the spatial spread of Ca^{2+} sparklets was calculated to be ~11 μm^2 in mouse mesenteric arterial ECs (Sonkusare *et al.*, 2012) and was remarkably similar in size to localized Na^+ transients observed in SMC, measured at ~ 9 μm^2 (Poburko *et al.*, 2007). Lastly, a proportion of these Ca^{2+} sparklets were found to occur within the IEL regions, where the PM and ER have been reported to be in close proximity to each other based on evidence of functional interaction between IP_3R, an ER Ca^{2+} channel, and IK_{Ca}, a PM channel (Ledoux *et al.*, 2008).

These observations indicate that NCX may play a role in the generation of these localized Ca^{2+} events; however, several questions remain to be answered: (1) does an increase in flow augment the frequency and/or amplitude of these TRPV4-mediated Ca^{2+} events? (2) are these TRPV4-mediated Ca^{2+} events inhibited by NCX blockers? and (3) are there Na^+ equivalents of Ca^{2+} sparklets occurring basally and at greater frequency upon shear stress stimulation? A more rigorous approach and co-localization studies will be needed in order to better understand the regulation of these TRPV4-mediated Ca^{2+} events and their functional relationship to NCX, both basally and in response to shear stress stimulation.

4.4.3 Role of Ca^{2+} in FMD

4.4.3.1 Necessity for $[Ca^{2+}]_i$ in FMD

The data presented in this chapter support the view that $[Ca^{2+}]_i$ is important in the regulation of FMD, consistent with the findings of several labs where TRPV4-mediated Ca^{2+} entry is associated with flow-mediated dilation in

multiple vascular beds (Pohl *et al.*, 1991; Earley *et al.*, 2009; Zhang *et al.*, 2009; Mendoza *et al.*, 2010; Bubolz *et al.*, 2012). In contrast, others have questioned whether an increase in endothelial $[Ca^{2+}]_i$ is necessary for FMD (Ayajiki *et al.*, 1996; Muller *et al.*, 1999). For example, acetylcholine and shear stress both increased $[Ca^{2+}]_i$ and elicited dilation in rabbit coronary artery; however, chelation of Ca^{2+} with BAPTA-AM treatment inhibited only acetylcholine- but not shear-induced vasodilation (Muller *et al.*, 1999). It needs to be considered that, while BAPTA-AM chelates bulk cytosolic Ca^{2+}, it is possible that a sub-PM localized increase in $[Ca^{2+}]_i$ (e.g. Ca^{2+} sparklets) is unaffected by BAPTA-AM. This could explain the persistence of flow-mediated vasodilation in the absence of a bulk cytosolic $[Ca^{2+}]_i$ increase. Thus, studying the generation of localized Ca^{2+} events during FMD could provide important insights into how $[Ca^{2+}]_i$ is involved in the regulation of FMD.

4.4.3.2 Interplay between $[Ca^{2+}]_{ER}$ and $[Ca^{2+}]_i$

Although TRPV4-mediated Ca^{2+} entry is associated with shear-induced increase in $[Ca^{2+}]_i$, TRPV4 has also been shown to be activated downstream of agonist stimulation and store depletion (Zhang *et al.*, 2009; Ma *et al.*, 2011a). Thus, the concurrent modulation of TRPV4 by shear stress and store modulation needs to be considered to allow for better understanding of mechanisms involved in the overall control of endothelial $[Ca^{2+}]_i$ in response to shear stimulation. Interestingly, shear-induced $[Ca^{2+}]_i$ increase in bovine aortic endothelial cells was found to consist of both ER Ca^{2+} release and Ca^{2+} influx (Liu *et al.*, 2011). Specifically, shear stress exposure was associated with an elevated intracellular

IP_3 concentration, leading to IP_3R-mediated Ca^{2+} release from the ER and increased $[Ca^{2+}]_i$. Interestingly, shear-induced activation of TRPV4 was shown to be modulated by $[Ca^{2+}]_{ER}$; TRPV4 activity was enhanced by ER Ca^{2+} depletion and inhibited by ER Ca^{2+} loading (Ma *et al.*, 2011a). Moreover, TRPV4s have also been reported to be activated downstream of agonist stimulation (Zhang *et al.*, 2009). These findings raise the question of whether Ca^{2+} influx alone is sufficient for initiation of endothelial $[Ca^{2+}]_i$ increase or if crosstalk between ER $[Ca^{2+}]$ and Ca^{2+} influx exists to facilitate changes in endothelial $[Ca^{2+}]_i$ in response to shear stress.

4.4.4 Molecular mechanisms underlying FMD

4.4.4.1 Phosphorylation of eNOS and NO-dependent mechanisms

Inhibition of eNOS by L-NAME significantly reduced FMD in RCAs, indicating that NO contributes to flow-induced dilation, in agreement with findings by several other groups (Pohl *et al.*, 1991; Canty & Schwartz, 1994; Koller & Huang, 1994). Here, we provided the first evidence that FMD was also associated with an increase in S1177-eNOS phosphorylation in myogenic RCA, which further supported the notion that activation of eNOS and subsequent NO production contributes to FMD. A flow rate of 9.6 µl/min (40-70 dyn/cm^2) increased phosphorylation of S1177-eNOS in RCAs by 2.6–fold, which was inhibited by 6H2 NCX antibody and KBR. This suggests flow-induced NCX-mediated Ca^{2+} entry is associated with increased phosphorylation of S1177-eNOS. However, the mechanism underlying flow-mediated phosphorylation of S1177-eNOS in RCA is uncertain. As mentioned previously, phosphorylation of

S1177-eNOS is under the control of several kinases, such CaMKII, Akt, and PKA. Although phosphorylation of S1177-eNOS by a Ca^{2+}/CaM/CaMKII-dependent mechanism in our experiment was postulated due to the sensitivity of S1177-eNOS phosphorylation to KBR and 6H2 antibody, Akt-dependent phosphorylation of S1177-eNOS has been observed in response to shear stress in cultured EC (Fleming *et al.*, 2005; Drouin & Thorin, 2009). Moreover, activation of Akt has been associated with flow-mediated dilation in mouse rat cerebral arteries (Drouin *et al.*, 2009). Therefore, a contribution of Akt in mediating S1177-eNOS phosphorylation cannot be excluded.

The Ca^{2+}-dependent phosphorylation of S1177-eNOS in response to shear stress has not been previously elucidated. This could be explained due to the fact that the majority of reported biochemical analyses of S1177-shear-induced phosphorylation have been performed in cultured ECs. Moreover, an argument has been made previously regarding the contribution of CaMKII and Akt to the phosphorylation of S1177-eNOS. The Sessa group showed that there were two populations of eNOS. One population of eNOS was located within the Golgi apparatus and Akt mediated the phosphorylation of S1177 in this group. A second population was anchored to the plasma membrane and phosphorylation of S1177-eNOS in this population was Ca^{2+} dependent (Garcia-Cardena *et al.*, 1996b). In the present study, total cellular eNOS phosphorylation was measured by western blotting and the two populations of eNOS were treated as a homogeneous population, thus Akt- and CaMKII-dependent phosphorylations of S1177-eNOS were not distinguished. Although both Akt- and CaMKII-dependent

phosphorylation of S1177 may be occurring in FMD, it was not detectable by our experimental approach. Further experiments will be required to identify the specific kinase(s) involved in the shear-induced phosphorylation of S1177-eNOS.

4.4.4.2 NO and EDHF

There is a strong association between the release of NO and FMD, but other EDRFs, such as hydrogen peroxide, reactive oxygen species, EETs, and EDHFs have been suggested as putative candidates that mediate flow-induced dilation. Our finding that intraluminal perfusion of apamin and TRAM34 inhibited FMD indicates IK_{Ca}/SK_{Ca} activation is involved in the regulation of FMD. Similarly, patch clamp experiments performed using bovine aortic endothelial cells showed that shear stress of 5-18 dyn/cm^2 increased both the frequency and magnitude of charybdotoxin-sensitive current, suggesting a role for K_{Ca}s in the shear-induced response (Hoyer *et al.*, 1998). However, in mouse mesenteric arteries pre-constricted with U46199, the combination of the K_{Ca} blockers, apamin and charybdotoxin, inhibited only acetylcholine-, but not flow-evoked vasodilatation that persisted in the presence of COX and eNOS inhibitors, indicating K_{Ca}s do not play a functional role in FMD in that vessel (Thorsgaard *et al.*, 2003).

While the differences in vascular bed could account for these mixed findings, variability in experimental conditions, such as intraluminal drug perfusion vs. superfusing drug solution could also have an impact. For example, Doughty *et al*. found that superfusing apamin and charybdotoxin did not affect endothelium-dependent relaxation, but when perfused intraluminally, this drug combination inhibited relaxation (Doughty *et al.*, 1999). This is consistent with our

finding that apamin and TRAM34 inhibited FMD only when applied intraluminally. Although SK_{Ca} and IK_{Ca} activation is associated with EDHF-mediated vasodilation, hyperpolarization of EC, E_m has been shown to influence NO production (Sheng & Braun, 2007). Inhibition of FMD by intraluminal perfusion of apamin and TRAM-34 in our experiments could be attributed to an indirect effect of these two drugs on eNOS activity, since eNOS and COX components of the endothelium-dependent relaxation were not inhibited prior to assessing the contribution of IK_{Ca} and SK_{Ca}.

4.4.5 TRPV4 as a mechanosensitive channel?

While TRPV4 expression and/or activity has been shown to contribute to increased $[Ca^{2+}]_i$ in response to flow, its role as a mechanosensor in intact cells is under intense scrutiny. Several observations indicate that TRPV4 is unlikely to be a mechanosensitive channel. Firstly, the initiation of the shear-induced $[Ca^{2+}]_i$ response was delayed for a few seconds after the onset of the stimulus in HEK cells overexpressing TRPV4. In contrast, rapid initiation was observed for TRPV4 agonist, 4α-PDD. (Wu *et al.*, 2007). The delayed onset of the response suggests TRPV4 was activated downstream of other signaling pathways and not by direct mechanical stimulation. Secondly, Ma *et al*. (2011a) showed that shear stress increased membrane expression of TRPV4 and C1; inhibition of vesicular translocation reduced membrane expression of TRPV4 and C1 and associated shear-mediated $[Ca^{2+}]_i$ increase (Ma *et al.*, 2011a). These data indicate that TRPV4 is unlikely to be a *bona fide* mechanosensor and its mechanism of activation remains elusive.

Although we focused on the role of TRPV4 and NCX1 in the regulation of FMD, other TRPs have been implicated as mechanosensitive channels as well. For example, TRPP1 and P2 channels have been demonstrated to be mechanosensitive in ECs (Nauli *et al.*, 2008; AbouAlaiwi *et al.*, 2009). TRPC6, M4, A1 subunit-containing channels have also been reported to be mechanosensitve (Spassova *et al.*, 2006; Morita *et al.*, 2007). Although a functional role for TRPM4 and TRPA1 in EC has not been clarified, the potential contribution of these other channels to the regulation of FMD cannot be excluded. It is conceivable that TRPV4 in not the only shear-activated cation-entry pathway in ECs.

Moreover, NCX1 has also been shown to be mechano-sensitive. An increase in flow enhanced reverse-mode NCX activity in conditions of reduced $[Na^+]_o$, whereas in conditions of normal physiological $[Na^+]_o$, flow enhanced forward NCX activity (Reeves *et al.*, 2008). Our experiments were carried out in the presence of physiological $[Na^+]_o$ (140 mM) and, if flow directly activated NCX, an increase in forward-mode NCX activity would have enhanced Ca^{2+} extrusion, leading to reduced $[Ca^{2+}]_i$. Since a decrease in $[Ca^{2+}]_i$ is not associated with activation of endothelium-dependent dilatory processes, it is unlikely that NCX is acting as a direct mechano-sensitive transporter in endothelium of intact RCA.

4.4.6 Limitations

4.4.6.1 Information gap

As mentioned previously, we found that inhibition of TRPV4 and NCX1 both significantly reduced FMD. Moreover, inhibition of NCX also significantly

reduced flow-mediated phosphorylation of S1177-eNOS. Although the effect of TRPV4 and NCX1 inhibition was likely due to a change in $[Ca^{2+}]_i$, further experiments will be necessary to assess the contribution of TRPV4 and NCX1 to changes in endothelial $[Ca^{2+}]_i$ during FMD. Characterization of endothelial Ca^{2+} dynamics in response to shear will allow for better understanding of the mechanisms underlying FMD (see Chapter 6).

4.4.6.2 Basal condition: pressure and flow

To determine the pressure-diameter relationship of isolated cerebral arterial segments, changes in diameter were monitored during a series of incremental increases in pressure. However, *in vivo*, mean changes in arterial blood pressure are graded, with superimposed pulsatile changes in pressure with each cardiac cycle. Thus, pressure myography does not fully simulate acute real-time changes in diameter due to fluctuations in pressure. Similarly, FMD was assessed by a sudden increase in flow from a zero-flow basal state in our experimental conditions, while arteries *in vivo* are subjected to constant flow with superimposed elevations in rate.

Interestingly, baseline flow rate that ECs are exposed to can alter their subsequent response to flow. For example, when ECs isolated from embryonic mice were exposed to pre-conditioning shear stress of 0, 1.1, or 7.2 dyn/cm^2 for 30 min prior to exposure to 10 dyn/cm^2 of shear stress (Nauli *et al.*, 2008), pre-conditioning with higher magnitude of shear stress was found to inhibit subsequent shear-induced Ca^{2+} responses (Nauli *et al.*, 2008). This finding indicates the presence of basal flow is important in the regulation of shear-

induced responses. Therefore, although our data provide evidence supporting a role for NCX in the regulation of FMD, our baseline condition of no-flow limits interpretation of our data as an artery *in vivo* is subjected to constant flow.

4.4.6.3 Pattern of flow

The changes in flow were carried out manually in our experiments in order to study the effect of flow on arterial diameter from an established baseline in the absence of flow. The consequence of this approach is that there is a delay before laminar flow can be achieved. This is significant because different patterns of flow, such as pulsatile and oscillatory flow, have been shown to exert physiological effects on ECs. For example, oscillatory flow, which exhibits sudden change in direction of the flow pattern, has been shown to alter gene expression and cell alignment in ECs (Vessieres *et al.*, 2012). Although it is unlikely that the initial non-laminar flow in our experimental set-up could contribute to the observed changes in arterial diameter in response to flow, the potential influence of the non-laminar flow needs to be considered for future experiments that may be of longer duration. Moreover, although the flow in our system is unidirectional, hence unlikely to be oscillatory, it is unclear whether the flow in our system is laminar or turbulent.

4.4.6.4 *Time course*

In our experimental set up, we opted to use short-term (< 2 min) increases in shear force to assess FMD and corresponding biochemical analysis of S1177-eNOS phosphorylation. It has been suggested that the shear-induced increase in $[Ca^{2+}]_i$ is transient and returns to base line within 5 min (Ayajiki *et al.*, 1996),

while others have reported a sustained (30 min) increase in S1177 phosphorylation in response to shear independent of $[Ca^{2+}]_i$ increase (Fleming *et al.*, 2005). Thus, time course experiments will be necessary to understand the contribution of TRPV4- and NCX1-mediated changes in $[Ca^{2+}]_i$ in association with S1177-eNOS phosphorylation (see Chapter 6).

4.5 Significance

FMD is an important physiological process involved in the regulation of blood flow. Shear stress has been suggested to play a significant role in the regulation of basal tone and act as a stimulus for long-term changes in endothelial morphology and phenotype. In human subjects, FMD also serves as a non-invasive NO bioassay and an indirect measure of endothelial function. The data in this chapter provide direct evidence of the molecular changes that occur during FMD in an intact RCA, which is important for understanding the regulation of FMD and its implication in maintenance of vascular tone.

Chapter 5: General Discussion

5.1 Summary of findings

Endothelial NO synthesis and release mechanisms have been extensively studied, particularly with respect to the role of $[Ca^{2+}]_i$. The work presented in this thesis outlines the molecular mechanisms responsible for regulating EC $[Ca^{2+}]_i$ and the implications to eNOS regulation.

In Chapter 3, our findings point to the possibility that a STIM1-TRPC1-NCX1 signaling complex may be an important component of the Ca^{2+} influx pathway necessary for the activation of eNOS. This was supported by evidence that histamine-induced $[Ca^{2+}]_i$ elevation and eNOS S1177 phosphorylation were significantly reduced during inhibition of NSCC by SKF, or NCX inhibition by KBR. Additionally, siRNA treatments to decrease expression of NCX1 and STIM1 were found to reduce the $[Ca^{2+}]_i$ elevation in response to histamine. The presence of a STIM1-TRPC1-NCX1 signaling complex was supported by TRPC1-NCX1 and STIM1-NCX co-immunoprecipitation and co-localization. Importantly, NCX1 co-localization with STIM1 was dependent on the expression of TRPC1. The data in Chapter 3 thus identified a novel signaling mechanism that is involved in the regulation of agonist-induced $[Ca^{2+}]_i$ increases in cultured endothelial cells.

Chapter 4 shows that NCX activity is associated with flow-mediated dilation in RCA and corresponding phosphorylation of S1177-eNOS. Na^+ entry through TRPV4/C1-containing channels was likely involved to drive reverse-mode NCX, resulting in elevated $[Ca^{2+}]_i$ and eNOS S1177 phosphorylation. Our

observation that TRPV4/C1 co-localized with NCX1 in intact RCA endothelium provided the physical basis for the involvement of NCX in FMD. The eNOS inhibitor, L-NAME, significantly reduced the magnitude of FMD, suggesting an NO-dependent mechanism in FMD. Inhibition of endothelial NCX by intraluminal perfusion of KBR or 6H2 NCX antibody also significantly reduced FMD. Moreover, FMD was associated with increased S1177-eNOS phosphorylation, which was inhibited in the presence of NCX blockers, KBR and 6H2 NCX antibody. The data in Chapter 4 thus provide additional evidence supporting the idea that NCX activity is important in the regulation of eNOS in response to shear stress, but in this case the data were derived from an intact artery. The combination of data from cell culture and intact vessel experiments provides strong support for the view that NCX plays a critical role in regulating endothelial Ca^{2+} dynamics and function in controlling vascular smooth muscle contractility.

5.2 Physiological role of NCX in ECs

5.2.1 Molecular mechanisms of Ca^{2+} regulation in ECs

The data presented here indicate that NCX activity regulates $[Ca^{2+}]_i$ and FMD in response to agonist- and shear-stimulation, respectively. This is consistent with findings from other labs demonstrating that NCX activities in ECs are sensitive to: (1) Na^+ concentration gradient manipulation, and (2) known NCX blockers that alter agonist-mediated changes in I_{NSCC} and $[Ca^{2+}]_i$ (Teubl *et al.*, 1999; Schneider *et al.*, 2002; Girardin *et al.*, 2010).

Although reports in the literature imply TRP subunit-containing channels are a major Ca^{2+} influx pathway contributing to the regulation of EC $[Ca^{2+}]_i$, these

findings do not necessarily preclude an involvement of NCX, as suggested by our data. In Chapter 3, we suggested that co-immunoprecipitation of TRPC1/C4 with NCX provides the physical basis for the $[Na^+]_i$-dependent activation of reverse-mode NCX. In Chapter 4, we argued that pharmacological inhibition of TRPV4 by RN1734 does not evaluate the role of TRPV4 as a Ca^{2+} entry mechanism and in reality it only shows that TRPV4 gating is required for these $[Ca^{2+}]_i$ elevations. A similar argument can be made regarding the presence of other TRP subunit-containing channels in ECs, especially if most TRP channels, with the exception of TRPM4/M5 and TRPV5/V6, display varying degrees of non-selectivity for cations (Owsianik *et al.*, 2006). For example, decreased protein expression of TRPC3, C6, C7, utilizing siRNA approaches, is associated with a reduction in agonist-induced Ca^{2+} influx in ECs (Tiruppathi *et al.*, 2002; Mehta *et al.*, 2003; Singh *et al.*, 2007; Antigny *et al.*, 2012). However, in these studies, the potential importance of Na^+ influx mediated by these channels to $[Ca^{2+}]_i$ dynamics was largely ignored. Na^+ entry through these channels could be significant, given that TRPC3, C6, C7 have reported P_{Ca}:P_{Na} values of ~ 1.6, ~ 5, and ~ 0.5, respectively (Owsianik *et al.*, 2006). Specifically, siRNA inhibition of TRPC6 significantly reduced the histamine-induced $[Ca^{2+}]_i$ increase in pulmonary arterial ECs (Singh *et al.*, 2007); however, TRPC6 has been implicated as a Na^+ entry pathway and has been shown to be functionally linked to reverse-mode NCX activity in SMCs (Poburko *et al.*, 2007). Given the significant Na^+ influx through TRP subunit-containing channels, the potential involvement of NCX in these

observed $[Ca^{2+}]_i$ responses needs to be considered, as was accomplished in the present study.

Several factors limit the interpretation of our data. Firstly, although we provided evidence that NCX plays an important regulatory role in EC $[Ca^{2+}]_i$ regulation and FMD, whether NCX is a *bona fide* Ca^{2+} entry pathway in our experimental conditions requires further investigation. A proposed increase in $[Na^+]_i$ in response to activation of TRP-containing channels would not only enhance Ca^{2+} influx through NCX, but also inhibit Ca^{2+} efflux. This phenomenon was demonstrated in dialyzed squid axons where increasing $[Na^+]_i$ enhanced Na^+-dependent Ca^{2+} influx (reverse mode) and inhibited Na^+-dependent Ca^{2+} efflux (forward mode), with forward-mode NCX completely inhibited at an intracellular $[Na^+]$ of 100 mM (DiPolo & Beauge, 1991). Although KBR is known as a selective reverse-mode NCX blocker, its directional selectivity has been questioned (Ruknudin *et al.*, 2007). Moreover, inhibition of NCX activity with an siRNA approach or blocking antibodies, which do not discriminate between forward- and reverse-mode activity, mimicked the effects of KBR. The tools utilized in this study thus do not discriminate between the relative contribution of forward- and reverse-mode NCX activity.

Convincing data demonstrating that $[Na^+]_i$ is elevated in ECs in response to agonist and shear stress has yet to be published. Measurements of $[Na^+]_i$ in ECs in response to agonist and shear stimulation are necessary for two major reasons: (1) $[Na^+]_i$ measurements would provide a functional link between TRP-channel activation and reversal of NCX, and (2) characterization of localized Na^+

transients (LNats) in ECs may provide valuable spatial information regarding the location of reverse-mode NCX activity. Specifically, agonist-stimulated LNats have been shown to correlate with reverse NCX activity, as reverse-mode NCX inhibition was associated with an increase in the frequency and amplitude of LNats in VSMCs (Poburko *et al.*, 2007). Thus, measurement of $[Na^+]_i$ and detection of LNats in ECs would allow for better understanding of the dynamic regulation of the TRPC-NCX signaling complex within ECs and the differential regulation of global and localized ionic events.

Lastly, the use of a cell culture model in Chapter 3 is a limitation of the present study. TRP protein expression has been reported to be altered by cell passages and culture conditions, so the composition of subunits of channels in native ECs may be different from that in the cultured cell model. For instance, TRPV4 mRNA transcript was not detected and $[Ca^{2+}]_i$ remained unchanged with the application of GSK in the Ea.Hy926 cells used here. This suggests TRPV4 is not expressed in Ea.Hy 926 cells. Thus, in Chapter 4, intact RCAs were used to evaluate the contribution of TRPV4 and NCX1 in FMD. However, here, a direct quantification of endothelial $[Ca^{2+}]_i$ change in response to flow was not possible. Therefore, other endpoints, such as sensitivity of FMD to known Ca^{2+} channel/transporter blockers (i.e. TRPV4 and NCX blockers) and phosphorylation of S1177-eNOS (see Chapter 5.2.2), were used as an indirect indication of changes in endothelial $[Ca^{2+}]_i$. Thus, caution must be taken in the interpretation of these data.

5.2.2 Phosphorylation of eNOS

5.2.2.1 Ca^{2+}-dependent regulation of eNOS

Our data indicate that NCX inhibition only reduces a component of the histamine-mediated increase in $[Ca^{2+}]_i$ in cultured cells, but it fully abolishes the histamine-induced phosphorylation of S1177. This suggests that a localized Ca^{2+} response rather than a change in bulk $[Ca^{2+}]_i$ may be the functionally relevant signal for the regulation of downstream physiological function. This could potentially explain why inhibition of NCX activity has an apparently greater effect on phosphorylation of S1177-eNOS than that of $[Ca^{2+}]_i$. Interestingly, shear stress-induced phosphorylation of S1177-eNOS was also completely abolished by inhibition of NCX activity. However, measurement of $[Ca^{2+}]_i$ in the ECs of RCAs during FMD would be necessary to better understand the association between NCX activity and S1177-eNOS phosphorylation in this case.

It is unclear why inhibition of NCX activity would eliminate shear- and agonist-induced phosphorylation of S1177-eNOS altogether, but this observation suggests NCX activity is crucial for the phosphorylation of S1177. On one hand, it is conceivable that NCX is closer to eNOS than NSCCs, providing a spatial advantage for the activation of eNOS. However, the area of LNats, which represent a functional link between TRPC and NCX activity, is measured at ~ 9 μm^2, putting the diameter of localized Na^+/Ca^{2+} signals near the NCX to be ~ 3 μm. This local area of signaling at 3 μm is much larger than the distance between TRPC1 and NCX1 or TRPV4 and NCX1 as indicated by our PLA experiments to be < 40 nm. Thus the location of NCX is unlikely to provide significant spatial

advantage over TRP subunit-containing channels in mediating Ca^{2+} entry for eNOS activation.

Another consideration is the difference between the kinetics of NCX- and NSCC-mediated Ca^{2+} entry. For example, NCX-mediated Ca^{2+} entry is on the order of 10^4-fold slower than Ca^{2+} entry through NSCC (Fameli *et al.*, 2009). The slower kinetics of NCX-mediated Ca^{2+} entry combined with inhibition of forward-mode NCX may prevent Ca^{2+} diffusion outside the PM-ER signaling hotspot and contribute to the sustained increase in subplasmalemmal $[Ca^{2+}]_i$ necessary for S1177-eNOS phosphorylation. However, further experiments and computer modeling relating Ca^{2+} entry kinetics to formation of the Ca^{2+}/CaM complex and subsequent activation of eNOS would be required to test this hypothesis.

In the present study, phosphorylation of S1177-eNOS was utilized as an indirect indicator of eNOS activation and NO production (Chapter 3 and 4), and $[Ca^{2+}]_i$ elevations (Chapter 4) based on known the Ca^{2+}-dependent mechanism of its phosphorylation (Fleming *et al.*, 2001). However, phosphorylation of S1177-eNOS is not under exclusive control of Ca^{2+}-calmodulin-dependent kinase. Moreover, phosphorylation of S1177-eNOS is associated with activation of eNOS, but it may not equate to NO production/release (Fleming *et al.*, 2001). Thus, although our data provide a correlation between NCX activity and S1177 phosphorylation, quantification of NO production would be a better endpoint of measurement. However, the short half-life of NO has limited the measurement of NO. Others have used fluorescent dyes for detection of NO *in situ* (Isshiki *et al.*, 2002b; Isshiki *et al.*, 2004; Sheng & Braun, 2007); however, technical difficulties

exist with simultaneous live imaging and arterial diameter measurement (discussed in Chapter 6). Griess reagent, a colorimetric assay that indirectly measures NO by detecting nitrite levels in samples, has been employed to measure serum NO levels (Fujita *et al.*, 2011). However, the Griess reagent does not allow for real-time measurement of NO released by the endothelium. Electrochemical based assays for detecting NO production (i.e. NO probe) may provide real-time measurements of NO with concurrent changes in arterial diameter and could be implemented for potential future studies (Schneider *et al.*, 2002), but at present, it is not clear that the sensitivity of the measurement will be sufficient to detect NO released from a 0.5-2 mm segment of RMCA.

Interpretation of our data is also limited by the specificity of the pharmacological tools utilized in this study. KBR, in addition to inhibition of NCX, has been reported to block TRPC channels (Kraft, 2007). Although we also employed 6H2 antibody as a more specific NCX blocker in our study, functional characterization of the 6H2 antibody has been limited. Similarly, our characterization of NSCC and TRPV4 activities was also heavily reliant on the use of pharmacological tools. Although an siRNA approach would provide more selective inhibition of targets, it is important to note that the siRNA approach requires short-term vessel culture for ~1-3 days. Not only can inappropriate culture conditions result in abnormal myogenic behaviour of vessels owing to a change in the properties of VSMCs due to removal from their normal environment, but the endothelium also becomes functionally compromised in tissue culture.

5.2.2.2 Shear and agonist modulation of eNOS

We showed that NCX activity is important for both agonist- and flow-mediated phosphorylation of S1177-eNOS, suggesting that S1177-eNOS phosphorylation is in part Ca^{2+} dependent. Both shear and agonist stimulation of ECs are associated with elevated $[Ca^{2+}]_i$ and increased S1177-eNOS phosphorylation. However, Ca^{2+}/CaM/CaM kinase II (CaMKII)-dependent phosphorylation of S1177 eNOS has been described primarily in situations of agonist stimulation whereas Akt-mediated S1177-eNOS phosphorylation appears to be common for both FMD and agonist-dependent stimulation (Forstermann *et al.*, 1991; Fleming *et al.*, 1998; Fleming *et al.*, 2001; Li *et al.*, 2004; Drouin & Thorin, 2009; Bevan *et al.*, 2011)

Interestingly, Ca^{2+}-dependent production of NO has been shown to be time dependent. For example, it was shown that $[Ca^{2+}]_I$- and CaMKII-dependent production of NO in response to shear was limited to early time points (< 15 min) in human umbilical vein endothelial cells (Kuchan & Frangos, 1994). Chelation of intracellular Ca^{2+} and inhibition of CaMKII with calmidazolium both significantly reduced shear-induced production of NO at 5 min post-stimulation, but the inhibitory effects of calmidazolium and Ca^{2+} chelation diminished after 15 min (Kuchan & Frangos, 1994). This implicates the involvement of non-Ca^{2+}-dependent mechanisms in the long-term maintenance of NO production. Thus, the discrepancy between our findings and those of others indicating that S1177 phosphorylation was Akt-dependent could be related to the time point employed for biochemical analysis. In our study, samples were collected 2 min after shear

stimulation, whereas in the majority of previous studies samples were collected after 15 min (Li *et al.*, 2004; Fleming *et al.*, 2005; Bevan *et al.*, 2011).

Although the short-term, acute exposure to shear stress in our study elucidated a potential Ca^{2+}-dependent phosphorylation of S1177-eNOS in response to flow, the short-term stimulus in itself is a weakness. As alluded to in Chapter 4, arteries *in vivo* are exposed to constant flow, which contributes to setting the basal level of eNOS phosphorylation and subsequently NO levels in determination of vascular tone. Thus, the physiological relevance of the acute application of shear in our experiments may be questioned.

5.3 Significance.

Hypertension is a condition characterized by an elevation in arterial blood pressure and is a major risk factor for stroke, myocardial infarction, and aneurysms. Salt-sensitive hypertension is of particular interest. It identifies dietary sodium as a parameter that strongly correlates with elevated blood pressure, with some individuals being more susceptible to increased dietary sodium intake (salt-sensitive) than others (salt-resistant). An upregulation of VSMC NCX protein expression level has been reported in Dahl salt-sensitive hypertensive rats (Pulina *et al.*, 2010), suggesting NCX could contribute to abnormal VSMC contraction in hypertension in response to elevated $[Na^+]_o$.

The contribution of endothelial NCX activity to salt-sensitive hypertension has not yet been elucidated; however, increased dietary Na^+ has been shown to alter endothelial function and NO production. For example, steady-state mRNA and protein levels of eNOS and Ca^{2+}-dependent NO production of isolated

glomeruli from animals on a high-NaCl (8.0%) diet were enhanced compared to animals on a low-NaCl diet (0.3%) (Ying & Sanders, 1998). Moreover, lysates from aortae and isolated glomeruli of rats on the 8.0% NaCl diet displayed increased phosphorylation of S1177-eNOS compared to samples from rats on the 0.3% NaCl diet (Ying *et al.*, 2008). Consistent with these observations, Shultz and Tolins (1993) showed that exposure of rats to high salt intake (1% NaCl drinking water) for 2 weeks induced increased serum concentration of the NO decomposition products, NO_2 + NO_3 (Shultz & Tolins, 1993). These data suggest an upregulation of eNOS expression and/or activity is associated with increased salt intake. In contrast, others have shown agonist-induced endothelial Ca^{2+} response and NO production were attenuated in aortas of rats on a high-salt diet, which was attributed to an increased level of reactive oxygen species (ROS) (Zhu *et al.*, 2006). Although it remains to be investigated whether there is a physiological basis for these varied observations (i.e. differences in regulatory mechanism in a vascular bed-specific manner, duration of high salt diet), elevated dietary Na^+ consumption appears to contribute to abnormal NO production.

Interestingly, in conditions of limited L-arginine and tetrahydrobiopterin (BH_4), a critical cofactor for eNOS activity, eNOS can become “uncoupled” and convert to a ROS-generating enzyme (Hoang *et al.*, 2013). Thus, although upregulation of eNOS expression may appear beneficial by increasing NO output, increased eNOS activity and/or expression can enhance depletion of L-arginine and BH_4 and contribute to ROS generation. The ROS generated by

eNOS can rapidly inactivate NO and further decrease NO bioavailability. Moreover, phosphorylation of eNOS at S1177 has been shown to enhance ROS production (Chen *et al.*, 2008). These data suggest that, depending on the physiological environment in the vasculature, increased eNOS activity could reduce NO bioavailability. In support of this idea, L-arginine administration was found to momentarily decrease blood pressure and correct for endothelial defects in rats maintained on a high-salt diet (Chen & Sanders, 1993). The increased availability of L-arginine was postulated to enhance NO production.

Although a role for endothelial NCX in salt-sensitive hypertension has not been elucidated, its potential role in response to sustained elevation in $[Na^+]_o$ needs to be considered, especially if NCX activity is important in the maintenance of endothelial $[Ca^{2+}]_i$ and phosphorylation of S1177 as our data suggest. The findings in this thesis provide evidence in support of a role for endothelial NCX in the physiological regulation of eNOS, which may permit elucidation of the potential involvement of this mechanism in dietary salt-induced alteration in eNOS function.

5.4 Conclusions

The endothelium is considered to be a key determinant of vascular health with the appropriate release of NO from ECs being critical for normal physiological functioning of the cardiovascular system. NO is a principal mediator of endothelial protective effects, contributing to blood pressure regulation through its ability to induce smooth muscle relaxation and arterial dilation, but also by its anti-inflammatory and anti-proliferative properties. Regulation of EC $[Ca^{2+}]_i$ plays

an important role in the coordinated release of NO. The findings presented in this thesis focused specifically on identifying novel elements in the regulation of endothelial $[Ca^{2+}]_i$, including: (1) NCX1 functionally and spatially interacts with TRPC1 to play a role in the regulation of agonist-induced $[Ca^{2+}]_i$ and (2) functional involvement of NCX1 in the regulation of FMD. Precisely how these mechanisms, represented in Figure 5.1, are integrated into the overall regulation of endothelial $[Ca^{2+}]_i$ and how these mechanisms are altered in cardiovascular disease represent intriguing areas for future study.

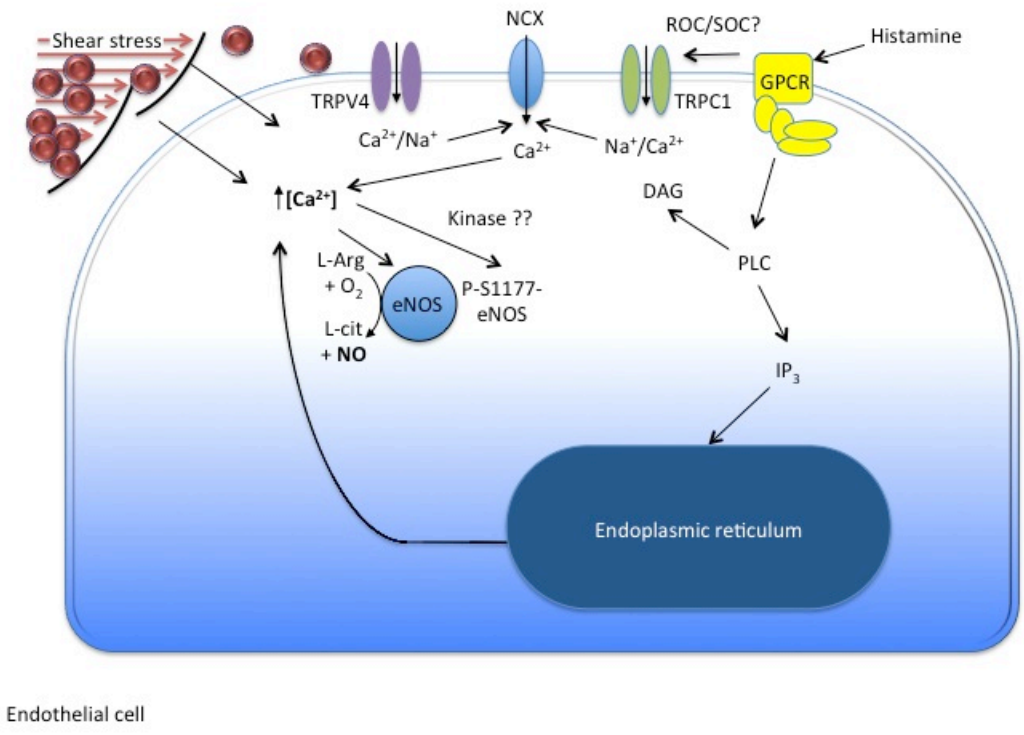

Figure 5.1: Proposed activation mechanism of NCX downstream of agonist and shear stress stimulation. In response to agonist stimulation, activation of TRPC1 subunit-containing channels allow for influx of Na^+ and Ca^{2+}, the increase in $[Na^+]_i$ can allow for Ca^{2+} entry through NCX. Shear, on the other hand, activates TRPV4-containing channels allowing for influx of Na^+ and Ca^{2+}, and subsequent increase in $[Na^+]_i$ allow for Ca^{2+} entry through NCX. In both scenarios, phosphorylation of eNOS at S1177 downstream NCX-mediated Ca^{2+} entry likely contributes to the activation of eNOS and NO production.

Chapter 6: Future Directions

6.1 Summary of the most intriguing future directions

Spatio-temporal control of $[Ca^{2+}]_i$ is important in the regulation of endothelial cell function and the coordinated release of NO. However, several aspects of EC $[Ca^{2+}]_i$ and consequent functional regulation warrant further investigation and these will be discussed in this chapter.

Firstly, our data indicate that inhibition of NCX in the endothelium in intact RCA reduced FMD and eNOS-S1177 phosphorylation. Although an NCX-mediated increase in $[Ca^{2+}]_i$ likely enhances CaM binding to eNOS and CaMKII-dependent phosphorylation of S1177 (Fleming *et al.*, 2001), further experiments will be necessary to determine the specific kinase(s) involved in the phosphorylation of S1177 in our experimental conditions. This may offer an understanding of the link between Ca^{2+} and eNOS activation in ECs in response to shear-stimulation. For example, the role of CaMKII could be tested by applying selective inhibitors of this kinase, such as KN-93 and KN-62, or peptide inhibitor, such as autocamtide 2-related inhibitory peptide, prior to stimulating Ca^{2+} influx with flow, and quantifying the extent of eNOS phosphorylation at S1177 by western blotting with phospho-specific anti-S1177-eNOS (Nie *et al.*, 2007; Brooks & Tavalin, 2011). KN-92, an inactive derivative of KN-93, could be used as a negative control (Brooks & Tavalin, 2011).

Secondly, the data presented in this thesis indicate that exposure of endothelium to shear stress contributes to regulation of RCA diameter. However,

the mechanisms by which flow alters smooth muscle contractility have not been extensively characterized. VSMCs are responsible for force generation in the regulation of arterial diameter; thus, understanding how factors that are intrinsic and extrinsic to VSMCs integrate and co-operatively control arterial diameter would contribute to our understanding of the regulation of vascular tone (see Chapter 6.2.3.4).

6.2 Additional future areas of research

6.2.1 Potential role of NCX as part of another signaling complex

NCX-mediated Ca^{2+} entry has been suggested to play an important functional role in several cell types. For example, NCX activity has been shown to be necessary in the maintenance of $[Ca^{2+}]_{ER}$ in SMC and inactivation of L-type VGCC in cardiomyocytes (Pott *et al.*, 2005; Dai *et al.*, 2007; Hirota *et al.*, 2007b). However, with the exception of a role for NCX-mediated Ca^{2+} entry in NO production, the functional implication of NCX-mediated Ca^{2+} entry in endothelial physiology is still largely unknown and warrants further investigation.

6.2.1.1 Possible role in EC permeability

As described in Chapter 1, the endothelium lines the blood vessel and maintains a barrier between blood and tissues. The endothelial barrier function is tightly maintained and, when compromised, pathophysiology ensues. Barrier function is influenced by endothelial contraction; as endothelial cells contract, intercellular junctions between cells become permeable, rendering the barrier leaky. Endothelial contraction is mediated by signaling mechanisms similar to those in SMC (see Chapter 1). For example, phosphorylation of LC_{20} activates

non-muscle myosin II and initiates cross-bridge cycling leading to contraction in ECs. Phosphorylation of LC_{20} is mediated by a Ca^{2+}-dependent MLCK pathway and is associated with RhoA activation (Mehta & Malik, 2006). Although activation of RhoA has been shown to be associated with an increased level of LC_{20} phosphorylation, the signaling mechanisms downstream of RhoA in ECs are less well characterized.

Barrier function is known to be altered due to increased $[Ca^{2+}]_i$, so the role of NCX in controlling this important facet of endothelial function should be determined. TRPC4- and TRPC6-mediated Ca^{2+} entry in response to stimulation by inflammatory agonists, such as thrombin and histamine, has been implicated in the regulation of pulmonary aortic EC barrier integrity (Mehta *et al.*, 2003; Paria *et al.*, 2004; Singh *et al.*, 2007). Ca^{2+} entry through TRPCs is thought to contribute to the $[Ca^{2+}]_i$ increase, which leads to LC_{20} phosphorylation and contraction (Singh *et al.*, 2007). Interestingly, decreased expression of TRPC6 has been shown to not only inhibit LC_{20} phosphorylation but also reduce RhoA activation and actin stress fiber formation (Singh *et al.*, 2007).

As our data in Chapter 3 indicated, NCX is important in the regulation of histamine- and thrombin-induced changes in $[Ca^{2+}]_i$. Its activity is likely to be functionally and spatially linked to TRPC1 and TRPC4, but the possibility of co-localization between NCX and other TRP channels in ECs cannot be excluded (Rosker *et al.*, 2004; Eder *et al.*, 2007; Poburko *et al.*, 2007). Given that changes in LC_{20} phosphorylation are in part dependent on $[Ca^{2+}]_i$ and that knockdown of TRPC reduces the agonist-evoked increase in $[Ca^{2+}]_i$, it is conceivable that NCX-

mediated Ca^{2+} entry in EC may play a role in the regulation of endothelial permeability. Investigation of whether NCX-mediated changes in $[Ca^{2+}]_i$ contribute to changes in EC barrier integrity would be an interesting future direction of study. For instance, Boyden chambers could be used to measure histamine- and/or thrombin-induced changes in transendothelial resistance and the contribution of NCX could be evaluated by inhibiting NCX activity by KBR or siRNA approaches.

6.2.1.2 Interplay between $[Ca^{2+}]_i$ and EC Em hyperpolarization

As mentioned previously (Chapter 1.8.1), endothelial E_m provides the driving force for Ca^{2+} entry. Several laboratories have shown that SK_{Ca}/IK_{Ca} activities influence agonist-induced $[Ca^{2+}]_i$ and NO production (Stankevicius *et al.*, 2006; Sheng & Braun, 2007; Raqeeb *et al.*, 2011). Conversely, $[Ca^{2+}]_i$ also contributes to the regulation of E_m; for example, TRPC3 inhibition has been reported to reduce K_{Ca}-mediated E_m changes in rat mesenteric arteries (Senadheera *et al.*, 2012). Moreover, activation of TRPV4 is thought to enhance IK_{Ca}/SK_{Ca}-mediated vasodilation (Kohler *et al.*, 2006; Earley *et al.*, 2010; Bagher *et al.*, 2012).

A role for NCX in E_m regulation has been suggested; inhibition of NCX by KBR has been shown to reduce acetylcholine-mediated hyperpolarization of EC in intact rabbit mesenteric artery (Bondarenko, 2004). It is unclear whether reverse NCX-dependent changes in E_m are due to the electrogenic nature of NCX during activation, or NCX-mediated Ca^{2+} entry is a necessary component for the activation of SK_{Ca}/IK_{Ca}. Certain experiments will help to clarify this issue,

such as concurrent $[Ca^{2+}]_i$ and E_m measurements in the presence and absence of NCX inhibitors and assessment of co-localization of NCX and the K_{Ca}s, based on the approaches employed in the present study.

6.2.1.3 Cellular distribution of NCX

As mentioned in Chapter 3, strategic positioning of ion channels/transporters in the endothelium is important for the regulation of specific physiological responses (e.g. activation of eNOS). In addition to the distribution of signaling molecules within the cell, apical versus basal (towards/away from the lumen of the blood vessel) organization of endothelial membrane proteins in intact arteries is important as well. Specifically, protein expression in the endothelium of intact RCA has been shown to display distinct polarity (Cornford & Hyman, 2005). Although the cellular locations of several proteins in ECs, such as eNOS, TRPC1 and IK_{Ca}, have been shown to be functionally important (Garcia-Cardena *et al.*, 1996b; Murata *et al.*, 2007; Ledoux *et al.*, 2008; Bagher *et al.*, 2012), systematic investigation of NCX distribution in endothelium of intact arteries from different vascular beds is lacking.

Systematic investigation of the distribution of NCX in the endothelium of an intact artery would help to identify potential downstream targets reliant on NCX-mediated Ca^{2+} entry for activation or inhibition. For example, our data demonstrated a role for NCX in FMD, suggesting NCX may be expressed apically if NCX was activated via a direct mechanosensitive mechanism. However, the presence of NCX at the basal surface may also be possible if NCX was activated by second messenger signals in response to shear stress. Thus,

studying the localization of NCX in EC may provide helpful insights concerning its functional role. Evaluation of NCX localization within ECs in multiple vascular beds would not only provide insights into the role of NCX as a Ca^{2+} regulatory mechanism, but also whether NCX is a common Ca^{2+} entry mechanism for ECs in different vascular beds.

6.2.2 Dynamic changes in $[Ca^{2+}]_i$ and $[Na^+]_i$

6.2.2.1 Concurrent measurements of endothelial $[Ca^{2+}]_i$ and pressure myography

As mentioned previously, a role for Ca^{2+} in FMD is debated. The observed inconsistencies in the findings of previous studies may arise from the exclusive Ca^{2+} measurements in cultured ECs rather than native cells *in situ*. Moreover, bulk $[Ca^{2+}]_i$ was measured rather than local changes, such as subplasmalemmal $[Ca^{2+}]_i$ as accomplished by Isshiki *et al* (2002b) using caveolae-targeted Ca^{2+} sensor molecules. FMD studies in ECs from intact arteries have mostly been limited to experiments in which arteries were cut open with the EC positioned upward, facing the direction of flow. Localized hot spots of Ca^{2+} signaling were recently detected in ECs of pressurized rat cremaster arteries and mouse mesenteric arteries (Bagher *et al.*, 2012; Sonkusare *et al.*, 2012), but the effect of flow on these Ca^{2+} hotspots was not characterized. Further experiments will be necessary to characterize $[Ca^{2+}]_i$ in response to shear stress in intact pressurized arteries in order to better understand the generation of localized Ca^{2+} signals and whether they contribute to the regulation of FMD.

The execution of these experiments is limited by a major technical difficulty associated with $[Ca^{2+}]_i$ measurements in pressurized arteries that exhibit the myogenic response. Live imaging requires tissue to remain static to ensure the obtained measurements are representative of cellular processes independent of movement artifacts resulting from arterial constriction or dilation. Although agents such as ML-7 and wortmannin, MLCK inhibitors, have been used to prevent contraction, inhibition of contraction could alter the $[Ca^{2+}]_i$ response. For instance, it has been suggested that changes in signaling in the smooth muscle layer during contraction can influence endothelial $[Ca^{2+}]_i$ levels (Dora *et al.*, 1997; Bohlen *et al.*, 2009). Despite such issues, measurement of endothelial $[Ca^{2+}]_i$ in response to FMD in intact myogenic RCA would be an important future direction of study as it would allow for characterization of the temporal relationship between changes in $[Ca^{2+}]_i$ and arterial diameter, which would provide valuable insight into the Ca^{2+} dependency of FMD.

6.2.2.2 Agonist- and shear-stimulated changes in $[Na^+]_i$

An increase in global and localized $[Na^+]_i$ upon agonist stimulation is the fundamental basis which favors the activation of reverse-mode NCX activity (Arnon *et al.*, 2000a; Paltauf-Doburzynska *et al.*, 2000; Poburko *et al.*, 2007). Although the presence of NSCC currents in cultured ECs provides evidence supporting the view that Na^+ entry occurs in response to agonist, a limited number of studies have characterized changes in $[Na^+]_i$ in native ECs (Paltauf-Doburzynska *et al.*, 2000). In Chapter 3, we provided evidence supporting the presence of a TRPC1-NCX1 signaling complex in EC but recognized that

agonist-induced changes in $[Na^+]_i$ warrant further study. In Chapter 4, we suggested that close apposition between TRPV4-NCX1 could provide the physical basis for their potential functional interaction. Given that TRPV4-containing channels have the capacity to carry Na^+, an increase in $[Na^+]_i$ in response to shear is likely (Ma *et al.*, 2010). Changes in $[Na^+]_i$ in response to stimulation, either agonist or shear, have never been visualized in ECs from intact arteries. Direct visualization of $[Na^+]_i$ in intact arterial endothelium in response to shear stimulation will provide direct functional support for the mechanism proposed in this thesis.

6.2.3 Molecular mechanisms of FMD

6.2.3.1 Regulation of basal tone

An artery *in vivo* is constantly exposed to flow and pressure. The interplay between flow and pressure basally would influence vascular tone due to: (1) inherent myogenic activity of VSMC in response to changes in luminal pressure, and (2) input from endothelium-dependent release of vasoactive substances from constant exposure to shear stress. The combined effects of these two mechanisms are important in the determination of the “basal” level of vascular tone and regulation of arterial diameter.

As mentioned in Chapter 4, a major limitation of our study is that FMD was assessed by acute increase in shear stress from a zero-flow resting state, compared to constant exposure to flow sensed by an artery *in vivo*. The magnitude of the “basal” flow experienced by ECs has been shown to affect resting levels of eNOS phosphorylation, for example, increased S1177-eNOS

phosphorylation was observed in ECs that experienced a prolonged elevation of shear stress (Gambillara *et al.*, 2006). Moreover, the magnitude of "pre-conditioning" basal flow also affected the ability of ECs to respond to a subsequent increase in flow (Nauli *et al.*, 2008). Thus, it would be necessary to study the effect of FMD in conditions where the artery is experiencing a basal level of constant flow in order to better reproduce the precise environment experienced by the artery *in vivo*. Using the experimental approaches employed in Chapter 4, the effect of constant flow on endothelial cellular mechanisms, such as eNOS activation and NO production, can be elucidated and may contribute to the understanding of basal tone regulation.

6.2.3.2 Time course studies

In our study, phospho-protein analysis of S1177-eNOS was accomplished using RCAs that were collected after 2-min exposure to intraluminal flow. To better understand the mechanism of eNOS activation in FMD, time-course studies will be necessary to establish whether maintenance of arterial diameter during FMD correlates with a sustained increase in S1177-eNOS phosphorylation. Moreover, pharmacological dissection of the specific kinases involved in phosphorylation of S1177-eNOS would contribute to our understanding of the interplay between Ca^{2+}-dependent (e.g. CaMKII) and Ca^{2+}-independent (e.g. Akt) flow-mediated phosphorylation of S1177-eNOS.

6.2.3.3 Integrated regulation of vasodilation by flow and agonist

Certain mechanisms described in this thesis have been shown to be activated in response to both agonist and shear; for example, in Chapters 3 and

4, we also provided evidence that both agonist and shear induced phosphorylation of S1177-eNOS. Moreover, TRPV4 subunit-containing channels have been shown to be activated in response to agonist and shear and contribute to endothelium-dependent vasodilation (Zhang *et al.*, 2009; Mendoza *et al.*, 2010). However, the integration of agonist and shear stimulation in the regulation of endothelium-dependent vasodilation has not been extensively characterized and would be another avenue of future study.

The integration of agonist and shear stimulation and the associated molecular changes in EC, such as alteration in eNOS phosphorylation, in the presence of these two stimuli would provide insights into the regulation of vasoactive factor release from EC. Certain questions would be of utmost interest, for example: (1) would application of acetylcholine in an artery that is dilated by flow further relax the artery? (2) if shear and agonist both increase S1177-eNOS independently, would the co-application of these two stimuli result in an additive increase in phosphorylation of S1177? and (3) would the relative contributions of EDHF and EDRF to endothelium-dependent dilation change in response to integration of the two stimuli?

6.2.3.4 Extrinsic modulation of the intrinsic myogenic response

As mentioned in Chapter 1, NO has been reported to act on the mechanisms responsible for the activation of SMC contraction through PKG-mediated phosphorylation or direct binding of cGMP (Carvajal *et al.*, 2000). For example, PKG has been reported to phosphorylate Ca^{2+} transport proteins to reduce $[Ca^{2+}]_i$ (i.e. phosphorylation of L-type VGCCs), reduce Ca^{2+} sensitization

(i.e. phosphorylation of MYPT1 at T696) and influence actin cytoskeletal rearrangement (i.e. phosphorylation of VASP). However, the molecular mechanisms by which flow regulates SMC contractility during the myogenic response are poorly understood. Previous experiments in the lab showed DEA-NONOate, a NO donor, and acetylcholine-induced dilation of RCAs were associated with an increased F-/G-actin ratio independent of changes in LC_{20} phosphorylation, indicating a role for cytoskeleton reorganization in endothelium-dependent relaxation of RCAs (Unpublished finding, Dr. Zoe Zhong, University of Calgary). The data in this thesis suggest that FMD in intact RCA is, in part, mediated by NO. Thus, reporting changes in several proteins that are associated with myogenic constriction, such as phosphorylation of LC_{20} and G-actin:F-actin ratio, in response to flow would provide essential information regarding how flow and pressure contribute to the regulation of cerebral arterial diameter.

6.3 Summary

While major advances have been made in the field of EC $[Ca^{2+}]_i$ regulation, there are several areas that warrant further study. For example, Na^+ entry through NSCC has been implicated as a pre-requisite for activation of NCX in endothelial cells; however, a direct measurement of $[Na^+]_i$ would provide a crucial piece of data linking TRP subunit-containing channels to NCX activity functionally. Secondly, integration of pressure and flow in the regulation of arteries will be necessary to allow for better understanding of basal tone regulation *in vivo*. Lastly, the impact of flow on the changes of molecular entities involved in SMC contractility has never been measured in small resistance

arteries, and would be an important future step in understanding how flow elicits endothelium-dependent SMC relaxation in an intact artery.

References

Abdullaev IF, Bisaillon JM, Potier M, Gonzalez JC, Motiani RK & Trebak M. (2008). Stim1 and Orai1 mediate CRAC currents and store-operated calcium entry important for endothelial cell proliferation. *Circ Res* **103,** 1289-1299.

AbouAlaiwi WA, Takahashi M, Mell BR, Jones TJ, Ratnam S, Kolb RJ & Nauli SM. (2009). Ciliary polycystin-2 is a mechanosensitive calcium channel involved in nitric oxide signaling cascades. *Circ Res* **104,** 860-869.

Abu-Soud HM & Stuehr DJ. (1993). Nitric oxide synthases reveal a role for calmodulin in controlling electron transfer. *Proc Natl Acad Sci USA* **90,** 10769-10772.

Ahmmed GU, Mehta D, Vogel S, Holinstat M, Paria BC, Tiruppathi C & Malik AB. (2004). Protein kinase Calpha phosphorylates the TRPC1 channel and regulates store-operated Ca2+ entry in endothelial cells. *J Biol Chem* **279,** 20941-20949.

Antigny F, Girardin N & Frieden M. (2012). Transient receptor potential canonical channels are required for in vitro endothelial tube formation. *J Biol Chem* **287,** 5917-5927.

Arnon A, Hamlyn JM & Blaustein MP. (2000a). Na(+) entry via store-operated channels modulates Ca(2+) signaling in arterial myocytes. *Am J Physiol Cell Physiol* **278,** C163-173.

Arnon A, Hamlyn JM & Blaustein MP. (2000b). Ouabain augments Ca(2+) transients in arterial smooth muscle without raising cytosolic Na(+). *Am J Physiol Heart Circ Physiol* **279,** H679-691.

Ayajiki K, Kindermann M, Hecker M, Fleming I & Busse R. (1996). Intracellular pH and tyrosine phosphorylation but not calcium determine shear stress-induced nitric oxide production in native endothelial cells. *Circ Res* **78,** 750-758.

Bae JH, Park JW & Kwon TK. (2003). Ruthenium red, inhibitor of mitochondrial Ca2+ uniporter, inhibits curcumin-induced apoptosis via the prevention of intracellular Ca2+ depletion and cytochrome c release. *Biochem Biophys Res Commun* **303,** 1073-1079.

Bagher P, Beleznai T, Kansui Y, Mitchell R, Garland CJ & Dora KA. (2012). Low intravascular pressure activates endothelial cell TRPV4 channels, local Ca2+ events, and IKCa channels, reducing arteriolar tone. *Proc Natl Acad Sci USA* **109,** 18174-18179.

Bellien J, Iacob M, Gutierrez L, Isabelle M, Lahary A, Thuillez C & Joannides R. (2006). Crucial role of NO and endothelium-derived hyperpolarizing factor in human sustained conduit artery flow-mediated dilatation. *Hypertension* **48,** 1088-1094.

Bellien J, Joannides R, Iacob M, Arnaud P & Thuillez C. (2005). Calcium-activated potassium channels and NO regulate human peripheral conduit artery mechanics. *Hypertension* **46,** 210-216.

Bergdahl A, Gomez MF, Dreja K, Xu SZ, Adner M, Beech DJ, Broman J, Hellstrand P & Sward K. (2003). Cholesterol depletion impairs vascular reactivity to endothelin-1 by reducing store-operated Ca2+ entry dependent on TRPC1. *Circ Res* **93,** 839-847.

Bernatchez PN, Bauer PM, Yu J, Prendergast JS, He P & Sessa WC. (2005). Dissecting the molecular control of endothelial NO synthase by caveolin-1 using cell-permeable peptides. *Proc Natl Acad Sci USA* **102,** 761-766.

Bevan HS, Slater SC, Clarke H, Cahill PA, Mathieson PW, Welsh GI & Satchell SC. (2011). Acute laminar shear stress reversibly increases human glomerular endothelial cell permeability via activation of endothelial nitric oxide synthase. *Am J Physiol Renal Physiol* **301,** F733-742.

Bohlen HG, Wang W, Gashev A, Gasheva O & Zawieja D. (2009). Phasic contractions of rat mesenteric lymphatics increase basal and phasic nitric oxide generation in vivo. *Am J Physiol Heart Circ Physiol* **297,** H1319-1328.

Bondarenko A. (2004). Sodium-calcium exchanger contributes to membrane hyperpolarization of intact endothelial cells from rat aorta during acetylcholine stimulation. *Br J Pharmacol* **143,** 9-18.

Bondarenko A & Sagach V. (2006). Na+-K+-ATPase is involved in the sustained ACh-induced hyperpolarization of endothelial cells from rat aorta. *Br J Pharmacol* **149,** 958-965.

Bosteels S, Matejovic P, Flameng W & Mubagwa K. (1999). Sodium influx via a non-selective pathway activated by the removal of extracellular divalent cations: possible role in the calcium paradox. *Cardiovasc Res* **43,** 417-425.

Braunstein TH, Inoue R, Cribbs L, Oike M, Ito Y, Holstein-Rathlou NH & Jensen LJ. (2009). The role of L- and T-type calcium channels in local and remote calcium responses in rat mesenteric terminal arterioles. *J Vasc Res* **46,** 138-151.

Brooks IM & Tavalin SJ. (2011). Ca2+/calmodulin-dependent protein kinase II inhibitors disrupt AKAP79-dependent PKC signaling to GluA1 AMPA receptors. *J Biol Chem* **286,** 6697-6706.

Bubolz AH, Mendoza SA, Zheng X, Zinkevich NS, Li R, Gutterman DD & Zhang DX. (2012). Activation of endothelial TRPV4 channels mediates flow-induced dilation in human coronary arterioles: role of Ca2+ entry and mitochondrial ROS signaling. *Am J Physiol Heart Circ Physiol* **302,** H634-642.

Bulley S, Neeb ZP, Burris SK, Bannister JP, Thomas-Gatewood CM, Jangsangthong W & Jaggar JH. (2012). TMEM16A/ANO1 channels contribute to the myogenic response in cerebral arteries. *Circ Res* **111,** 1027-1036.

Busse R, Fichtner H, Luckhoff A & Kohlhardt M. (1988). Hyperpolarization and increased free calcium in acetylcholine-stimulated endothelial cells. *Am J Physiol* **255,** H965-969.

Busse R & Mulsch A. (1990). Calcium-dependent nitric oxide synthesis in endothelial cytosol is mediated by calmodulin. *FEBS Lett* **265,** 133-136.

Canty JM, Jr. & Schwartz JS. (1994). Nitric oxide mediates flow-dependent epicardial coronary vasodilation to changes in pulse frequency but not mean flow in conscious dogs. *Circulation* **89,** 375-384.

Carroll MA, Garcia MP, Falck JR & McGiff JC. (1990). 5,6-epoxyeicosatrienoic acid, a novel arachidonate metabolite. Mechanism of vasoactivity in the rat. *Circ Res* **67,** 1082-1088.

Carvajal JA, Germain AM, Huidobro-Toro JP & Weiner CP. (2000). Molecular mechanism of cGMP-mediated smooth muscle relaxation. *J Cell Physiol* **184,** 409-420.

Casteel DE, Boss GR & Pilz RB. (2005). Identification of the interface between cGMP-dependent protein kinase Ibeta and its interaction partners TFII-I and IRAG reveals a common interaction motif. *J Biol Chem* **280,** 38211-38218.

Caulin-Glaser T, Garcia-Cardena G, Sarrel P, Sessa WC & Bender JR. (1997). 17 beta-estradiol regulation of human endothelial cell basal nitric oxide release, independent of cytosolic Ca2+ mobilization. *Circ Res* **81,** 885-892.

Cha SH, Shin SY, Jung SY, Kim YT, Park YJ, Kwak JO, Kim HW & Suh CK. (2004). Evidence for Na+/Ca2+ exchanger 1 association with caveolin-1 and -2 in C6 glioma cells. *IUBMB Life* **56,** 621-627.

Chen CA, Druhan LJ, Varadharaj S, Chen YR & Zweier JL. (2008). Phosphorylation of endothelial nitric-oxide synthase regulates superoxide generation from the enzyme. *J Biol Chem* **283,** 27038-27047.

Chen G, Suzuki H & Weston AH. (1988). Acetylcholine releases endothelium-derived hyperpolarizing factor and EDRF from rat blood vessels. *Br J Pharmacol* **95,** 1165-1174.

Chen GF & Suzuki H. (1990). Calcium dependency of the endothelium-dependent hyperpolarization in smooth muscle cells of the rabbit carotid artery. *J Physiol* **421,** 521-534.

Chen PY & Sanders PW. (1993). Role of nitric oxide synthesis in salt-sensitive hypertension in Dahl/Rapp rats. *Hypertension* **22,** 812-818.

Chen ZP, Mitchelhill KI, Michell BJ, Stapleton D, Rodriguez-Crespo I, Witters LA, Power DA, Ortiz de Montellano PR & Kemp BE. (1999). AMP-activated protein kinase phosphorylation of endothelial NO synthase. *FEBS Lett* **443,** 285-289.

Cheng KT, Liu X, Ong HL, Swaim W & Ambudkar IS. (2011). Local Ca(2)+ entry via Orai1 regulates plasma membrane recruitment of TRPC1 and controls cytosolic Ca(2)+ signals required for specific cell functions. *PLoS Biol* **9,** e1001025.

Cho HJ, Xie QW, Calaycay J, Mumford RA, Swiderek KM, Lee TD & Nathan C. (1992). Calmodulin is a subunit of nitric oxide synthase from macrophages. *J Exp Med* **176,** 599-604.

Cioffi DL, Wu S, Chen H, Alexeyev M, St Croix CM, Pitt BR, Uhlig S & Stevens T. (2012). Orai1 determines calcium selectivity of an endogenous TRPC heterotetramer channel. *Circ Res* **110,** 1435-1444.

Cipolla MJ. (2009). *The Cerebral Circulation*. 2010 by Morgan & Claypool Life Sciences., San Rafael CA.

Cipolla MJ, Gokina NI & Osol G. (2002). Pressure-induced actin polymerization in vascular smooth muscle as a mechanism underlying myogenic behavior. *FASEB journal : official publication of the Federation of Am Soc Exp Biol* **16,** 72-76.

Cipolla MJ & Osol G. (1998). Vascular smooth muscle actin cytoskeleton in cerebral artery forced dilatation. *Stroke* **29,** 1223-1228.

Cohen KD & Jackson WF. (2005). Membrane hyperpolarization is not required for sustained muscarinic agonist-induced increases in intracellular Ca2+ in arteriolar endothelial cells. *Microcirculation* **12,** 169-182.

Colden-Stanfield M, Schilling WP, Ritchie AK, Eskin SG, Navarro LT & Kunze DL. (1987). Bradykinin-induced increases in cytosolic calcium and ionic currents in cultured bovine aortic endothelial cells. *Circ Res* **61,** 632-640.

Cole WC & Welsh DG. (2011). Role of myosin light chain kinase and myosin light chain phosphatase in the resistance arterial myogenic response to intravascular pressure. *Arch Biochem Biophys* **510,** 160-173.

Cornford EM & Hyman S. (2005). Localization of brain endothelial luminal and abluminal transporters with immunogold electron microscopy. *NeuroRx* **2,** 27-43.

Cornwell TL, Pryzwansky KB, Wyatt TA & Lincoln TM. (1991). Regulation of sarcoplasmic reticulum protein phosphorylation by localized cyclic GMP-dependent protein kinase in vascular smooth muscle cells. *Mol Pharmacol* **40,** 923-931.

Corson MA, James NL, Latta SE, Nerem RM, Berk BC & Harrison DG. (1996). Phosphorylation of endothelial nitric oxide synthase in response to fluid shear stress. *Circ Res* **79,** 984-991.

Dai J, Kuo KH, Leo JM, van Breemen C & Lee CH. (2005). Rearrangement of the close contact between the mitochondria and the sarcoplasmic reticulum in airway smooth muscle. *Cell Calcium* **37,** 333-340.

Dai J, Lee CH, Poburko D, Szado T, Kuo KH & van Breemen C. (2007). Endothelin-1-mediated wave-like [Ca2+]i oscillations in intact rabbit inferior vena cava. *J Vasc Res* **44,** 495-503.

Davis MJ & Hill MA. (1999). Signaling mechanisms underlying the vascular myogenic response. *Physiol Rev* **79,** 387-423.

Dedio J, Konig P, Wohlfart P, Schroeder C, Kummer W & Muller-Esterl W. (2001). NOSIP, a novel modulator of endothelial nitric oxide synthase activity. *FASEB J* **15,** 79-89.

Dekker N, van Dussen L, Hollak CE, Overkleeft H, Scheij S, Ghauharali K, van Breemen MJ, Ferraz MJ, Groener JE, Maas M, Wijburg FA, Speijer D, Tylki-Szymanska A, Mistry PK, Boot RG & Aerts JM. (2011). Elevated

plasma glucosylsphingosine in Gaucher disease: relation to phenotype, storage cell markers, and therapeutic response. *Blood* **118,** e118-127.

Dietrich A & Gudermann T. (2011). TRP channels in the cardiopulmonary vasculature. *Adv Exp Med Biol* **704,** 781-810.

Dimmeler S, Fleming I, Fisslthaler B, Hermann C, Busse R & Zeiher AM. (1999). Activation of nitric oxide synthase in endothelial cells by Akt-dependent phosphorylation. *Nature* **399,** 601-605.

DiPolo R & Beauge L. (1991). Regulation of Na-Ca exchange. An overview. *Ann NYk Acad Sci* **639,** 100-111.

Dora KA, Doyle MP & Duling BR. (1997). Elevation of intracellular calcium in smooth muscle causes endothelial cell generation of NO in arterioles. *Proc Natl Acad Sci USA* **94,** 6529-6534.

Doughty JM & Langton PD. (2001). Measurement of chloride flux associated with the myogenic response in rat cerebral arteries. *J Physiol* **534,** 753-761.

Doughty JM, Plane F & Langton PD. (1999). Charybdotoxin and apamin block EDHF in rat mesenteric artery if selectively applied to the endothelium. *Am J Physiol* **276,** H1107-1112.

Drouin A & Thorin E. (2009). Flow-induced dilation is mediated by Akt-dependent activation of endothelial nitric oxide synthase-derived hydrogen peroxide in mouse cerebral arteries. *Stroke* **40,** 1827-1833.

Dudzinski DM & Michel T. (2007). Life history of eNOS: partners and pathways. *Cardiovasc Res* **75,** 247-260.

Dyer LA & Patterson C. (2010). Development of the endothelium: an emphasis on heterogeneity. *Semin Thromb Hemost* **36,** 227-235.

Earley S, Gonzales AL & Garcia ZI. (2010). A dietary agonist of transient receptor potential cation channel V3 elicits endothelium-dependent vasodilation. *Mol Pharmacol* **77,** 612-620.

Earley S, Heppner TJ, Nelson MT & Brayden JE. (2005). TRPV4 forms a novel Ca2+ signaling complex with ryanodine receptors and BKCa channels. *Circ Res* **97,** 1270-1279.

Earley S, Pauyo T, Drapp R, Tavares MJ, Liedtke W & Brayden JE. (2009). TRPV4-dependent dilation of peripheral resistance arteries influences arterial pressure. *Am J Physiol Heart Circ Physiol* **297,** H1096-1102.

Eder P, Probst D, Rosker C, Poteser M, Wolinski H, Kohlwein SD, Romanin C & Groschner K. (2007). Phospholipase C-dependent control of cardiac calcium homeostasis involves a TRPC3-NCX1 signaling complex. *Cardiovasc Res* **73,** 111-119.

Edwards G, Dora KA, Gardener MJ, Garland CJ & Weston AH. (1998). K+ is an endothelium-derived hyperpolarizing factor in rat arteries. *Nature* **396,** 269-272.

Edwards G, Feletou M & Weston AH. (2010). Endothelium-derived hyperpolarising factors and associated pathways: a synopsis. *Pflugers Arch* **459,** 863-879.

Estrada IA, Donthamsetty R, Debski P, Zhou MH, Zhang SL, Yuan JX, Han W & Makino A. (2012). STIM1 restores coronary endothelial function in type 1 diabetic mice. *Circ Res* **111,** 1166-1175.

Fameli N, Kuo KH & van Breemen C. (2009). A model for the generation of localized transient [Na+] elevations in vascular smooth muscle. *Biochem Biophys Res Commun* **389,** 461-465.

Feletou M & Vanhoutte PM. (1999). The third pathway: endothelium-dependent hyperpolarization. *J Physiol Pharmacol* **50,** 525-534.

Fisslthaler B, Loot AE, Mohamed A, Busse R & Fleming I. (2008). Inhibition of endothelial nitric oxide synthase activity by proline-rich tyrosine kinase 2 in response to fluid shear stress and insulin. *Circ Res* **102,** 1520-1528.

Flavahan NA, Bailey SR, Flavahan WA, Mitra S & Flavahan S. (2005). Imaging remodeling of the actin cytoskeleton in vascular smooth muscle cells after mechanosensitive arteriolar constriction. *Am J Physiol Heart Circ Physiol* **288,** H660-669.

Fleming I, Bauersachs J, Fisslthaler B & Busse R. (1998). Ca2+-independent activation of the endothelial nitric oxide synthase in response to tyrosine phosphatase inhibitors and fluid shear stress. *Circ Res* **82,** 686-695.

Fleming I & Busse R. (1999). NO: the primary EDRF. *J Mol Cell Cardiol* **31,** 5-14.

Fleming I, Fisslthaler B, Dimmeler S, Kemp BE & Busse R. (2001). Phosphorylation of Thr(495) regulates Ca(2+)/calmodulin-dependent endothelial nitric oxide synthase activity. *Circ Res* **88,** E68-75.

Fleming I, Fisslthaler B, Dixit M & Busse R. (2005). Role of PECAM-1 in the shear-stress-induced activation of Akt and the endothelial nitric oxide synthase (eNOS) in endothelial cells. *J Cell Sci* **118,** 4103-4111.

Forstermann U, Pollock JS, Schmidt HH, Heller M & Murad F. (1991). Calmodulin-dependent endothelium-derived relaxing factor/nitric oxide synthase activity is present in the particulate and cytosolic fractions of bovine aortic endothelial cells. *Proc Natl Acad Sci USA* **88,** 1788-1792.

Forstermann U & Sessa WC. (2012). Nitric oxide synthases: regulation and function. *Eur Heart J* **33,** 829-837, 837a-837d.

Fujita K, Wada K, Nozaki Y, Yoneda M, Endo H, Takahashi H, Kirikoshi H, Inamori M, Saito S & Nakajima A. (2011). Serum nitric oxide metabolite as a biomarker of visceral fat accumulation: clinical significance of measurement for nitrate/nitrite. *Med Sci Monit* **17,** CR123-131.

Fulton D, Babbitt R, Zoellner S, Fontana J, Acevedo L, McCabe TJ, Iwakiri Y & Sessa WC. (2004). Targeting of endothelial nitric-oxide synthase to the cytoplasmic face of the Golgi complex or plasma membrane regulates Akt-versus calcium-dependent mechanisms for nitric oxide release. *J Biol Chem* **279,** 30349-30357.

Fulton D, Gratton JP & Sessa WC. (2001). Post-translational control of endothelial nitric oxide synthase: why isn't calcium/calmodulin enough? *J Pharmacol Exp Ther* **299,** 818-824.

Fulton D, Ruan L, Sood SG, Li C, Zhang Q & Venema RC. (2008). Agonist-stimulated endothelial nitric oxide synthase activation and vascular relaxation. Role of eNOS phosphorylation at Tyr83. *Circ Res* **102,** 497-504.

Furchgott RF & Zawadzki JV. (1980). The obligatory role of endothelial cells in the relaxation of arterial smooth muscle by acetylcholine. *Nature* **288,** 373-376.

Gambillara V, Chambaz C, Montorzi G, Roy S, Stergiopulos N & Silacci P. (2006). Plaque-prone hemodynamics impair endothelial function in pig carotid arteries. *Am J Physiol Heart Circ Physiol* **290,** H2320-2328.

Garcia-Cardena G, Fan R, Shah V, Sorrentino R, Cirino G, Papapetropoulos A & Sessa WC. (1998). Dynamic activation of endothelial nitric oxide synthase by Hsp90. *Nature* **392,** 821-824.

Garcia-Cardena G, Fan R, Stern DF, Liu J & Sessa WC. (1996a). Endothelial nitric oxide synthase is regulated by tyrosine phosphorylation and interacts with caveolin-1. *J Biol Chem* **271,** 27237-27240.

Garcia-Cardena G, Martasek P, Masters BS, Skidd PM, Couet J, Li S, Lisanti MP & Sessa WC. (1997). Dissecting the interaction between nitric oxide synthase (NOS) and caveolin. Functional significance of the nos caveolin binding domain in vivo. *J Biol Chem* **272,** 25437-25440.

Garcia-Cardena G, Oh P, Liu J, Schnitzer JE & Sessa WC. (1996b). Targeting of nitric oxide synthase to endothelial cell caveolae via palmitoylation: implications for nitric oxide signaling. *Proc Natl Acad Sci USA* **93,** 6448-6453.

Girardin NC, Antigny F & Frieden M. (2010). Electrophysiological characterization of store-operated and agonist-induced Ca2+ entry pathways in endothelial cells. *Pflugers Arch* **460,** 109-120.

Gokina NI, Park KM, McElroy-Yaggy K & Osol G. (2005). Effects of Rho kinase inhibition on cerebral artery myogenic tone and reactivity. *J Appl Physiol* **98,** 1940-1948.

Grassie ME, Moffat LD, Walsh MP & MacDonald JA. (2011). The myosin phosphatase targeting protein (MYPT) family: a regulated mechanism for achieving substrate specificity of the catalytic subunit of protein phosphatase type 1delta. *Arch Biochem Biophys* **510,** 147-159.

Gryglewski RJ, Moncada S & Palmer RM. (1986). Bioassay of prostacyclin and endothelium-derived relaxing factor (EDRF) from porcine aortic endothelial cells. *Br J Pharmacol* **87,** 685-694.

Gunst SJ & Tang DD. (2000). The contractile apparatus and mechanical properties of airway smooth muscle. *Eur Respir J* **15,** 600-616.

Gunst SJ & Zhang W. (2008). Actin cytoskeletal dynamics in smooth muscle: a new paradigm for the regulation of smooth muscle contraction. *Am J Physiol Cell Physiol* **295,** C576-587.

Gwack Y, Srikanth S, Feske S, Cruz-Guilloty F, Oh-hora M, Neems DS, Hogan PG & Rao A. (2007). Biochemical and functional characterization of Orai proteins. *J Biol Chem* **282,** 16232-16243.

Hardie RC & Minke B. (1992). The trp gene is essential for a light-activated Ca2+ channel in Drosophila photoreceptors. *Neuron* **8,** 643-651.

Harris D, Martin PE, Evans WH, Kendall DA, Griffith TM & Randall MD. (2000). Role of gap junctions in endothelium-derived hyperpolarizing factor responses and mechanisms of K(+)-relaxation. *Eur J Pharmacol* **402,** 119-128.

Hicks K, O'Neil RG, Dubinsky WS & Brown RC. (2010). TRPC-mediated actin-myosin contraction is critical for BBB disruption following hypoxic stress. *Am J Physiol Cell Physiol* **298,** C1583-1593.

Hill MA, Zou H, Potocnik SJ, Meininger GA & Davis MJ. (2001). Invited review: arteriolar smooth muscle mechanotransduction: Ca(2+) signaling pathways underlying myogenic reactivity. *J Appl Physiol* **91,** 973-983.

Hirota S, Helli P & Janssen LJ. (2007a). Ionic mechanisms and Ca2+ handling in airway smooth muscle. *Eur Respir J* **30,** 114-133.

Hirota S, Pertens E & Janssen LJ. (2007b). The reverse mode of the Na(+)/Ca(2+) exchanger provides a source of Ca(2+) for store refilling following agonist-induced Ca(2+) mobilization. *Am J Physiol Lung Cell Mol Physiol* **292,** L438-447.

Hoang HH, Padgham SV & Meininger CJ. (2013). L-arginine, tetrahydrobiopterin, nitric oxide and diabetes. *Curr Opin Clin Nutr Metab Care* **16,** 76-82.

Hofmann T, Obukhov AG, Schaefer M, Harteneck C, Gudermann T & Schultz G. (1999). Direct activation of human TRPC6 and TRPC3 channels by diacylglycerol. *Nature* **397,** 259-263.

Hooper WC, Catravas JD, Heistad DD, Sessa WC & Mensah GA. (2007). Vascular endothelium summary statement I: Health promotion and chronic disease prevention. *Vascul Pharmacol* **46,** 315-317.

Hoyer J, Kohler R & Distler A. (1998). Mechanosensitive Ca2+ oscillations and STOC activation in endothelial cells. *FASEB J* **12,** 359-366.

Huang A, Sun D, Carroll MA, Jiang H, Smith CJ, Connetta JA, Falck JR, Shesely EG, Koller A & Kaley G. (2001a). EDHF mediates flow-induced dilation in skeletal muscle arterioles of female eNOS-KO mice. *Am J Physiol Heart Circ Physiol* **280,** H2462-2469.

Huang A, Wu Y, Sun D, Koller A & Kaley G. (2001b). Effect of estrogen on flow-induced dilation in NO deficiency: role of prostaglandins and EDHF. *J Appl Physiol* **91,** 2561-2566.

Huang GN, Zeng W, Kim JY, Yuan JP, Han L, Muallem S & Worley PF. (2006a). STIM1 carboxyl-terminus activates native SOC, I(crac) and TRPC1 channels. *Nat Cell Biol* **8,** 1003-1010.

Huang J, van Breemen C, Kuo KH, Hove-Madsen L & Tibbits GF. (2006b). Store-operated Ca2+ entry modulates sarcoplasmic reticulum Ca2+ loading in

neonatal rabbit cardiac ventricular myocytes. *Am J Physiol Cell Physiol* **290,** C1572-1582.

Ilan N & Madri JA. (2003). PECAM-1: old friend, new partners. *Curr Opin Cell Biol* **15,** 515-524.

Ishibazawa A, Nagaoka T, Takahashi T, Yamamoto K, Kamiya A, Ando J & Yoshida A. (2011). Effects of shear stress on the gene expressions of endothelial nitric oxide synthase, endothelin-1, and thrombomodulin in human retinal microvascular endothelial cells. *Invest Ophthalmol Vis Sci* **52,** 8496-8504.

Isshiki M, Ando J, Korenaga R, Kogo H, Fujimoto T, Fujita T & Kamiya A. (1998). Endothelial Ca2+ waves preferentially originate at specific loci in caveolin-rich cell edges. *Proc Natl Acad Sci USA* **95,** 5009-5014.

Isshiki M, Ando J, Yamamoto K, Fujita T, Ying Y & Anderson RG. (2002a). Sites of Ca(2+) wave initiation move with caveolae to the trailing edge of migrating cells. *J Cell Sci* **115,** 475-484.

Isshiki M, Mutoh A & Fujita T. (2004). Subcortical Ca2+ waves sneaking under the plasma membrane in endothelial cells. *Circ Res* **95,** e11-21.

Isshiki M, Ying YS, Fujita T & Anderson RG. (2002b). A molecular sensor detects signal transduction from caveolae in living cells. *J Biol Chem* **277,** 43389-43398.

Jho D, Mehta D, Ahmmed G, Gao XP, Tiruppathi C, Broman M & Malik AB. (2005). Angiopoietin-1 opposes VEGF-induced increase in endothelial permeability by inhibiting TRPC1-dependent Ca2 influx. *Circ Res* **96,** 1282-1290.

Johns A, Lategan TW, Lodge NJ, Ryan US, Van Breemen C & Adams DJ. (1987). Calcium entry through receptor-operated channels in bovine pulmonary artery endothelial cells. *Tissue Cell* **19,** 733-745.

Johnson RP, El-Yazbi AF, Takeya K, Walsh EJ, Walsh MP & Cole WC. (2009). Ca2+ sensitization via phosphorylation of myosin phosphatase targeting subunit at threonine-855 by Rho kinase contributes to the arterial myogenic response. *J Physiol* **587,** 2537-2553.

Jousset H, Malli R, Girardin N, Graier WF, Demaurex N & Frieden M. (2008). Evidence for a receptor-activated Ca2+ entry pathway independent from Ca2) store depletion in endothelial cells. *Cell Calcium* **43,** 83-94.

Ju H, Zou R, Venema VJ & Venema RC. (1997). Direct interaction of endothelial nitric-oxide synthase and caveolin-1 inhibits synthase activity. *J Biol Chem* **272,** 18522-18525.

Kang H, Bayless KJ & Kaunas R. (2008). Fluid shear stress modulates endothelial cell invasion into three-dimensional collagen matrices. *Am J Physiol Heart Circ Physiol* **295,** H2087-2097.

Kiselyov K, Xu X, Mozhayeva G, Kuo T, Pessah I, Mignery G, Zhu X, Birnbaumer L & Muallem S. (1998). Functional interaction between InsP3 receptors and store-operated Htrp3 channels. *Nature* **396,** 478-482.

Knot HJ & Nelson MT. (1998). Regulation of arterial diameter and wall [Ca2+] in cerebral arteries of rat by membrane potential and intravascular pressure. *J Physiol* **508,** 199-209.

Kohler R, Heyken WT, Heinau P, Schubert R, Si H, Kacik M, Busch C, Grgic I, Maier T & Hoyer J. (2006). Evidence for a functional role of endothelial transient receptor potential V4 in shear stress-induced vasodilatation. *Arterioscler Thromb Vasc Biol* **26,** 1495-1502.

Koller A & Huang A. (1994). Impaired nitric oxide-mediated flow-induced dilation in arterioles of spontaneously hypertensive rats. *Circ Res* **74,** 416-421.

Koller A & Toth P. (2012). Contribution of flow-dependent vasomotor mechanisms to the autoregulation of cerebral blood flow. *J Vasc Res* **49,** 375-389.

Kraft R. (2007). The Na+/Ca2+ exchange inhibitor KB-R7943 potently blocks TRPC channels. *Biochem Biophys Res Commun* **361,** 230-236.

Kruse HJ, Grunberg B, Siess W & Weber PC. (1994). Formation of biologically active autacoids is regulated by calcium influx in endothelial cells. *Arterioscler Thromb* **14,** 1821-1828.

Kuchan MJ & Frangos JA. (1994). Role of calcium and calmodulin in flow-induced nitric oxide production in endothelial cells. *Am J Physiol* **266,** C628-636.

Kumar B, Dreja K, Shah SS, Cheong A, Xu SZ, Sukumar P, Naylor J, Forte A, Cipollaro M, McHugh D, Kingston PA, Heagerty AM, Munsch CM, Bergdahl A, Hultgardh-Nilsson A, Gomez MF, Porter KE, Hellstrand P & Beech DJ. (2006). Upregulated TRPC1 channel in vascular injury in vivo and its role in human neointimal hyperplasia. *Circ Res* **98,** 557-563.

Kuo IY, Wolfle SE & Hill CE. (2011). T-type calcium channels and vascular function: the new kid on the block? *J Physiol* **589,** 783-795.

Kuo L, Arko F, Chilian WM & Davis MJ. (1993). Coronary venular responses to flow and pressure. *Circ Res* **72,** 607-615.

Kuo L, Davis MJ & Chilian WM. (1990). Endothelium-dependent, flow-induced dilation of isolated coronary arterioles. *Am J Physiol* **259,** H1063-1070.

Kwiatek AM, Minshall RD, Cool DR, Skidgel RA, Malik AB & Tiruppathi C. (2006). Caveolin-1 regulates store-operated Ca2+ influx by binding of its scaffolding domain to transient receptor potential channel-1 in endothelial cells. *Mol Pharmacol* **70,** 1174-1183.

Lagaud G, Gaudreault N, Moore ED, Van Breemen C & Laher I. (2002). Pressure-dependent myogenic constriction of cerebral arteries occurs independently of voltage-dependent activation. *Am J Physiol Heart Circ Physiol* **283,** H2187-2195.

Ledoux J, Taylor MS, Bonev AD, Hannah RM, Solodushko V, Shui B, Tallini Y, Kotlikoff MI & Nelson MT. (2008). Functional architecture of inositol 1,4,5-trisphosphate signaling in restricted spaces of myoendothelial projections. *ProcNatiAcadSci USA* **105,** 9627-9632.

Lee RH, Tseng TY, Wu CY, Chen PY, Chen MF, Kuo JS & Lee TJ. (2012). Memantine inhibits alpha3beta2-nAChRs-mediated nitrergic neurogenic vasodilation in porcine basilar arteries. *PLoS One* **7,** e40326.

Lemos VS, Poburko D, Liao CH, Cole WC & van Breemen C. (2007). Na+ entry via TRPC6 causes Ca2+ entry via NCX reversal in ATP stimulated smooth muscle cells. *Biochem Biophys Res Commun* **352,** 130-134.

Li J, Cubbon RM, Wilson LA, Amer MS, McKeown L, Hou B, Majeed Y, Tumova S, Seymour VA, Taylor H, Stacey M, O'Regan D, Foster R, Porter KE, Kearney MT & Beech DJ. (2011a). Orai1 and CRAC channel dependence of VEGF-activated Ca2+ entry and endothelial tube formation. *Circ Res* **108,** 1190-1198.

Li J, Godecke T, Chen SN, Imai A, Lankin DC, Farnsworth NR, Pauli GF, van Breemen RB & Nikolic D. (2011b). In vitro metabolic interactions between black cohosh (Cimicifuga racemosa) and tamoxifen via inhibition of cytochromes P450 2D6 and 3A4. *Xenobiotica VOLUME & PAGE #s*.

Li J, Sukumar P, Milligan CJ, Kumar B, Ma ZY, Munsch CM, Jiang LH, Porter KE & Beech DJ. (2008). Interactions, functions, and independence of plasma

membrane STIM1 and TRPC1 in vascular smooth muscle cells. *Circ Res* **103,** e97-104.

Li Y, Zheng J, Bird IM & Magness RR. (2004). Mechanisms of shear stress-induced endothelial nitric-oxide synthase phosphorylation and expression in ovine fetoplacental artery endothelial cells. *Biol Reprod* **70,** 785-796.

Li Z, Lu J, Xu P, Xie X, Chen L & Xu T. (2007). Mapping the interacting domains of STIM1 and Orai1 in Ca2+ release-activated Ca2+ channel activation. *J Biol Chem* **282,** 29448-29456.

Liang GH, Park S, Kim JA, Choi S & Suh SH. (2009). Stimulation of large-conductance Ca2+-activated K+ channels by the Na+/Ca2+ exchanger inhibitor dichlorobenzamil in cultured human umbilical vein endothelial cells and mouse aortic smooth muscle cells. *J Physiol Pharmacol* **60,** 43-50.

Lievremont JP, Bird GS & Putney JW, Jr. (2004). Canonical transient receptor potential TRPC7 can function as both a receptor- and store-operated channel in HEK-293 cells. *Am J Physiol Cell Physiol* **287,** C1709-1716.

Liou J, Fivaz M, Inoue T & Meyer T. (2007). Live-cell imaging reveals sequential oligomerization and local plasma membrane targeting of stromal interaction molecule 1 after Ca2+ store depletion. *Proc Natl Acad Sci USA* **104,** 9301-9306.

Liou J, Kim ML, Heo WD, Jones JT, Myers JW, Ferrell JE, Jr. & Meyer T. (2005). STIM is a Ca2+ sensor essential for Ca2+-store-depletion-triggered Ca2+ influx. *Curr Biol* **15,** 1235-1241.

Liu B, Peel SE, Fox J & Hall IP. (2010). Reverse mode Na+/Ca2+ exchange mediated by STIM1 contributes to Ca2+ influx in airway smooth muscle following agonist stimulation. *Respir Res* **11,** 168.

Liu H, Xiong Z & Sperelakis N. (1997). Cyclic nucleotides regulate the activity of L-type calcium channels in smooth muscle cells from rat portal vein. *J Mol Cell Cardiol* **29,** 1411-1421.

Liu J, Garcia-Cardena G & Sessa WC. (1996). Palmitoylation of endothelial nitric oxide synthase is necessary for optimal stimulated release of nitric oxide: implications for caveolae localization. *Biochemistry* **35,** 13277-13281.

Liu X, Singh BB & Ambudkar IS. (2003). TRPC1 is required for functional store-operated Ca2+ channels. Role of acidic amino acid residues in the S5-S6 region. *J Biol Chem* **278,** 11337-11343.

Liu Y, Bubolz AH, Mendoza S, Zhang DX & Gutterman DD. (2011). H2O2 is the transferrable factor mediating flow-induced dilation in human coronary arterioles. *Circ Res* **108,** 566-573.

Lockwich T, Singh BB, Liu X & Ambudkar IS. (2001). Stabilization of cortical actin induces internalization of transient receptor potential 3 (Trp3)-associated caveolar Ca2+ signaling complex and loss of Ca2+ influx without disruption of Trp3-inositol trisphosphate receptor association. *J Biol Chem* **276,** 42401-42408.

Loutzenhiser R, Bidani AK & Wang X. (2004). Systolic pressure and the myogenic response of the renal afferent arteriole. *Acta Physiol Scand* **181,** 407-413.

Luckhoff A & Busse R. (1990a). Activators of potassium channels enhance calcium influx into endothelial cells as a consequence of potassium currents. *Naunyn Schmiedebergs Arch Pharmacol* **342,** 94-99.

Luckhoff A & Busse R. (1990b). Calcium influx into endothelial cells and formation of endothelium-derived relaxing factor is controlled by the membrane potential. *Pflugers Arch* **416,** 305-311.

Luckhoff A, Pohl U, Mulsch A & Busse R. (1988). Differential role of extra- and intracellular calcium in the release of EDRF and prostacyclin from cultured endothelial cells. *Br J Pharmacol* **95,** 189-196.

Luksha L, Agewall S & Kublickiene K. (2009). Endothelium-derived hyperpolarizing factor in vascular physiology and cardiovascular disease. *Atherosclerosis* **202,** 330-344.

Luksha N, Luksha L, Carrero JJ, Hammarqvist F, Stenvinkel P & Kublickiene K. (2011). Impaired resistance artery function in patients with end-stage renal disease. *Clin Sci (Lond)* **120,** 525-536.

Lytton J. (2007). Na+/Ca2+ exchangers: three mammalian gene families control Ca2+ transport. *Biochem J* **406,** 365-382.

Lyu RM, Smith L & Smith JB. (1992). Ca2+ influx via Na(+)-Ca2+ exchange in immortalized aortic myocytes. I. Dependence on [Na+]i and inhibition by external Na+. *Am J Physiol* **263,** C628-634.

Ma X, Cao J, Luo J, Nilius B, Huang Y, Ambudkar IS & Yao X. (2010). Depletion of intracellular Ca2+ stores stimulates the translocation of vanilloid transient receptor potential 4-c1 heteromeric channels to the plasma membrane. *Arterioscler Thromb Vasc Biol* **30,** 2249-2255.

Ma X, Cheng KT, Wong CO, O'Neil RG, Birnbaumer L, Ambudkar IS & Yao X. (2011a). Heteromeric TRPV4-C1 channels contribute to store-operated Ca(2+) entry in vascular endothelial cells. *Cell Calcium* **50,** 502-509.

Ma X, Nilius B, Wong JW, Huang Y & Yao X. (2011b). Electrophysiological properties of heteromeric TRPV4-C1 channels. *Biochimica et biophysica acta* **1808,** 2789-2797.

Maack C, Ganesan A, Sidor A & O'Rourke B. (2005). Cardiac sodium-calcium exchanger is regulated by allosteric calcium and exchanger inhibitory peptide at distinct sites. *Circ Res* **96,** 91-99.

Martinez-Lemus LA. (2012). The dynamic structure of arterioles. *Basic Clin Pharmacol Toxicol* **110,** 5-11.

McCabe TJ, Fulton D, Roman LJ & Sessa WC. (2000). Enhanced electron flux and reduced calmodulin dissociation may explain "calcium-independent" eNOS activation by phosphorylation. *J Biol Chem* **275,** 6123-6128.

McCarron JG, Crichton CA, Langton PD, MacKenzie A & Smith GL. (1997). Myogenic contraction by modulation of voltage-dependent calcium currents in isolated rat cerebral arteries. *J Physiol* **498 (Pt 2),** 371-379.

McNeish AJ, Sandow SL, Neylon CB, Chen MX, Dora KA & Garland CJ. (2006). Evidence for involvement of both IKCa and SKCa channels in hyperpolarizing responses of the rat middle cerebral artery. *Stroke* **37,** 1277-1282.

McSherry IN, Spitaler MM, Takano H & Dora KA. (2005). Endothelial cell Ca2+ increases are independent of membrane potential in pressurized rat mesenteric arteries. *Cell Calcium* **38,** 23-33.

Mehta D, Ahmmed GU, Paria BC, Holinstat M, Voyno-Yasenetskaya T, Tiruppathi C, Minshall RD & Malik AB. (2003). RhoA interaction with inositol 1,4,5-trisphosphate receptor and transient receptor potential channel-1 regulates Ca2+ entry. Role in signaling increased endothelial permeability. *J Biol Chem* **278,** 33492-33500.

Mehta D & Malik AB. (2006). Signaling mechanisms regulating endothelial permeability. *Physiol Rev* **86,** 279-367.

Mendoza SA, Fang J, Gutterman DD, Wilcox DA, Bubolz AH, Li R, Suzuki M & Zhang DX. (2010). TRPV4-mediated endothelial Ca2+ influx and vasodilation in response to shear stress. *Am J Physiol Heart Circ Physiol* **298,** H466-476.

Mergler S, Valtink M, Coulson-Thomas VJ, Lindemann D, Reinach PS, Engelmann K & Pleyer U. (2010). TRPV channels mediate temperature-sensing in human corneal endothelial cells. *Exp Eye Res* **90,** 758-770.

Michel JB, Feron O, Sacks D & Michel T. (1997a). Reciprocal regulation of endothelial nitric-oxide synthase by Ca2+-calmodulin and caveolin. *J Biol Chem* **272,** 15583-15586.

Michel JB, Feron O, Sase K, Prabhakar P & Michel T. (1997b). Caveolin versus calmodulin. Counterbalancing allosteric modulators of endothelial nitric oxide synthase. *J Biol Chem* **272,** 25907-25912.

Michell BJ, Chen Z, Tiganis T, Stapleton D, Katsis F, Power DA, Sim AT & Kemp BE. (2001). Coordinated control of endothelial nitric-oxide synthase phosphorylation by protein kinase C and the cAMP-dependent protein kinase. *J Biol Chem* **276,** 17625-17628.

Moore JP, Weber M & Searles CD. (2010). Laminar shear stress modulates phosphorylation and localization of RNA polymerase II on the endothelial nitric oxide synthase gene. *Arterioscler Thromb Vasc Biol* **30,** 561-567.

Moreno-Dominguez A, Colinas O, El-Yazbi A, Walsh EJ, Hill MA, Walsh MP & Cole WC. (2013). Ca2+ sensitization due to myosin light chain phosphatase inhibition and cytoskeletal reorganization in the myogenic response of skeletal muscle resistance arteries. *J Physiol* **591,** 1235-1250.

Morita H, Honda A, Inoue R, Ito Y, Abe K, Nelson MT & Brayden JE. (2007). Membrane stretch-induced activation of a TRPM4-like nonselective cation channel in cerebral artery myocytes. *J Pharmacol Sci* **103,** 417-426.

Motley ED, Eguchi K, Patterson MM, Palmer PD, Suzuki H & Eguchi S. (2007). Mechanism of endothelial nitric oxide synthase phosphorylation and activation by thrombin. *Hypertension* **49,** 577-583.

Mufti RE, Brett SE, Tran CH, Abd El-Rahman R, Anfinogenova Y, El-Yazbi A, Cole WC, Jones PP, Chen SR & Welsh DG. (2010). Intravascular pressure augments cerebral arterial constriction by inducing voltage-insensitive Ca2+ waves. *J Physiol* **588,** 3983-4005.

Muller JM, Davis MJ, Kuo L & Chilian WM. (1999). Changes in coronary endothelial cell Ca2+ concentration during shear stress- and agonist-induced vasodilation. *Am J Physiol* **276,** H1706-1714.

Murata T, Lin MI, Stan RV, Bauer PM, Yu J & Sessa WC. (2007). Genetic evidence supporting caveolae microdomain regulation of calcium entry in endothelial cells. *J Biol Chem* **282,** 16631-16643.

Mustafa AK, Sikka G, Gazi SK, Steppan J, Jung SM, Bhunia AK, Barodka VM, Gazi FK, Barrow RK, Wang R, Amzel LM, Berkowitz DE & Snyder SH. (2011). Hydrogen sulfide as endothelium-derived hyperpolarizing factor sulfhydrates potassium channels. *Circ Res* **109,** 1259-1268.

Nauli SM, Kawanabe Y, Kaminski JJ, Pearce WJ, Ingber DE & Zhou J. (2008). Endothelial cilia are fluid shear sensors that regulate calcium signaling and nitric oxide production through polycystin-1. *Circulation* **117,** 1161-1171.

Ng LC, O'Neill KG, French D, Airey JA, Singer CA, Tian H, Shen XM & Hume JR. (2012). TRPC1 and Orai1 interact with STIM1 and mediate capacitative Ca(2+) entry caused by acute hypoxia in mouse pulmonary arterial smooth muscle cells. *Am J Physiol Cell Physiol* **303,** C1156-1172.

Nie HG, Hao LY, Xu JJ, Minobe E, Kameyama A & Kameyama M. (2007). Distinct roles of CaM and Ca(2+)/CaM -dependent protein kinase II in Ca(2+) -dependent facilitation and inactivation of cardiac L-type Ca(2+) channels. *J Physiol Sci* **57,** 167-173.

Nilius B & Droogmans G. (2001). Ion channels and their functional role in vascular endothelium. *Physiol Rev* **81,** 1415-1459.

Oelze M, Mollnau H, Hoffmann N, Warnholtz A, Bodenschatz M, Smolenski A, Walter U, Skatchkov M, Meinertz T & Munzel T. (2000). Vasodilator-stimulated phosphoprotein serine 239 phosphorylation as a sensitive monitor of defective nitric oxide/cGMP signaling and endothelial dysfunction. *Circ Res* **87,** 999-1005.

Osol G, Brekke JF, McElroy-Yaggy K & Gokina NI. (2002). Myogenic tone, reactivity, and forced dilatation: a three-phase model of in vitro arterial myogenic behavior. *Am J Physiol Heart Circ Physiol* **283,** H2260-2267.

Owsianik G, Talavera K, Voets T & Nilius B. (2006). Permeation and selectivity of TRP channels. *Annu Rev Physiol* **68,** 685-717.

Paffett ML, Naik JS, Riddle MA, Menicucci SD, Gonzales AJ, Resta TC & Walker BR. (2011). Altered membrane lipid domains limit pulmonary endothelial calcium entry following chronic hypoxia. *Am J Physiol Heart Circ Physiol* **301,** H1331-1340.

Palmer RM, Ferrige AG & Moncada S. (1987). Nitric oxide release accounts for the biological activity of endothelium-derived relaxing factor. *Nature* **327,** 524-526.

Paltauf-Doburzynska J, Frieden M, Spitaler M & Graier WF. (2000). Histamine-induced Ca2+ oscillations in a human endothelial cell line depend on transmembrane ion flux, ryanodine receptors and endoplasmic reticulum Ca2+-ATPase. *J Physiol* **524 Pt 3,** 701-713.

Pani B, Ong HL, Brazer SC, Liu X, Rauser K, Singh BB & Ambudkar IS. (2009). Activation of TRPC1 by STIM1 in ER-PM microdomains involves release of the channel from its scaffold caveolin-1. *Proc Natl Acad Sci USA* **106,** 20087-20092.

Papaioannou TG, Karatzis EN, Vavuranakis M, Lekakis JP & Stefanadis C. (2006). Assessment of vascular wall shear stress and implications for atherosclerotic disease. *Int J Cardiol* **113,** 12-18.

Papapetropoulos A, Rudic RD & Sessa WC. (1999). Molecular control of nitric oxide synthases in the cardiovascular system. *Cardiovasc Res* **43,** 509-520.

Parekh AB & Putney JW, Jr. (2005). Store-operated calcium channels. *Physiol Rev* **85,** 757-810.

Paria BC, Vogel SM, Ahmmed GU, Alamgir S, Shroff J, Malik AB & Tiruppathi C. (2004). Tumor necrosis factor-alpha-induced TRPC1 expression amplifies store-operated Ca2+ influx and endothelial permeability. *Am J Physiol Lung Cell Mol Physiol* **287,** L1303-1313.

Pedersen SF, Owsianik G & Nilius B. (2005). TRP channels: an overview. *Cell Calcium* **38,** 233-252.

Perrotta I. (2013). Ultrastructural features of human atherosclerosis. *Ultrastruct Pathol* **37,** 43-51.

Pfitzer G. (2001). Invited review: regulation of myosin phosphorylation in smooth muscle. *J Appl Physiol* **91,** 497-503.

Poburko D, Liao CH, Lemos VS, Lin E, Maruyama Y, Cole WC & van Breemen C. (2007). Transient receptor potential channel 6-mediated, localized cytosolic [Na+] transients drive Na+/Ca2+ exchanger-mediated Ca2+ entry in purinergically stimulated aorta smooth muscle cells. *Circ Res* **101,** 1030-1038.

Pohl U, Herlan K, Huang A & Bassenge E. (1991). EDRF-mediated shear-induced dilation opposes myogenic vasoconstriction in small rabbit arteries. *Am J Physiol* **261,** H2016-2023.

Potocnik SJ & Hill MA. (2001). Pharmacological evidence for capacitative Ca(2+) entry in cannulated and pressurized skeletal muscle arterioles. *Br J Pharmacol* **134,** 247-256.

Pott C, Philipson KD & Goldhaber JI. (2005). Excitation-contraction coupling in Na+-Ca2+ exchanger knockout mice: reduced transsarcolemmal Ca2+ flux. *Circ Res* **97,** 1288-1295.

Prakriya M, Feske S, Gwack Y, Srikanth S, Rao A & Hogan PG. (2006). Orai1 is an essential pore subunit of the CRAC channel. *Nature* **443,** 230-233.

Presley T, Vedam K, Velayutham M, Zweier JL & Ilangovan G. (2008). Activation of Hsp90-eNOS and increased NO generation attenuate respiration of hypoxia-treated endothelial cells. *Am J Physiol Cell Physiol* **295,** C1281-1291.

Pulina MV, Zulian A, Berra-Romani R, Beskina O, Mazzocco-Spezzia A, Baryshnikov SG, Papparella I, Hamlyn JM, Blaustein MP & Golovina VA. (2010). Upregulation of Na+ and Ca2+ transporters in arterial smooth muscle from ouabain-induced hypertensive rats. *Am J Physiol Heart Circ Physiol* **298,** H263-274.

Raina H, Ella SR & Hill MA. (2008). Decreased activity of the smooth muscle Na+/Ca2+ exchanger impairs arteriolar myogenic reactivity. *J Physiol* **586,** 1669-1681.

Raqeeb A, Sheng J, Ao N & Braun AP. (2011). Purinergic P2Y2 receptors mediate rapid Ca(2+) mobilization, membrane hyperpolarization and nitric oxide production in human vascular endothelial cells. *Cell Calcium* **49,** 240-248.

Reeves JP, Abdellatif M & Condrescu M. (2008). The sodium-calcium exchanger is a mechanosensitive transporter. *J Physiol* **586,** 1549-1563.

Rosker C, Graziani A, Lukas M, Eder P, Zhu MX, Romanin C & Groschner K. (2004). Ca(2+) signaling by TRPC3 involves Na(+) entry and local coupling to the Na(+)/Ca(2+) exchanger. *J Biol Chem* **279,** 13696-13704.

Rudic RD & Sessa WC. (1999). Nitric oxide in endothelial dysfunction and vascular remodeling: clinical correlates and experimental links. *Am J Hum Genet* **64,** 673-677.

Ruknudin AM, Wei SK, Haigney MC, Lederer WJ & Schulze DH. (2007). Phosphorylation and other conundrums of Na/Ca exchanger, NCX1. *Ann NY Acad Sci* **1099,** 103-118.

Sandow SL, Haddock RE, Hill CE, Chadha PS, Kerr PM, Welsh DG & Plane F. (2009). What's where and why at a vascular myoendothelial microdomain signalling complex. *Clin Exp Pharmacol Physiol* **36,** 67-76.

Sandow SL & Hill CE. (2000). Incidence of myoendothelial gap junctions in the proximal and distal mesenteric arteries of the rat is suggestive of a role in endothelium-derived hyperpolarizing factor-mediated responses. *Circ Res* **86,** 341-346.

Sandow SL, Neylon CB, Chen MX & Garland CJ. (2006). Spatial separation of endothelial small- and intermediate-conductance calcium-activated potassium channels (K(Ca)) and connexins: possible relationship to vasodilator function? *J Anat* **209,** 689-698.

Satchell SC & Braet F. (2009). Glomerular endothelial cell fenestrations: an integral component of the glomerular filtration barrier. *Am J Physiol Renal Physiol* **296,** F947-956.

Schafer A, Burkhardt M, Vollkommer T, Bauersachs J, Munzel T, Walter U & Smolenski A. (2003). Endothelium-dependent and -independent relaxation and VASP serines 157/239 phosphorylation by cyclic nucleotide-elevating vasodilators in rat aorta. *Biochem Pharmacol* **65,** 397-405.

Schneider JC, El Kebir D, Chereau C, Mercier JC, Dall'Ava-Santucci J & Dinh-Xuan AT. (2002). Involvement of Na(+)/Ca(2+) exchanger in endothelial NO production and endothelium-dependent relaxation. *Am J Physiol Heart Circ Physiol* **283,** H837-844.

Sedova M & Blatter LA. (1999). Dynamic regulation of [Ca2+]i by plasma membrane Ca(2+)-ATPase and Na+/Ca2+ exchange during capacitative Ca2+ entry in bovine vascular endothelial cells. *Cell Calcium* **25,** 333-343.

Senadheera S, Kim Y, Grayson TH, Toemoe S, Kochukov MY, Abramowitz J, Housley GD, Bertrand RL, Chadha PS, Bertrand PP, Murphy TV, Tare M, Birnbaumer L, Marrelli SP & Sandow SL. (2012). Transient receptor potential canonical type 3 channels facilitate endothelium-derived hyperpolarization-mediated resistance artery vasodilator activity. *Cardiovasc Res* **95,** 439-447.

Shaul PW, Smart EJ, Robinson LJ, German Z, Yuhanna IS, Ying Y, Anderson RG & Michel T. (1996). Acylation targets emdothelial nitric-oxide synthase to plasmalemmal caveolae. *J Biol Chem* **271,** 6518-6522.

Sheng JZ & Braun AP. (2007). Small- and intermediate-conductance Ca2+-activated K+ channels directly control agonist-evoked nitric oxide

synthesis in human vascular endothelial cells. *Am J Physiol Cell Physiol* **293,** C458-467.

Shultz PJ & Tolins JP. (1993). Adaptation to increased dietary salt intake in the rat. Role of endogenous nitric oxide. *J Clinical Invest***91,** 642-650.

Silver AE & Vita JA. (2006). Shear-stress-mediated arterial remodeling in atherosclerosis: too much of a good thing? *Circulation* **113,** 2787-2789.

Singer HA & Peach MJ. (1982). Calcium- and endothelial-mediated vascular smooth muscle relaxation in rabbit aorta. *Hypertension* **4,** 19-25.

Singh I, Knezevic N, Ahmmed GU, Kini V, Malik AB & Mehta D. (2007). Galphaq-TRPC6-mediated Ca2+ entry induces RhoA activation and resultant endothelial cell shape change in response to thrombin. *J Biol Chem* **282,** 7833-7843.

Sobie EA, Dilly KW, dos Santos Cruz J, Lederer WJ & Jafri MS. (2002). Termination of cardiac Ca(2+) sparks: an investigative mathematical model of calcium-induced calcium release. *Biophys J* **83,** 59-78.

Somlyo AP & Somlyo AV. (2003). Ca2+ sensitivity of smooth muscle and nonmuscle myosin II: modulated by G proteins, kinases, and myosin phosphatase. *Physiol Rev* **83,** 1325-1358.

Sonkusare SK, Bonev AD, Ledoux J, Liedtke W, Kotlikoff MI, Heppner TJ, Hill-Eubanks DC & Nelson MT. (2012). Elementary Ca2+ signals through endothelial TRPV4 channels regulate vascular function. *Science* **336,** 597-601.

Spassova MA, Hewavitharana T, Xu W, Soboloff J & Gill DL. (2006). A common mechanism underlies stretch activation and receptor activation of TRPC6 channels. *Proc Natl Acad Sci USA* **103,** 16586-16591.

Stankevicius E, Lopez-Valverde V, Rivera L, Hughes AD, Mulvany MJ & Simonsen U. (2006). Combination of Ca2+ -activated K+ channel blockers inhibits acetylcholine-evoked nitric oxide release in rat superior mesenteric artery. *Br J Pharmacol* **149,** 560-572.

Strubing C, Krapivinsky G, Krapivinsky L & Clapham DE. (2001). TRPC1 and TRPC5 form a novel cation channel in mammalian brain. *Neuron* **29,** 645-655.

Strubing C, Krapivinsky G, Krapivinsky L & Clapham DE. (2003). Formation of novel TRPC channels by complex subunit interactions in embryonic brain. *J Biol Chem* **278,** 39014-39019.

Sullivan MN, Francis M, Pitts NL, Taylor MS & Earley S. (2012). Optical recording reveals novel properties of GSK1016790A-induced vanilloid transient receptor potential channel TRPV4 activity in primary human endothelial cells. *Mol Pharmacol* **82,** 464-472.

Sundivakkam PC, Freichel M, Singh V, Yuan JP, Vogel SM, Flockerzi V, Malik AB & Tiruppathi C. (2012). The Ca(2+) sensor stromal interaction molecule 1 (STIM1) is necessary and sufficient for the store-operated Ca(2+) entry function of transient receptor potential canonical (TRPC) 1 and 4 channels in endothelial cells. *Mol Pharmacol* **81,** 510-526.

Sundivakkam PC, Kwiatek AM, Sharma TT, Minshall RD, Malik AB & Tiruppathi C. (2009). Caveolin-1 scaffold domain interacts with TRPC1 and IP3R3 to regulate Ca2+ store release-induced Ca2+ entry in endothelial cells. *Am J Physiol Cell Physiol* **296,** C403-413.

Syyong HT, Poburko D, Fameli N & van Breemen C. (2007). ATP promotes NCX-reversal in aortic smooth muscle cells by DAG-activated Na+ entry. *Biochem Biophys Res Commun* **357,** 1177-1182.

Takahashi S & Mendelsohn ME. (2003). Synergistic activation of endothelial nitric-oxide synthase (eNOS) by HSP90 and Akt: calcium-independent eNOS activation involves formation of an HSP90-Akt-CaM-bound eNOS complex. *J Biol Chem* **278,** 30821-30827.

Takeya K, Loutzenhiser K, Shiraishi M, Loutzenhiser R & Walsh MP. (2008). A highly sensitive technique to measure myosin regulatory light chain phosphorylation: the first quantification in renal arterioles. *Am JPhysiol Renal Physiol* **294,** F1487-1492.

Tang EH & Vanhoutte PM. (2009). Prostanoids and reactive oxygen species: team players in endothelium-dependent contractions. *Pharmacol Ther* **122,** 140-149.

Teubl M, Groschner K, Kohlwein SD, Mayer B & Schmidt K. (1999). Na(+)/Ca(2+) exchange facilitates Ca(2+)-dependent activation of endothelial nitric-oxide synthase. *J Biol Chem* **274,** 29529-29535.

Thors B, Halldorsson H & Thorgeirsson G. (2004). Thrombin and histamine stimulate endothelial nitric-oxide synthase phosphorylation at Ser1177 via an AMPK mediated pathway independent of PI3K-Akt. *FEBS Lett* **573,** 175-180.

Thorsgaard M, Lopez V, Buus NH & Simonsen U. (2003). Different modulation by Ca2+-activated K+ channel blockers and herbimycin of acetylcholine- and

flow-evoked vasodilatation in rat mesenteric small arteries. *Br JPharmacol* **138,** 1562-1570.

Tiruppathi C, Freichel M, Vogel SM, Paria BC, Mehta D, Flockerzi V & Malik AB. (2002). Impairment of store-operated Ca2+ entry in TRPC4(-/-) mice interferes with increase in lung microvascular permeability. *Circ Res* **91,** 70-76.

Tran QK, Leonard J, Black DJ & Persechini A. (2008). Phosphorylation within an autoinhibitory domain in endothelial nitric oxide synthase reduces the Ca(2+) concentrations required for calmodulin to bind and activate the enzyme. *Biochemistry* **47,** 7557-7566.

Trebak M, Vazquez G, Bird GS & Putney JW, Jr. (2003). The TRPC3/6/7 subfamily of cation channels. *Cell Calcium* **33,** 451-461.

Varnai P, Toth B, Toth DJ, Hunyady L & Balla T. (2007). Visualization and manipulation of plasma membrane-endoplasmic reticulum contact sites indicates the presence of additional molecular components within the STIM1-Orai1 Complex. *J Biol Chem* **282,** 29678-29690.

Vennekens R. (2011). Emerging concepts for the role of TRP channels in the cardiovascular system. *J Physiol* **589,** 1527-1534.

Vessieres E, Freidja ML, Loufrani L, Fassot C & Henrion D. (2012). Flow (shear stress)-mediated remodeling of resistance arteries in diabetes. *Vascul Pharmacol* **57,** 173-178.

Viana F, de Smedt H, Droogmans G & Nilius B. (1998). Calcium signalling through nucleotide receptor P2Y2 in cultured human vascular endothelium. *Cell Calcium* **24,** 117-127.

Vig M, Peinelt C, Beck A, Koomoa DL, Rabah D, Koblan-Huberson M, Kraft S, Turner H, Fleig A, Penner R & Kinet JP. (2006). CRACM1 is a plasma membrane protein essential for store-operated Ca2+ entry. *Science* **312,** 1220-1223.

Vincent F, Acevedo A, Nguyen MT, Dourado M, DeFalco J, Gustafson A, Spiro P, Emerling DE, Kelly MG & Duncton MA. (2009). Identification and characterization of novel TRPV4 modulators. *BiochemBiophys Res Commun* **389,** 490-494.

Walsh MP & Cole WC. (2013). The role of actin filament dynamics in the myogenic response of cerebral resistance arteries. *J Cereb Blood Flow Metab* **33,** 1-12.

Wang R, Wang Z & Wu L. (1997). Carbon monoxide-induced vasorelaxation and the underlying mechanisms. *Br J Pharmacol* **121,** 927-934.

Watanabe H, Vriens J, Suh SH, Benham CD, Droogmans G & Nilius B. (2002). Heat-evoked activation of TRPV4 channels in a HEK293 cell expression system and in native mouse aorta endothelial cells. *J BiolChem* **277,** 47044-47051.

Watanabe S, Yashiro Y, Mizuno R & Ohhashi T. (2005). Involvement of NO and EDHF in flow-induced vasodilation in isolated hamster cremasteric arterioles. *J Vasc Res* **42,** 137-147.

Welsh DG, Morielli AD, Nelson MT & Brayden JE. (2002). Transient receptor potential channels regulate myogenic tone of resistance arteries. *Circ Res* **90,** 248-250.

Wong MS & Vanhoutte PM. (2010). COX-mediated endothelium-dependent contractions: from the past to recent discoveries. *Acta Pharmacol Sin* **31,** 1095-1102.

Wright RS, Wei CM, Kim CH, Kinoshita M, Matsuda Y, Aarhus LL, Burnett JC, Jr. & Miller WL. (1996). C-type natriuretic peptide-mediated coronary vasodilation: role of the coronary nitric oxide and particulate guanylate cyclase systems. *J Am Coll Cardiol* **28,** 1031-1038.

Wu L, Gao X, Brown RC, Heller S & O'Neil RG. (2007). Dual role of the TRPV4 channel as a sensor of flow and osmolality in renal epithelial cells. *Am JPhysiol Renal Physiol* **293,** F1699-1713.

Wu S, Haynes J, Jr., Taylor JT, Obiako BO, Stubbs JR, Li M & Stevens T. (2003). Cav3.1 (alpha1G) T-type Ca2+ channels mediate vaso-occlusion of sickled erythrocytes in lung microcirculation. *Circ Res* **93,** 346-353.

Wu Y, Miyamoto T, Li K, Nakagomi H, Sawada N, Kira S, Kobayashi H, Zakohji H, Tsuchida T, Fukazawa M, Araki I & Takeda M. (2011). Decreased expression of the epithelial Ca2+ channel TRPV5 and TRPV6 in human renal cell carcinoma associated with vitamin D receptor. *J Urol* **186,** 2419-2425.

Xu SZ, Boulay G, Flemming R & Beech DJ. (2006). E3-targeted anti-TRPC5 antibody inhibits store-operated calcium entry in freshly isolated pial arterioles. *Am J Physiol Heart Circ Physiol* **291,** H2653-2659.

Yeromin AV, Zhang SL, Jiang W, Yu Y, Safrina O & Cahalan MD. (2006). Molecular identification of the CRAC channel by altered ion selectivity in a mutant of Orai. *Nature* **443,** 226-229.

Ying WZ, Aaron K & Sanders PW. (2008). Dietary salt activates an endothelial proline-rich tyrosine kinase 2/c-Src/phosphatidylinositol 3-kinase complex to promote endothelial nitric oxide synthase phosphorylation. *Hypertension* **52,** 1134-1141.

Ying WZ & Sanders PW. (1998). Dietary salt enhances glomerular endothelial nitric oxide synthase through TGF-beta1. *AmJ Physiol* **275,** F18-24.

Yip H, Chan WY, Leung PC, Kwan HY, Liu C, Huang Y, Michel V, Yew DT & Yao X. (2004). Expression of TRPC homologs in endothelial cells and smooth muscle layers of human arteries. *Histochem Cell Biol* **122,** 553-561.

Zembowicz A, Hatchett RJ, Jakubowski AM & Gryglewski RJ. (1993). Involvement of nitric oxide in the endothelium-dependent relaxation induced by hydrogen peroxide in the rabbit aorta. *Br J Pharmacol* **110,** 151-158.

Zhang DX & Gutterman DD. (2011). Transient receptor potential channel activation and endothelium-dependent dilation in the systemic circulation. *J Cardiovasc Pharmacol* **57,** 133-139.

Zhang DX, Mendoza SA, Bubolz AH, Mizuno A, Ge ZD, Li R, Warltier DC, Suzuki M & Gutterman DD. (2009). Transient receptor potential vanilloid type 4-deficient mice exhibit impaired endothelium-dependent relaxation induced by acetylcholine in vitro and in vivo. *Hypertension* **53,** 532-538.

Zhang J, Ren C, Chen L, Navedo MF, Antos LK, Kinsey SP, Iwamoto T, Philipson KD, Kotlikoff MI, Santana LF, Wier WG, Matteson DR & Blaustein MP. (2010). Knockout of Na+/Ca2+ exchanger in smooth muscle attenuates vasoconstriction and L-type Ca2+ channel current and lowers blood pressure. *Am J Physiol Heart Circ Physiol* **298,** H1472-1483.

Zhong XZ, Abd-Elrahman KS, Liao CH, El-Yazbi AF, Walsh EJ, Walsh MP & Cole WC. (2010). Stromatoxin-sensitive, heteromultimeric Kv2.1/Kv9.3 channels contribute to myogenic control of cerebral arterial diameter. *J Physiol* **588,** 4519-4537.

Zhou C, Chen H, King JA, Sellak H, Kuebler WM, Yin J, Townsley MI, Shin HS & Wu S. (2010). Alpha1G T-type calcium channel selectively regulates P-selectin surface expression in pulmonary capillary endothelium. *Am J Physiol Lung Cell Mol Physiol* **299,** L86-97.

Zhu J, Drenjancevic-Peric I, McEwen S, Friesema J, Schulta D, Yu M, Roman RJ & Lombard JH. (2006). Role of superoxide and angiotensin II suppression

in salt-induced changes in endothelial Ca2+ signaling and NO production in rat aorta. *Am J Physiol Heart Circ Physiol* **291,** H929-938.